GROUNDWATER-SURFACEWATER INTERACTION MEASUREMENT IMPROVEMENT AND MODEL APPLICATIONS

A Dissertation

by

XIN PENG

Submitted to the Office of Graduate and Professional Studies of
Texas A&M University
in partial fulfillment of the requirements for the degree of

DOCTOR OF PHILOSOPHY

Chair of Committee,	Hongbin Zhan
Committee Members,	Mark Everett
	David Sparks
	Peter Knappett
Head of Department,	Mike Pope

December 2018

Major Subject: Geophysics

ABSTRACT

A hyporheic zone is the region underneath or near the streambed that has interaction with groundwater and surface water. It serves many functions including exchange of water, nutrients and organic matter. Hydraulic parameters such as permeability and hydraulic gradient across streambeds control the water flow in the hyporheic zone. The accuracy of measurements of those parameters is important for learning and interpreting the hyporheic zone properties. The first part of this study will focus on the air compressibility effect on the Bouwer and Rice (B&R) seepage meter. The second part of the study will focus on the process of baseflow to a stream with a low hydraulic conductivity thin layer streambed. The third part of the study will focus on the bank storage effect in unsaturated and saturated zone with a streambed.

A correction is obtained for calculating the seepage flux rate that includes consideration of air compressibility inside the manometer of a Bouwer and Rice seepage meter. The result shows that the effect of air compressibility in the manometer increases with the volume of air in the manometer. The correction of this study will work as a quantitative tool to determine if air compressibility can be neglected or not for a Bouwer and Rice seepage meter test.

For the baseflow to a stream process, a low hydraulic conductivity thin layer streambed is considered along with an unsaturated-saturated coupled model. The hydraulic head in unsaturated and saturated zones are analytically derived. The integration of lateral seepage flux across both unsaturated and saturated zones are calculated afterwards. The study suggests that streambed affects the total discharge rate into the stream at early and late times in quite different manners, where the total discharge rate includes the horizontal discharge rates of both saturated and unsaturated zones. The peak of total discharge rate which occurs in early time is lowered and

the baseflow decay process is prolonged when there is a streambed. In slope recession hydrograph analysis, the streambed affects early time slope and has little impact on late time slope. This results in an underestimation of hydraulic conductivity, specific yield and saturated aquifer thickness if the streambed effect is not considered in the analysis.

Bank storage effect in unsaturated and saturated zone can be influenced by the streambed. A lower streambed hydraulic conductance value will lead to a lower peak value of the flux exchange rate between the aquifer and the stream. The total bank storage volume will also be lower if the streambed hydraulic conductance is lower. The bank storage releasing time is slightly shorter in the unsaturated zone than that in the saturated zone, which means that bank storage is released faster in the unsaturated zone than that in the saturated zone. The distribution of bank storage between saturated and unsaturated zones can be influenced by a thin layer of streambed and the unsaturated zone properties.

DEDICATION

To my family

ACKNOWLEDGEMENTS

I would like to thank my advisor, Dr. Hongbin Zhan for guiding me into the field of hydrogeology and helping me get through my Ph.D. study. His guidance helped me in all the time of research and writing of this thesis. I could not have imagined having a better advisor and mentor for my Ph.D. study. Dr. Zhan, thank you very much for your encouragements, patience, motivation and immense knowledge, thank you very much for paying attention not only to our students' school education but also to life experiences, and thank you very much for all the group members get-together fun times!

Besides my advisor, I would like to thank my committee members, Dr. Mark Everett, Dr. David Sparks and Dr. Peter Knappett, for their guidance and support throughout this research, for their insightful comments and encouragement, and also for the hard questions which incented me to widen my research from various perspectives.

Thanks also go to my friends and colleagues for making my time at Texas A&M University a great experience. Thanks go to the department of Geology & Geophysics staff and faculty. I sincerely thank the financial support from the department of Geology & Geophysics, which gave me the opportunity to work as a teaching assistant and finish my Ph.D. studies.

Finally, thanks to my mother and father, my family members for their persistent support and selfless love.

CONTRIBUTORS AND FUNDING SOURCES

This work was supported by a dissertation committee consisting of Professor Hongbin Zhan [advisor] and Professor Mark Everett, Professor David Sparks of the Department of Geology and Geophysics and Professor Peter Knappett of the Department of Water Management. All other work conducted for the dissertation was completed by the student independently.

Graduate study was supported by financial aid from department of Geology and Geophysics, Texas A&M University.

TABLE OF CONTENTS

Page

ABSTRACT ii

DEDICATION iv

ACKNOWLEDGEMENTS v

CONTRIBUTORS AND FUNDING SOURCES vi

TABLE OF CONTENTS vii

LIST OF FIGURES ix

LIST OF TABLES xii

1. INTRODUCTION 1

1.1 Background 1
1.2 Objective 3
1.3 Organization 3

2. AIR COMPRESSIBILITY EFFECT ON BOUWER AND RICE SEEPAGE METER 5

2.1 Introduction 5
2.2 Principle of the seepage meter 6
2.3 Improvement of interpretation considering air compressibility 11
2.4 Comparison of equation (2.2) with equation (2.1) 13
2.5 Conclusions 15

3. BASEFLOW RECESSION IN AN UNSATURATED-SATURATED ZONE WITH A STREAMBED 17

3.1 Introduction 17
3.2 Mathematical model 19
3.3 Semi-analytical solution 25
3.4 Validation through COMSOL Multiphysics numerical simulation 28
3.5 Results 31
3.6 Discussion 52
3.7 Conclusions 54

4. BANK STORAGE IN UNSATURATED AND SATURATED ZONE WITH A STREAMBED 56

4.1 Introduction 56
4.2 Mathematical model 58
4.3 Semi-analytical solution 65
4.4 Validation through COMSOL Multiphysics numerical simulation 67
4.5 Results 70
4.6 Discussion 84
4.7 Conclusion 85

5. SUMMARY 87

5.1 Summary and conclusions 87
5.2 Contribution 89
5.3 Future scope 90

REFERENCES 92

APPENDIX A 101

APPENDIX B 104

LIST OF FIGURES

Page

Figure 2. 1 B&R seepage meter from Bouwer and Rice (1963). (1) The seepage bell on the streambed. (2) The falling-level reservoir. (3) A manometer for measuring the hydraulic head inside the seepage bell. The dash line at the bottom represents the interface of stream water and streambed. The solid line right above the seepage bell represents the stream water level. Valve K_1 on top of the manometer is for providing vacuum in the manometer as well as controlling the air volume inside the manometer. 7

Figure 2. 2 Improved B&R seepage meter from Wang et al. (2014). The dash line at the bottom represents the interface of stream water and streambed. The solid line inside the seepage cylinder right above the seepage bell represents the simulated stream water level, which is controlled by valve K_4 in this figure. 8

Figure 2. 3 Example of water levels in manometer tube A and tube B versus time. Point 1 is the intersection of curve A and curve B which represents tube A water level equals the tube B water level and the seepage rate inside the seepage bell (V_b) will be equal to the seepage rate outside the seepage bell (V_e) at this point. 11

Figure 3. 1 The diagram of the baseflow model with a low-hydraulic conductivity streambed in a watershed, considering the coupled unsaturated and saturated flow processes. 20

Figure 3. 2 The zoom in picture of the concept model near the low-permeability streambed. 24

Figure 3. 3 Mesh plot for present model in the finite element simulation using COMSOL Multiphysics. 29

Figure 3. 4 Comparison between the numerical simulation from COMSOL Multiphysics and the present solution. 30

Figure 3. 5 Hydraulic head response in the saturated and unsaturated zones after two infiltration events. The first infiltration event starts at t_D = 1 and ends at t_D = 1.5 with a constant rate of I_D=0.5. The second infiltration event starts at t_D = 4.5 and ends at t_D = 5 with a constant rate of I_D=1. 32

Figure 3. 6 Hydraulic head response in the saturated zone with κ_D=1. 34

Figure 3. 7 Hydraulic head response in the saturated zone with κ_D=10. 35

Figure 3. 8 Dimensionless discharge from the saturated zone and unsaturated zone to the stream. a) Infiltration events. b) Dimensionless discharge rate to the

stream in the saturated zone. c) Dimensionless discharge rate to the stream in the unsaturated zone. 36

Figure 3. 9 The ratio of unsaturated zone dimensionless discharge to saturated zone dimensionless discharge. The Liang (2017) solution stands for no streambed case. Present solution K_{LD}=0.1 and K_{LD}=0.2 stand for different streambed index cases. 37

Figure 3. 10 The saturated zone dimensionless discharge difference between no streambed and with streambed. a) Infiltration events. b) Dimensionless discharge difference between K_{LD}=0.1 case and no streambed case. c) Dimensionless discharge ratio between K_{LD}= 0.1 case (present solution) and no streambed case (Liang solution). 38

Figure 3. 11 The ratio of horizontal flow versus vertical flow (γ) as a function of time at different locations when z_D= 0.1 (in the unsaturated zone). 40

Figure 3. 12 The ratio of horizontal flow versus vertical flow (γ) as a function of time at different locations when z_D= 0 (at free water table surface). 41

Figure 3. 13 The ratio of horizontal flow versus vertical flow (γ) as a function of time at different locations when z_D= -0.2 (in the saturated zone). 42

Figure 3. 14 The 3D view of the γ value varies over x_D and t_D when z_D= 0 and K_{LD}= 0.1. 44

Figure 3. 15 The log-log plot of Q_s $m^2 day^{-1}$ versus time (day). Q_s is the saturated discharge rate to the stream. The solid lines stand for the case without a streambed, which is the Liang solution. The dash lines stand for present solution considering streambed effect. 46

Figure 3. 16 The effect of streambed on slope recession hydrographs. The solid lines stand for no streambed case (Liang solution) and dash lines stand for present solution with a streambed index of K_{LD}=0.1. 48

Figure 3. 17 The effect of K_{LD} value on recession slope curves. 49

Figure 3. 18 Sensitivity analysis for different model parameters.K_{LD}=0.1 is the streambed index. H_{sD} is the dimensionless saturated zone thickness. H_{uD} is the dimensionless unsaturated zone thickness. H_D is the dimensionless stream water level. κ_D is the dimensionless parameter relates to unsaturated zone effect. S_y is the specific yield. S_s is the specific storativity. K_D is the ratio of vertical hydraulic conductivity to horizontal hydraulic conductivity. 51

Figure 3. 19 Sensitivity analysis for no streambed model for comparison.K_{LD}=0 is the no streambed case. H_{sD} is the dimensionless saturated zone thickness.

H_{uD} is the dimensionless unsaturated zone thickness. H_D is the dimensionless stream water level. κ_D is the dimensionless parameter relates to unsaturated zone effect. S_y is the specific yield. S_s is the specific storativity. K_D is the ratio of vertical hydraulic conductivity to horizontal hydraulic conductivity. 52

Figure 4. 1 Schematic model of unsaturated-saturated zone with a low permeability streambed. 59

Figure 4. 2 Zoom in near the low permeability streambed. The hydraulic head on the right side of low permeability layer is the same value as $H(t)$. 63

Figure 4. 3 Mesh plot for present model in the finite element simulation using COMSOL Multiphysics. 68

Figure 4. 4 Comparison between numerical solution and semi-analytical solution. The observation point is at x_D=0.9, z_D=0.1 for unsaturated zone (u_D) and (x_D=0.9, z_D=-0.1) for saturated zone (h_D). 70

Figure 4. 5 Hydraulic response at the location of x_D=0.9 73

Figure 4. 6 Hydraulic response at the location of x_D=0.5 74

Figure 4. 7 Hydraulic response at the location of x_D=0.1 74

Figure 4. 8 Saturated zone and unsaturated zone flux exchange rate across the streambed. (at the location of x_D=1) 76

Figure 4. 9 Bank storage in unsaturated zone and saturated zone. 78

Figure 4. 10 Semi-log plot of bank storage v.s. t_D 79

Figure 4. 11 Characteristic releasing time T_r value for unsaturated zone and saturated zone. 79

Figure 4. 12 The distribution of storage between unsaturated zone and saturated zone when κ_D=10. 81

Figure 4. 13 The distribution of storage between unsaturated zone and saturated zone when κ_D=100. 82

Figure 4. 14 The distribution of storage between unsaturated zone and saturated zone when κ_D=1000. 83

Figure 4. 15 Sensitivity analysis for different model parameters. 84

LIST OF TABLES

Page

Table 2. 1 Relative correction calculation results. 14

Table 3. 1 The dimensionless variables. 28

Table 3. 2 Simulation parameters 31

Table 3. 3 Simulation parameters for studying slope recession hydrographs 45

Table 4. 1 The dimensionless variables. 67

Table 4. 2 Simulation parameters for part 4.5.1 68

1. INTRODUCTION

1.1 Background

Recently topics related to stream-aquifer interaction has drawn much attention. For streams or lakes that are gaining water from groundwater the seepage flux is upward, and flux is downward where surface water flows to groundwater. In arid and semi-arid regions, streams and lakes may become disconnected from the underlying groundwater, in which case seepage flux is still downward but occurs through unsaturated sediments (Sophocleous, 2002; Brunner et al., 2009a; Brunner et al., 2009b; Brunner et al., 2011).

To determine the seepage flux across a streambed, we need a seepage mater. The first seepage meter was designed for measuring water loss in irrigation by Israelsen and Reeve in 1944. Later, a comprehensive review about seepage meters was given by Carr and Winter (1980). This review collected many seepage meter designs including the Salinity Laboratory seepage meter (Israelsen and Reeve, 1944; Warnick, 1951), the U.S. Bureau of Reclamation seepage meter (Lee and Cherry, 1979), the Weber Basin or Mariotte siphon seepage meter (Warnick, 1951; Hendricks and Warnick, 1961), the Soil Conservation Service seepage meter (Robinson and Rohwer, 1952), and the Bouwer and Rice seepage meter (Bouwer and Rice, 1963).

In the years since the Carr and Winter (1980) seepage meter review was published, other seepage meters have been designed such as the remotely operated seepage meter (Cherkauer and McBride, 1988), the heat pulse method seepage meter (Taniguchi and Fukuo, 1993; Zhu et al., 2015), the seepage meter for use in flowing water (Rosenberry, 2008; Rosenberry and Pitlick,

2009), and the tube seepage meter (Solder et al., 2016). There were some improvements to the Bouwer and Rice seepage meter to achieve better flux rate measurements and error analysis (Belanger and Montgomery, 1992; Murdoch and Kelly, 2003; Taniguchi et al., 2003). Recently, Wang et al. (2014) used the Bouwer and Rice seepage meter in his article but he didn't mention about the air compressibility in Bouwer and Rice seepage meter, which could impact the measurement results during the experiment. Therefore the first part of this study will focus on the air compressibility in Bouwer and Rice seepage meter.

The second part of this study focuses on baseflow recession problem. The governing equations of flow in this part are based upon Boussinesq's work, which is the problem of a horizontal unconfined aquifer fully penetrated by a stream (Boussinesq, 1877; Boussinesq, 1903a; Boussinesq, 1903b; Boussinesq, 1904). Brutsaert and Nieber (1977) presented a baseflow analysis based on data collected on streams located within the Finger Lakes region of New York State. They proposed that the changing rate of river discharge dQ/dt is a function of the discharge Q itself. One of the simplest models they assumed took the form of a power function, i.e., $\frac{dQ}{dt} = -aQ^b$, where a and b are constants. Since then, this method has been used widely to determine aquifer parameters (Brutsaert and Lopez, 1998; Szilagyi and Parlange, 1998; Rupp and Selker, 2005; Pauwels and Troch, 2010).

Zlotnik and Huang (1999) proposed an analytical model to assess the impact of thin, low-permeability stream bed sediments on head responses. However, the effect of the unsaturated zone flow process is ignored because of the problem complexity. Hilberts et al. (2005) proposed an analytical expression for specific yield (S_y) that is dependent on the water table and the retention capacity(κ) of the unsaturated zone based on the van Genuchten (1980) model. Because the lateral flux in the unsaturated zone is still ignored by Hillslope-storage Boussinesq

model(Troch et al., 2003), Kong et al. (2016) showed that it is necessary to consider unsaturated flow to improve the accuracy of predicting groundwater flux rates to the river during recession. Liang et al. (2017) constructed a model with an algorithm describing both unsaturated lateral and vertical flows.

1.2 Objective

The objective of this study is to investigate stream-aquifer interactions. Specifically, this study focuses on the following goals:

1. Study the effects of air compressibility on the Bouwer and Rice seepage meter and make suggestions for future seepage meter measurements.

2. Investigate theoretical rates of baseflow with an unsaturated-saturated coupled model with a low hydraulic conductivity streambed.

3. Explore the present unsaturated-saturated coupled model with different decay κ constant.

4. Investigate the bank storage effect with present unsaturated-saturated coupled model. Analyze the impact of a low permeability streambed on bank storage distribution among unsaturated zone and saturated zone.

1.3 Organization

This dissertation is organized as follows: in section 2, the air compressibility on the Bouwer and Rice seepage meter is studied and suggestions are provided to accurately conduct Bouwer and Rice seepage meter measurements; in section 3, a semi-analytical solution of spatiotemporal distributions of hydraulic heads and discharges in both the saturated and

unsaturated zones is acquired. The process of baseflow to a stream with thin, low hydraulic conductivity streambed is investigated using this solution; in section 4, a 2D conceptual model of flux exchange between an unsaturated-saturated zone and a stream with a thin low-permeability streambed is established. It considers both the unsaturated zone and saturated zone flow process. Lastly, a mathematical model describing the coupled unsaturated and saturated flow processes is introduced and the semi-analytical solutions of the spatiotemporal distributions of hydraulic heads in both the saturated and unsaturated zones are obtained. The streambed index, which reflects the impact of streambed, is studied for its effect on bank storage distribution among unsaturated zone and saturated zone; this dissertation is ended with a brief summary and several conclusions in section 6.

2. AIR COMPRESSIBILITY EFFECT ON BOUWER AND RICE SEEPAGE METER*

2.1 Introduction

A hyporheic zone is the region underneath or near the streambed that has interaction with groundwater and surface water. It serves many functions including exchange of water, nutrients and organic matter (Boulton et al., 1998). Hydraulic parameters such as permeability and hydraulic gradient of streambeds control the water flow in the hyporheic zone (Yamada et al., 2005). The accuracy of measurements of those parameters is important for learning and interpreting the hyporheic zone properties. One of the most commonly measured data is the seepage flux across the streambed. For streams or lakes that are gaining water from groundwater the seepage flux is upward, and flux is downward where surface water flows to groundwater. In arid and semi-arid areas, streams and lakes may become disconnected with the underlying groundwater, in which case seepage flux is still downward but occurs through unsaturated sediments (Sophocleous, 2002; Brunner et al., 2009a; Brunner et al., 2009b; Brunner et al., 2011).

To measure the seepage flux, there are different designs of seepage meter including the Bouwer and Rice seepage meter (Bouwer and Rice, 1963), remotely operated seepage meter (Cherkauer and McBride, 1988), heat pulse method seepage meter (Taniguchi and Fukuo, 1993; Zhu et al., 2015), seepage meter for use in flowing water (Rosenberry, 2008; Rosenberry and Pitlick, 2009), and tube seepage meter (Solder et al., 2016). This study will only discuss the Bouwer and Rice seepage meter which will be called B&R seepage meter for abbreviation

*Reprinted with permission from "Air Compressibility Effect on Bouwer and Rice Seepage Meter" by Peng, X., and H. Zhan (2017). Ground Water, 55, 899-905, Copyright [2017] by John Wiley & Sons, Inc.

hereinafter.

The first detailed operation of such a B&R seepage meter was given by Lee (1977). A comprehensive review about B&R seepage meters was given by Carr and Winter (1980). There were some improvements to B&R seepage meters for better flux rate measurements and error analysis (Belanger and Montgomery, 1992; Murdoch and Kelly, 2003; Taniguchi et al., 2003). However, none of them have considered the air compressibility effect in the B&R seepage meter.

2.2 Principle of the seepage meter

Figure 2.1 shows a sketch of a field B&R seepage meter, which has three main parts: (1) a seepage bell on the streambed, (2) a falling-level reservoir, and (3) a manometer for measuring the hydraulic head inside the seepage bell. A common size for a seepage bell is 25.4 cm in diameter. The seepage bell is inserted into the streambed to maintain a good seal. The falling-level reservoir is filled with water and can be adjusted for proper height (H_f). The total needed measurement time is depended on the streambed hydraulic conductivity as well as the size of the falling-level reservoir. A lower hydraulic conductivity or a larger diameter of the falling-level reservoir can result in a longer measurement. If the water level in the falling-level reservoir is higher than in the stream, the seepage rate inside the seepage bell (V_b) will have a higher value than the outside (actual streambed) seepage rate (V_e). The seepage rate of streambed (V_e) is related to the vertical hydraulic gradient at the streambed interface. And this vertical hydraulic gradient is defined by the stream water depth M. The manometer is a "U"-shape tube with a height of H. A ruler is attached to the manometer for reading the water level in tube A (h_A) and tube B (h_B) (see Figure 2.1). Valve K_1 on top of the manometer is for providing vacuum in the manometer as well as controlling the air volume inside the manometer. If valve K_1 is closed, the

manometer shows the head difference between the inside and outside of the seepage bell. If one plots h_A and h_B as functions of time in one diagram, one will see h_A decreasing with time and h_B increasing with time. The intersection of these two curves represents a condition that the head difference inside and outside of the seepage bell is zero, and the seepage rate inside seepage bell is the same as that outside seepage bell.

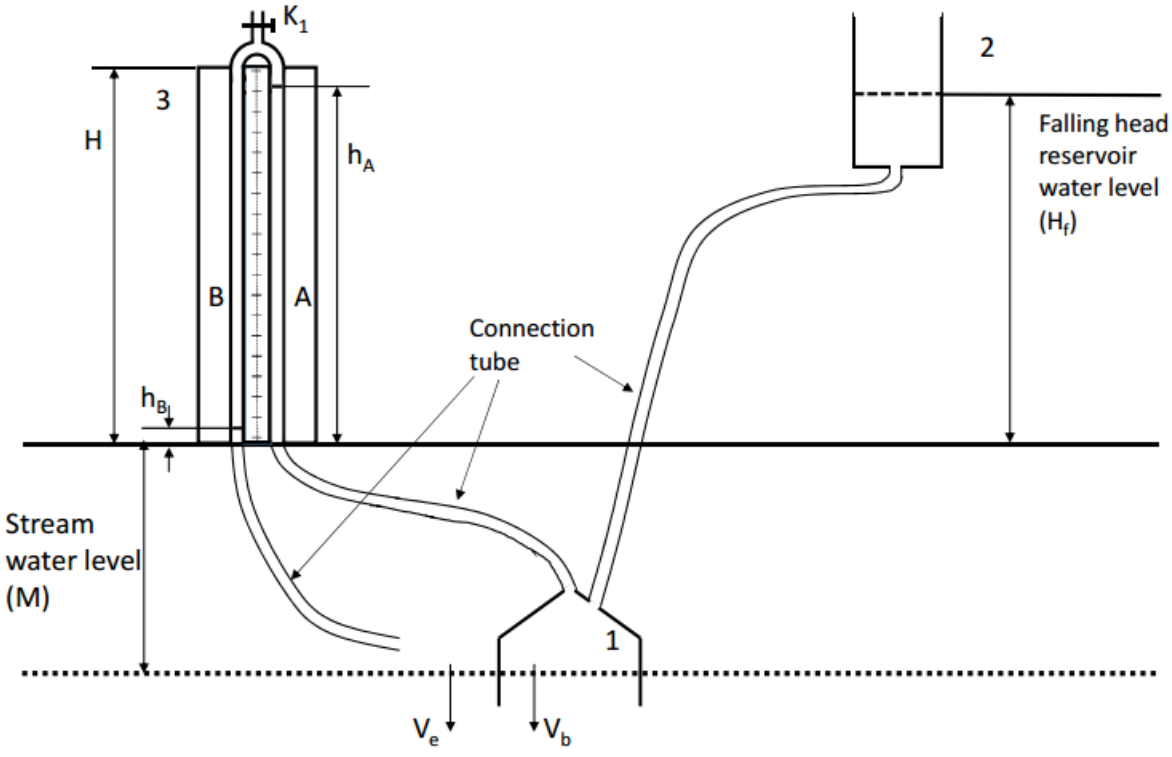

Figure 2. 1 B&R seepage meter from Bouwer and Rice (1963). (1) The seepage bell on the streambed. (2) The falling-level reservoir. (3) A manometer for measuring the hydraulic head inside the seepage bell. The dash line at the bottom represents the interface of stream water and streambed. The solid line right above the seepage bell represents the stream water level. Valve K_1 on top of the manometer is for providing vacuum in the manometer as well as controlling the air volume inside the manometer.(Peng and Zhan, 2017)

The test can be conducted in two different modes: suction and no-suction. For the suction mode, the air inside the manometer will be partially pumped out before closing valve K_1 to start the measurement. For the no-suction mode, the air inside the manometer will not be pumped out before closing valve K_1 to start the measurement. For either mode, the air mass inside the manometer remains constant during the entire duration of test because valve K_1 is closed. The difference is that less air mass is kept inside the manometer for the suction mode than for the no-suction mode.

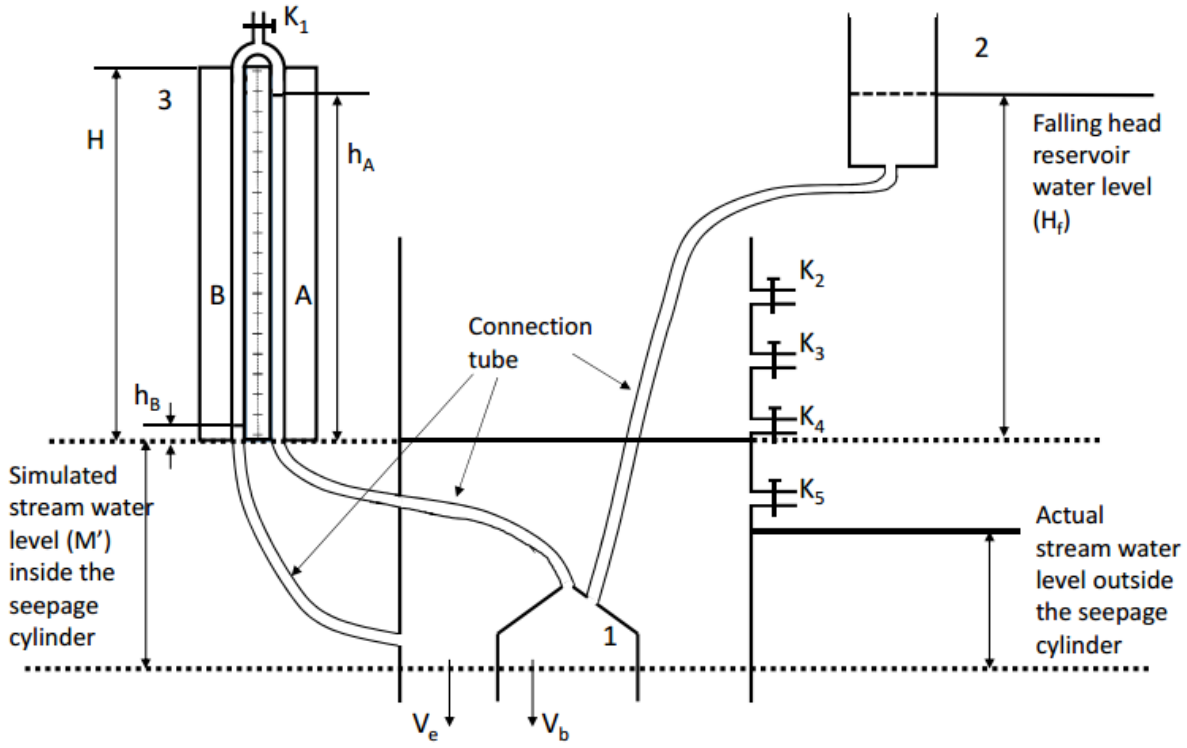

Figure 2. 2 Improved B&R seepage meter from Wang et al. (2014). The dash line at the bottom represents the interface of stream water and streambed. The solid line inside the seepage cylinder right above the seepage bell represents the simulated stream water level, which is controlled by valve K_4 in this figure.(Peng and Zhan, 2017)

Wang et al. (2014) improved the B&R seepage meter with a seepage cylinder outside the seepage bell (Figure 2.2). The seepage cylinder is 0.85 m in diameter and 1.5 m in height. The seepage cylinder is for creating an adjustable simulated water depth (M') around the seepage bell. It has to be inserted into the streambed and to maintain a good seal as well. In Figure 2.2, Valve K_1 on top of the manometer is also for providing vacuum in the manometer as well as controlling the air volume inside the manometer. There are several other valves (K_2, K_3, K_4, K_5) on the cylinder that can be opened or closed and the water depth inside the cylinder will be maintained at the first open valve. For instance, the water depth inside the cylinder is maintained at valve K_4 in Figure 2.2. The purpose to use multiple valves in the seepage cylinder of Figure 2.2 is enable us to determine the seepage flux under different and controllable stream water levels at a given location. By doing so, one is not limited to the actual stream water level outside the seepage cylinder. However, if one is only interested in the seepage flux under the actual stream water level, then the seepage cylinder is not needed and can be removed.

In the experiments reported by Wang et al. (2014), the seepage bell and the falling-level reservoir both are 25.4 cm in diameter. The manometer with a ruler attached has a length of 0.8 m and the lower end of the manometer is at the same level as the water level in the seepage cylinder. Before the measurement, water is filled into the falling-level reservoir to a height of H_f above the water level in the cylinder (Figure 2.2). Valve K_1 is open before the measurement and the water level in tube A (h_A) will be the same as the water level in the falling-level reservoir (H_f). The water level in tube B (h_B) will stay at the same level as the water level in the cylinder, so the water level reading in tube B (h_B) will be 0 m for the no-suction mode. Because a portion of air is removed through valve K_1 for the suction mode before the experiment, both the water levels in tube A and tube B will be lifted up by the same amount and the difference between the

water level in tube A (h_A) and the water level in tube B (h_B) will remain the same as H_f since both reservoirs are open to the atmosphere.

To start the measurement, valve K_1 is closed and water in the seepage bell starts to infiltrate into the streambed. The water level in tube A (h_A) will decrease with time and the water level in tube B (h_B) will increase with time. The seepage rate inside the seepage bell (V_b) will be equal to the seepage rate outside the seepage bell (V_e) when tube A water level equals the tube B water level. Both tube A and tube B water level readings are recorded with time and plotted in the same chart (Figure 2.3). Point 1 is the intersection of curve A (for tube A) and curve B (for tube B). The magnitude of the slope at point 1 on curve A is V_s (Figure 2.3). So the vertical seepage flux rate (V_e) is given by Wang et al. (2014) as:

$$V_e = 2V_s. \tag{2.1}$$

Wang et al. (2014) did not provide a physical explanation on equation (2.1). Here we offer an illustration about this equation based on Figure 2.1. First of all, we need to point out that Wang et al. (2014) did not consider the air compressibility. In another word, air volume inside the manometer of Figure 2.1 remains constant but its pressure is allowed to change. This assumption is obviously not physically sound. In fact, this is the motivation for us to develop this correction to the method of Wang et al. (2014). Nevertheless, if the water level in tube A drops by 1 unit length, then the water level in tube B has to rise by 1 unit length because the air volume inside the manometer must remain the same according to Wang et al. (2014). The rise of water level in tube B by 1 unit length must be supplemented by 1 unit length drop of pressure head above tube B because the hydraulic head at the base of the tube B does not change with time as long as the stream water level remains the same. One also notes that the pressure head above tube B is the same as the pressure head above tube A because the whole air body inside the

manometer has the same pressure and pressure head. Thus the pressure head above tube A will drop 1 unit length as well if the pressure head above tube B drops by 1 unit length. As the total hydraulic head inside the seepage bell is the summation of the water level in tube A and the pressure head above tube A, thus 1 unit length drop in tube A combined with 1 unit length drop of pressure head above tube A will lead to a total of 2 unit lengths drop of hydraulic head inside the seepage bell. Therefore, the rate of hydraulic head change over time in the seepage bell (V_e) is twice of the rate of water level drop in tube A (or water level rise in tube B) over time (V_s). We have to emphasize that equation (2.1) is based on a constant air volume but variable air pressure inside the manometer, which is not physically true.

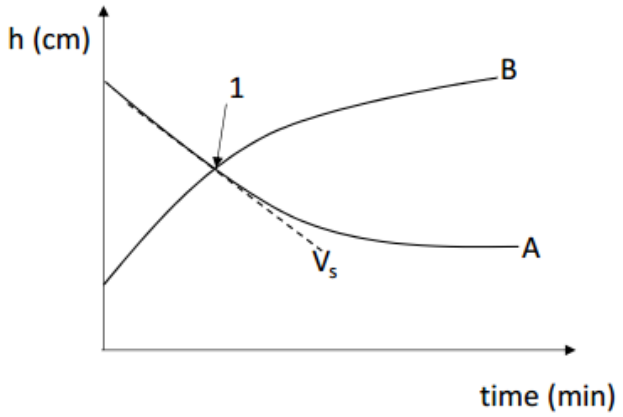

Figure 2. 3 Example of water levels in manometer tube A and tube B versus time. Point 1 is the intersection of curve A and curve B which represents tube A water level equals the tube B water level and the seepage rate inside the seepage bell (V_b) will be equal to the seepage rate outside the seepage bell (V_e) at this point. (Peng and Zhan, 2017)

2.3 Improvement of interpretation considering air compressibility

A careful check of the above-mentioned B&R seepage meter and equation (2.1) indicates that the air inside the manometer is assumed to be incompressible during the entire duration of

experiment. The validity of such an assumption has never been rigorously checked, as far as we know. We question the validity of such an assumption based on the following observation. As the water level in tube A declines, the air pressure inside the manometer decreases and the volume of air increases. Therefore, the increase of the water level in tube B should be smaller than the decrease of the water level in tube A. This difference will generate an error when estimating the total seepage flux using equation (2.1).

Here, we present a correction considering air compressibility as follows:

$$V_e' = \frac{2+\kappa}{1+\kappa} V_s, \tag{2.2}$$

where V_e' is the modified vertical seepage flux rate at the streambed considering the air compressibility effect and

$$\kappa = \frac{2H - h_A - h_B}{(P_0 / \rho g) - h_B}, \tag{2.3}$$

where the atmospheric air pressure above the stream water surface is noted as P_0 (101.3 kPa) and can be corrected for the topographical elevation at the stream, ρ is water density (998.2 kg/m^3 at 20 ° C), g is acceleration constant (9.81 m/s^2), the height of manometer is H, and the bottom of the manometer is set at the stream water surface. Detailed derivation of equations (2.2)-(2.3) is provided in the Appendix A.

Equation (2.3) can be rewritten into:

$$\kappa = \frac{(P_0 - \rho g h_B)(2H - h_A - h_B)}{(P_0 - \rho g h_B)[(P_0 / \rho g) - h_B]} = \frac{\rho g (P_0 - \rho g h_B)(2H - h_A - h_B)}{(P_0 - \rho g h_B)^2} = \frac{C'}{(P_0 - \rho g h_B)^2}, \tag{2.4}$$

where the numerator is a constant based on Boyle's ideal gas law and denoted as C' (See Appendix A equation (A10)). During an experiment, h_B increases with time so the κ value increases with time as well. The value of the denominator in equation (2.4) is mainly controlled

by P_0 since $\rho g h_B$ is usually considerably smaller than P_0 as the typical h_B value is within 0.5 m. For an experimental case with H of 0.8 m, h_A of 0.3 m and h_B of 0 m at the initial state, the κ value is calculated to be 0.126. At point 1 in Figure 2.3, h_A and h_B are both equal to 0.15 m, and the κ value is calculated to be 0.128. From this example, one can see that the κ value only increases slightly over the entire measurement duration. Therefore, one may treat the κ value as approximately constant.

2.4 Comparison of equation (2.2) with equation (2.1)

The relative error is commonly defined as "(true value - approximate value)/true value" (Burden and Faires, 2010). Comparing equation (2.2) (the corrected method) with equation (2.1), we define a relative correction factor, denoted as α, due to air compressibility as:

$$\alpha = \frac{V_e' - V_e}{V_e'} = -\frac{\kappa}{2+\kappa} \quad (5)$$

The α value can be regarded as a relative error associated with the use of equation (2.1) for neglecting the effect of air compressibility. The magnitude of the α value will increase when κ increases. The negative sign on the right side of equation (2.5) means that the seepage rate from the corrected method is smaller than that from the old method. In other words, the seepage rate will be overestimated if the air compressibility effect is not taken into consideration.

As an example, we have calculated the α value for one set of experiments based on the data from Wang et al. (2014), noted as cases 1-4 in Table 2.1, while cases 5-6 in Table 2.1 are hypothetical cases without suction. Cases 1-4 have the same manometer heights of 0.8 m and are operated under the suction mode. The setups for cases 5 and 1 are identical except that case 5 and case 1 are operated under no-suction and suction modes, respectively. The setups for cases 5 and 6 are identical except that case 6 has a larger manometer height of 1.5 m.

Table 2. 1 Relative correction calculation results.

Case No.	h_A(m)	h_B(m)	H(m)	κ value (-)	α value (-)
1	0.35	0.15	0.8	0.108	5.12%
2	0.45	0.36	0.8	0.079	3.81%
3	0.64	0.56	0.8	0.041	2.00%
4	0.51	0.39	0.8	0.071	3.40%
5	0.20	0.00	0.8	0.136	6.34%
6	0.20	0.00	1.5	0.272	11.92%

Note: cases 1-4 are from Wang et al. (2014) with suction, while cases 5-6 are hypothetical cases without suction. (Peng and Zhan, 2017)

We can use equation (2.3) to calculate the κ value, and then use equation (2.5) to calculate the α value. One can see that the α values are between 2.00% (for case 3) to 5.12% (for case 1), but they are much larger for cases 5 and 6 with the α values of 6.34% and 11.92%, respectively.

Case 5 shows that if the manometer height is 0.8 m and no suction is applied, the α value will be as high as 6.34%. Case 6 shows that if manometer height is increased from 0.8 m to 1.5 m without applying any suction, the α value will increase from 6.34% to 11.92%. A manometer length of 1.5 m or more may be required where the streambed is less permeable, such as when larger percentages of clay and silt are present.

From the above analysis, one can see that equation (2.1) (without considering the air compressibility) may be appropriate for cases 1-4 (with suction) as the relative errors are usually around or less than 5%. However, for the zero-suction cases 5 and 6, equation (2.2) should be used because the relative errors associated with use of equation (2.1) would be as large as

11.92%. A larger manometer height will lead to an even larger discrepancy between equations (2.1) and (2.2).

Wang et al. (2014) stated that the actual water levels in the manometer was arbitrary. This implies that the amount of air removed from the manometer, including zero air removal for the zero-suction mode, is site dependent. For a particular site, one may have to try multiple tests with different amounts of suction or no-suction at all to find an optimal measurement. In general, a larger degree of suction will lead to smaller air masses in tube A and tube B, and thus a smaller air compressibility effect eventually. In this regard, suction is recommended if one wants to limit the air compressibility effect in the measurement.

We do not consider the temperature effect in this study. If temperature is found to change considerably during the experiment, its effect on air compressibility may have to be taken into account, which is a subject out of the scope of this study, but certainly deserves further investigation.

2.5 Conclusions

In this study, we provided a correction for calculating the seepage flux rate that includes consideration of air compressibility inside the manometer of a B&R seepage meter. Previous works of Bouwer and Rice (1963) and Wang et al. (2014) excluded the effect of air compressibility. We calculated the error for ignoring the air compressibility in experiments of Wang et al. (2014) for the suction mode, and extended the calculation for two more cases for the no-suction mode. The following conclusions can be drawn:

1. The effect of air compressibility in the manometer increases with the volume of air in the manometer. Applying suction to the manometer reduces the air compressibility effect and is preferred.
2. The relative error (α) associated with neglecting the air compressibility can be kept around 5% if the manometer height is shorter than 0.8 m and suction is applied. For manometers longer than 0.8 m, the relative error will be larger than 5% and it may become over 10% if the manometer height is longer than 1.5 m and no suction is applied.
3. The correction of this study will work as a quantitative tool to determine if air compressibility can be neglected or not for a B&R seepage meter test with and without suction applied.

3. BASEFLOW RECESSION IN AN UNSATURATED-SATURATED ZONE WITH A STREAMBED

3.1 Introduction

Baseflow refers to water that entering a stream from a groundwater reservoir with very slow varying rates (Hall, 1968; Sophocleous, 2002). It plays a crucial role in providing water recharge to streams. Baseflow recession is the process that baseflow flux to the stream decreases with time when there is a lack of groundwater recharge (Freeze and Cherry, 1979; Domenico and Schwartz, 1998; Fetter, 2001). Information of the baseflow recession can provide hydraulic properties of the aquifer in a watershed scale (Brutsaert and Nieber, 1977; Brutsaert and Lopez, 1998). Brutsaert and Nieber (1977) proposed a low stream flow analysis procedure and related the baseflow recession process with aquifer characteristics. They suggested that the temporal changing rate of discharge $\frac{dQ}{dt}$ was a function of discharge Q itself. One of the simplest models is in the form of a power function, i.e., $\frac{dQ}{dt} = -aQ^b$, where a and b are constants. Since then, this power-law function model has been widely used to determine aquifer parameters in a watershed scale (Brutsaert and Lopez, 1998; Szilagyi et al., 1998; Rupp and Selker, 2005; Pauwels and Troch, 2010).

Zlotnik and Huang (1999) proposed an analytical model to assess the impact of stream shallow penetration and low-permeability streambed sediments on head responses. They ignored the effect of the unsaturated flow process, as commonly done by other similar studies as well (Huang et al., 2010; Huang et al., 2012), apparently for the sake of simplifying the problem. Hilberts et al. (2005) considered the unsaturated-saturated zone interaction and proposed an analytical expression for the specific yield that is dependent on the water table and the retention

capacity of the unsaturated zone using the van Genuchten (1980) model. However, the horizontal flux in the unsaturated zone is ignored in Hilberts et al. (2005). Kong et al. (2016) showed that it was necessary to consider unsaturated flow process to improve the accuracy of predicting groundwater flux rates in hillslope drainage processes. Liang et al. (2017) constructed a new model containing the unsaturated lateral flow along with the unsaturated vertical flow and is the newest one with unsaturated-saturated zone coupling for the baseflow study. But Liang et al. (2017) did not consider the low-permeability streambed that may affect the stream-aquifer interaction profoundly. Since most baseflow studies have not considered the unsaturated-saturated zone interaction with the presence of a streambed, we decided to fill this knowledge gap with the purpose to understand how important the impact of a streambed is on baseflow. We have two specific objectives here. The first is to quantify the streambed effect on the overall unsaturated and saturated flow processes. The second is to quantify the streambed effect on stream hydrographs during baseflow recession. To serve this purpose, we will build a two-dimensional (2D) model that contains both unsaturated-saturated flow processes and a streambed structure.

To achieve the above mentioned objectives, it is crucial to have a geologically based streambed conceptual model, a nontrivial task in many occasions, as the stream geomorphology is dynamic, and the streambed keeps changing with time and space (Hatch et al., 2010). Kalbus et al. (2009) stated that the variation of groundwater discharge to a stream is closely related to the heterogeneous properties of aquifer and streambed permeability. Sebok et al. (2015) showed the complexity of streambed structure which may have multiple layers with different grain sizes of sand, gravel, and organic layers that hindering groundwater discharge. Such complexities regarding streambed geomorphology will not be taken into account in this study because of a few

considerations. First, this study is the first attempt ever to include the interaction of streambed with saturated-unsaturated flow processes. Therefore, we like to start with a simple streambed model first and to use the established new model and associated solutions as benchmarks or references for further investigation considering more complex forms of streambed geomorphology in the future. Second, up to the present, there is still not a commonly accepted concept model to describe the spatiotemporally variable, heterogeneous streambed. Therefore, in this article, the streambed is represented by a thin lower-permeability layer with a uniform thickness.

The structure of this paper includes four parts. First, we will build a 2D mathematical model and derive the hydraulic head responses in both unsaturated and saturated zones. We will further test the new solution against a finite element numerical simulation using COMSOL Multiphysics. Second, we will compare the new solution against a previous model of Liang et al. (2017) which excluded the streambed effect. Third, we will analyze the effect of low-permeability streambed on baseflow and baseflow recession within a coupled saturated and unsaturated flow system. Fourth, we will conduct a sensitivity analysis of the new model to identify the important controlling parameters of the model. At last, we will also outline a few research directions in the future on the basis of this study, with the ultimate goal of understanding the complex streambed geomorphology impact on baseflow and baseflow recession.

3.2 Mathematical model

A 2D cross-sectional model of coupled saturated and unsaturated flow to a stream in a watershed is schematically shown in Figure 3.1. A low-permeability streambed with a uniform thickness and a constant hydraulic conductivity is presented. The hydraulic conductivity of the

streambed is much less (at least two orders of magnitude smaller) than the hydraulic conductivity of the aquifer. The aquifer is homogeneous and anisotropic in both saturated and unsaturated zones. The streambed thickness is small compared to aquifer length and assumed to be homogeneous and isotropic. The aquifer is fully penetrated by a stream.

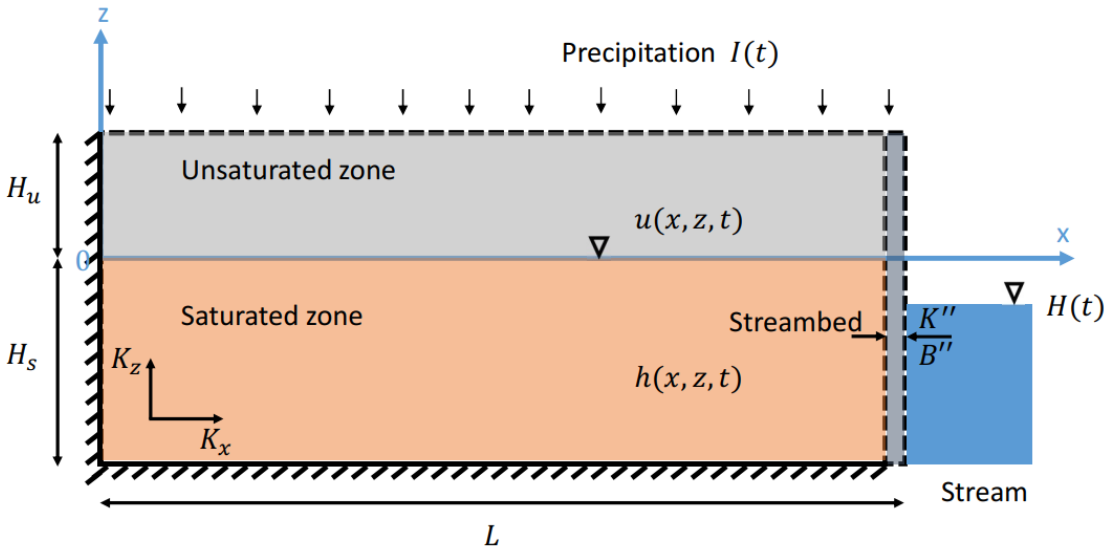

Figure 3. 1 The diagram of the baseflow model with a low-hydraulic conductivity streambed in a watershed, considering the coupled unsaturated and saturated flow processes.

The x-axis is horizontal and z-axis is vertically upward. The left side boundary ($x = 0$) represents the water divide (no flow boundary). The right side boundary ($x = L$) represents the streambed. Because the L represents the distance from the water divide to the stream channel, for a watershed, $2L$ then will be the watershed area divided by the total length of upstream channels. The streambed hydraulic conductivity is K'' and streambed thickness is B''. The initial water table is at $z = 0$. So the origin is set at the intercept of the initial water table with the left water

divide. The stream stage is dependent on time and is described as a function of $H(t)$. The unsaturated zone extends from $z = 0$ to $z = H_u$, and the saturated zone extends from $z = -H_s$ to $z = 0$. The saturated horizontal and vertical hydraulic conductivities are K_x and K_z, respectively. The base of the aquifer is impermeable. The top of the aquifer is the flat ground surface which has a second-kind flow boundary condition with a prescribed, spatially uniform but temporally variable downward flux $I(t)$. One may regard $I(t)$ as the net downward infiltration rate just below the ground surface. Topographic variation of the ground surface is likely to exist in the real world setting but is not considered here for the sake of simplicity. The topographic effect should be considered in a future study on the basis of this investigation.

After describing the conceptual model for a 2D cross-sectional flow, the governing equation for the saturated zone $-H_s \leq z \leq 0$ follows:

$$K_x \frac{\partial^2 h}{\partial x^2} + K_z \frac{\partial^2 h}{\partial z^2} = S_s \frac{\partial h}{\partial t}, \quad (3.1a)$$

$$h(x, z, 0) = 0, \quad (3.1b)$$

$$\frac{\partial h}{\partial x}(x, z, t)|_{x=0} = 0, \quad (3.1c)$$

$$\frac{K''(h(L,z,t)-H(t))}{B''} = -K_x \frac{\partial h}{\partial x}(x, z, t)|_{x=L}, \quad (3.1d)$$

$$\frac{\partial h}{\partial z}(x, z, t)|_{z=-H_s} = 0, \quad (3.1e)$$

where h is the hydraulic head in the saturated zone [L]; S_s is the specific storage [L^{-1}]; t is time [T]; H_s is the initial thickness of the saturated zone [L]; L is the distance from the water divide to the stream [L]; $H(t)$ is the time-dependent stream water level [L]. Other symbols have been explained above.

Equation (3.1a) is the general governing equation of flow in an unconfined aquifer. Equation (3.1b) is the initial condition of hydraulic head in the saturated zone. Equation (3.1c) is

the left boundary condition representing the water divide. Equation (3.1d) is the right boundary condition describing the aquifer-streambed-stream system. We choose the third type boundary condition described by Equation (3.1d) for the following reasons: first, the streambed is very thin and therefore has a negligible storage effect; second, flow in the streambed is horizontal, i.e., it is perpendicular with the aquifer-streambed interface (vertical). This is because the contrast of hydraulic conductivities of the streambed and the aquifer is significant (more than two orders of magnitude), thus flow in the low-permeability streambed is nearly perpendicular with the vertical aquifer-streambed interface, a principle sometimes called the law of refraction of flow in many hydrogeology textbooks (Freeze and Cherry, 1979; Domenico and Schwartz, 1998; Fetter, 2001). Equation (3.1e) is the no-flow lower boundary condition, which represents the impermeable aquifer bottom.

In the unsaturated zone $0 \le z \le H_u$, flow induced by infiltrations is governed by Richards' equation. However, it is difficult to directly solve Richards' equation without making approximations. Here, we propose to use the linearized method developed by Kroszynski and Dagan (1975). The linearized 2D unsaturated flow equation can be written as follows,

$$k_0(z)K_x\frac{\partial^2 u}{\partial x^2} + K_z\frac{\partial}{\partial z}\left(k_0(z)\frac{\partial u}{\partial z}\right) = C_0(z)\frac{\partial u}{\partial t}, \tag{3.2a}$$

$$u(x,z,0) = 0, \tag{3.2b}$$

$$\frac{\partial u}{\partial x}(x,z,t)|_{x=0} = 0, \tag{3.2c}$$

$$\frac{K''(u(L,z,t)-H(t))}{B''} = -K_x\frac{\partial u}{\partial x}(x,z,t)|_{x=L}\,, \tag{3.2d}$$

$$K_z k_0(z)\frac{\partial u}{\partial z}(x,z,t)|_{z=H_u} = I(t), \tag{3.2e}$$

where u is the hydraulic head in the unsaturated zone [L], $k_0(z)$ is the zero-order approximation of the relative hydraulic conductivity [-], $C_0(z)$ is the zero-order approximation of the soil

moisture capacity [L^{-1}] at the initial water content of θ_0. $k_0(z) = k(\theta_0)$ and $C_0(z) = C(\theta_0)$; k ($0 \leq k \leq 1$) and $C(\geq 0)$ are the relative hydraulic conductivity [-] and specific moisture capacity [L^{-1}], respectively, at an arbitrary water content of θ; H_u is the initial thickness of the unsaturated zone [L]. One notable point is that the saturated hydraulic conductivity of the unsaturated zone is the same as its counterpart of the saturated zone. Equation (3.2b) is the initial condition of hydraulic head in the unsaturated zone. Equation (3.2c) is the left boundary condition representing the water divide. Equation (3.2d) is the right boundary condition. Equation (3.2e) is the upper boundary at the flat ground surface. There are several reasons about why we chose Equation (3.2d) for the right boundary condition. We assume the water movement is horizontal in the low-permeability layer. The right side of low-permeability layer is considered as an equipotential surface. Figure 3.2 shows the assumed conceptual model near the low-permeability layer. Because the low-permeability layer is thin, the water flow inside the low-permeability layer is horizontal. As soon as water moves out to the right side boundary, water will go to the stream without head loss (frictionless flow). In this way, the right side boundary can be an equipotential surface.

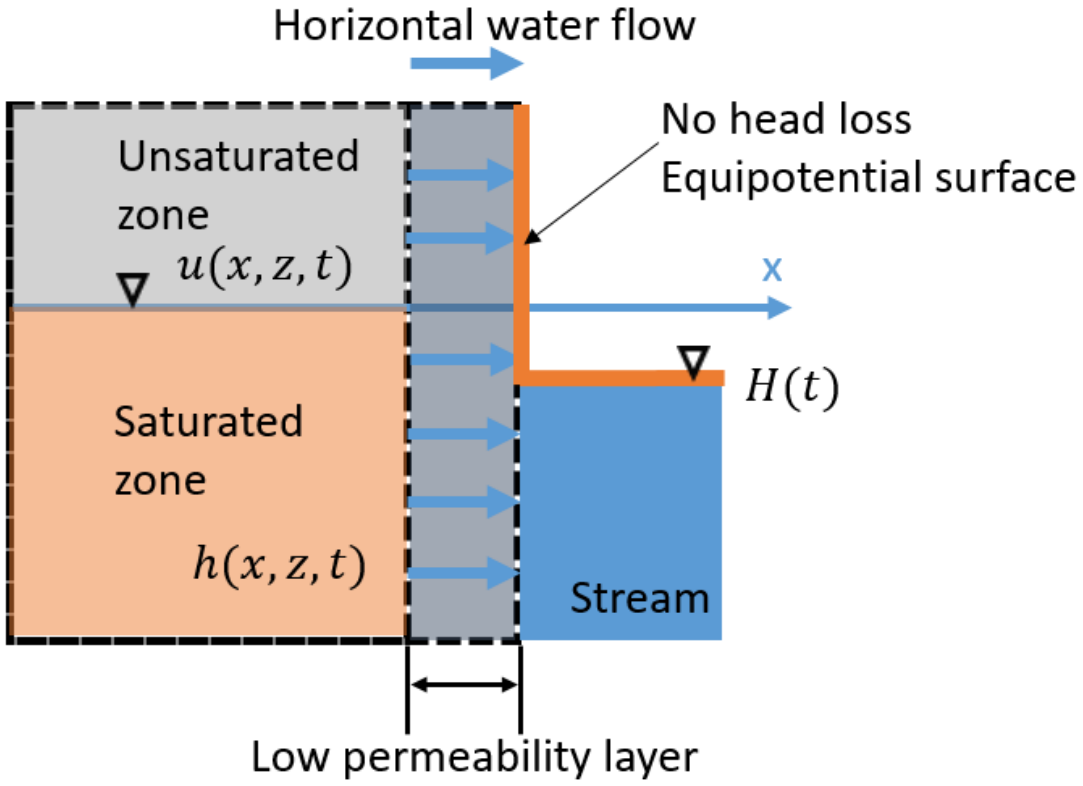

Figure 3. 2 The zoom in picture of the concept model near the low-permeability streambed.

To deal with $k_0(z)$ and $C_0(z)$ in Equation (3.2a), many previous researchers have used the Gardner (1958) exponential constitutive model for the unsaturated zone (Gardner, 1958; Kroszynski and Dagan, 1975; Tartakovsky and Neuman, 2007; Liang et al., 2017). The model is shown as follows:

$$k_0(z) = e^{-\kappa z}, \tag{3.2f}$$

$$C_0(z) = S_y \kappa e^{-\kappa z}, \tag{3.2g}$$

where $\kappa > 0$ is a constitutive exponent that describes the unsaturated zone medium properties [L^{-1}], S_y is the specific yield or drainable porosity [-]. We have to point out that the choice of the

Gardner (1958) exponential model is simply for the purpose of facilitating analytical treatment of the problem. If one decides to solve the problem numerically, then one is free to choose any other types of constitutive model, such as the Brooks and Corey (1966) model or the van Genuchten (1980) model. Nevertheless, the use of the Gardner (1958) exponential model here is to demonstrate the methodology in an analytical framework. In the future, it will be useful to check if the methodology and conclusions of this study still hold or not if a different constitutive model is used.

The continuous boundary condition at the saturated-unsaturated interface is as follows:

$$h(x,0,t) - u(x,0,t) = 0, \tag{3.3a}$$

$$\frac{\partial h}{\partial z}(x,0,t) - \frac{\partial u}{\partial z}(x,0,t) = 0. \tag{3.3b}$$

Base on the equation groups of (3.1a)-(3.3b), we can get the semi-analytic solution for the hydraulic head distribution in both unsaturated and saturated zones, provided that the change of hydraulic head in the saturated zone is relatively small as compared to the initial saturated thickness. After that, one can calculate the baseflow fluxes per unit width along the river in the saturated zone Q_s and unsaturated zone Q_u as:

$$Q_s(t) = \int_{-H_s}^{0} \left(-K_x \frac{\partial h}{\partial x}(x,z,t)|_{x=L}\right) dz, \tag{3.4a}$$

$$Q_u(t) = \int_{0}^{H_u} \left(-K_x k_0(z) \frac{\partial u}{\partial x}(x,z,t)|_{x=L}\right) dz\,. \tag{3.4b}$$

Total discharge rate per unit width along the river $Q(t)$ is the sum of discharge rates in the unsaturated and saturated zones.

$$Q(t) = Q_s(t) + Q_u(t). \tag{3.4c}$$

3.3 Semi-analytical solution

We prefer to solve the mathematical model in a dimensionless format. Nondimensionlization can reduce the number of parameters involved in the mathematical model

and can recover some characteristic properties that are key controls of the dynamic system. We have obtained a new semi-analytical solution in dimensionless form and the dimensionless variables are referred to subscript "*D*" which are defined in Table 3.1. $K_D, \kappa_D, \beta, \alpha, K_{LD}$ are dimensionless parameters describing the aquifer. Specifically, K_D is the anisotropy ratio defined as the ratio of K_x to K_z. κ_D and β are two dimensionless constitutive exponents. κ_D is related to the unsaturated zone influence to the flow. β is associated with the ratio of maximum soil moisture capacity C_0 and specific storativity S_s. K_{LD} is the ratio of hydraulic conductance of aquifer over that of streambed for horizontal flow, where the hydraulic conductance is defined as the ratio of hydraulic conductivity [LT^{-1}] over distance of flow [L]. K_{LD} is a key dimensionless parameter reflecting the streambed effect, and is called the "streambed index" hereinafter.

In Laplace domain, we have the semi-analytical solution as:

$$\bar{h}_D(x_D, z_D, p) = \bar{H}_D(p) + \sum_{n=0}^{\infty}\left[C_1\, exp(-\Omega_n z_D) + C_2\, exp(\Omega_n z_D) - \frac{A_n p\, sin(\omega_n)\bar{H}_D}{(\omega_n^2+p)\omega_n}\right] A_n\, cos(\omega_n x_D), \quad (3.5a)$$

$$\bar{u}_D(x_D, z_D, p) = \bar{H}_D(p) + \sum_{n=0}^{\infty}\left[C_3\, exp(M z_D) + C_4\, exp(N z_D) - \frac{p\beta \bar{H}_D(p) A_n sin\omega_n}{(\omega_n^2+p\beta)\omega_n}\right] A_n\, cos(\omega_n x_D), \quad (3.5b)$$

$$\bar{Q}_{sD}(p) = \sum_{n=0}^{\infty}\left[C_2 - C_1 + C_1\, exp(\Omega_n H_{sD}) - C_2\, exp(-\Omega_n H_{sD}) - \frac{A_n p\, sin(\omega_n)\bar{H}_D H_{sD}}{K_D \Omega_n \omega_n}\right] \frac{\omega_n sin(\omega_n)}{\Omega_n} A_n \ , \quad (3.6a)$$

$$\bar{Q}_{uD}(p) = \sum_{n=0}^{\infty}\left[-\frac{C_3}{M-\kappa_D} - \frac{C_4}{N-\kappa_D} + \frac{C_3\, exp\left((M-\kappa_D)H_{uD}\right)}{M-\kappa_D} + \frac{C_4\, exp\left((N-\kappa_D)H_{uD}\right)}{N-\kappa_D} + (exp(-\kappa_D H_{uD}) - 1)\frac{A_n p\beta\, sin(\omega_n)\bar{H}_D}{K_D \Psi_n^2 \kappa_D \omega_n}\right] \omega_n sin(\omega_n)\, A_n \ , \quad (3.6b)$$

where the overhead bar stands for Laplace domain and the subscript "*D*" refers to the dimensionless variable, *p* is the Laplace transform parameter in respect to the dimensionless time defined in Table 3.1. The detailed derivation of the solution is presented in Appendix B. Since the closed-form analytical inverse Laplace transform is difficult to execute, a numerical inverse Laplace transform method is implemented to obtain the real time solution. The numerical inverse Laplace transform technique chosen here is the de Hoog et al. (1982) algorithm, which is based on accelerating the convergence of the Fourier series for calculation. A MATLAB script file to facilitate numerical inverse Laplace transform was modified from Hollenbeck (1998) and has a better overall accuracy than other numerical inverse Laplace transform methods (Liang et al., 2017).

Table 3. 1 The dimensionless variables.

$h_D = \frac{h}{H_s}$	$t_D = \frac{K_x}{S_s L^2} t$
$x_D = \frac{x}{L}$	$z_D = \frac{z}{L}$
$K_D = \frac{K_z}{K_x}$	$H_{sD} = \frac{H_s}{L}$
$H_{uD} = \frac{H_u}{L}$	$H_D = \frac{H}{H_s}$
$u_D = \frac{u}{H_s}$	$\kappa_D = \kappa L$
$\beta = \frac{\kappa s_y}{S_s}$	$\alpha = H_{sD} \exp(-\kappa_D H_{uD})$
$I_D = \frac{I}{K_z}$	$K_{LD} = \frac{K_x B''}{K'' L}$
$Q_{sD} = \frac{Q_s}{K_x H_s}$	$Q_{uD} = \frac{Q_u}{K_x H_s}$

3.4 Validation through COMSOL Multiphysics numerical simulation

To check the solution robustness, we use COMSOL Multiphysics (COMSOL Inc., Burlington, MA, USA) to solve Equations (3.1)-(3.3). Then we compare the new semi-analytical solution with the numerical solution under a streambed index $K_{LD} = 0.1$. The parameters used for simulation are given in Table 3.2. Those parameters are from the previous study by Liang et al. (2017).

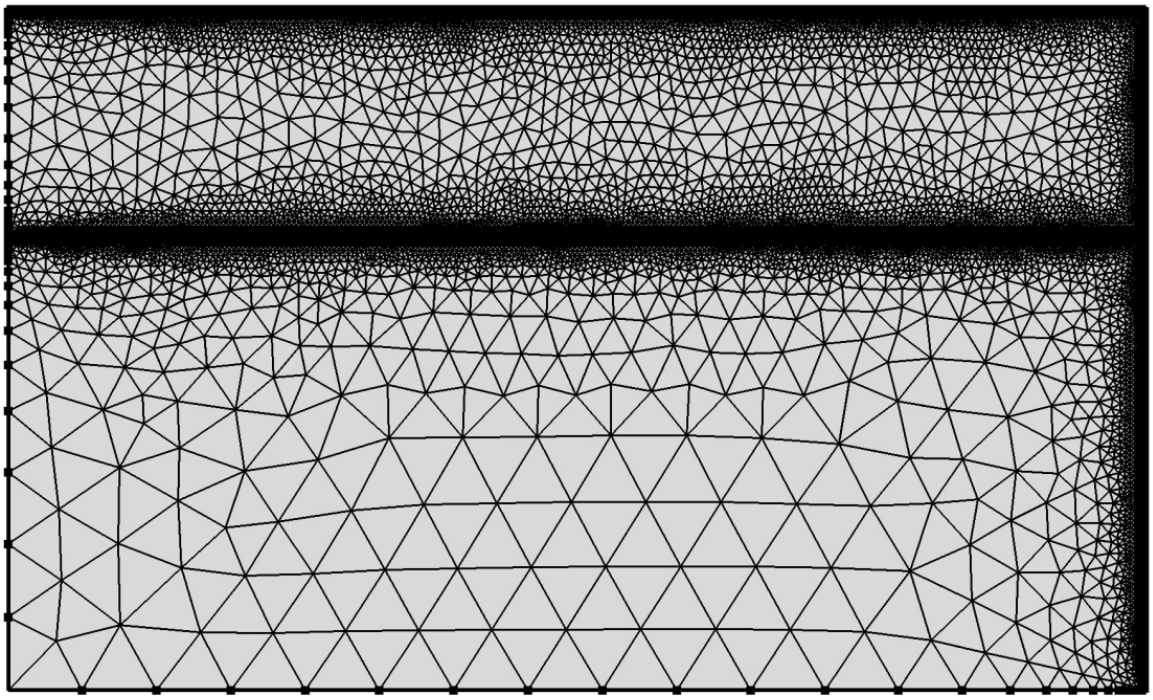

Figure 3. 3 Mesh plot for present model in the finite element simulation using COMSOL Multiphysics.

Figure 3.3 shows the mesh plot for the model. We can see that the elements near the water table and boundaries are refined to reduce numerical errors. The number of triangular elements is 23086. The average element quality is 0.8419, which is good for simulation accuracy. In general, if the average element quality is below 0.1, it is considered as a poor mesh which then has to be redesigned to achieve an average element quality above 0.1. Numerical exercises demonstrate that the mesh used here is sufficiently fine so that additional elements do not impact the results of the simulation.

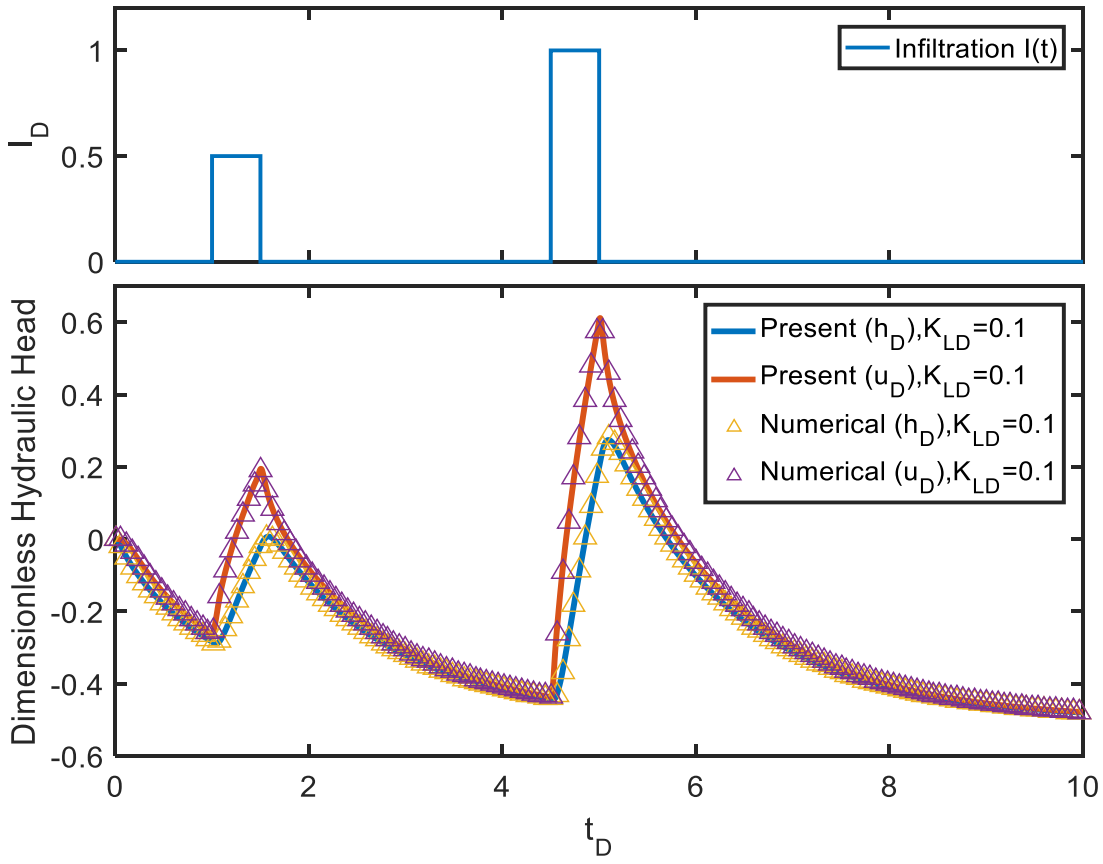

Figure 3. 4 Comparison between the numerical simulation from COMSOL Multiphysics and the present solution.

Table 3. 2 Simulation parameters

$K_D = 1.0$	$H_{sD} = 0.4$
$H_{uD} = 0.2$	$H_D = -0.5$
$K_{LD} = \frac{K_x B''}{K'' L} = 0.1$	$\kappa_D = 10$
$\beta = 10$	$I_D = \begin{cases} 0.5 & \text{when } 1.0 < \mathrm{t_D} < 1.5 \\ 1.0 & when\ 4.5 < t_D < 5.0 \\ 0 & otherwise \end{cases}$

The simulation time step is $\Delta t_D = 0.01$, and the total number of time steps is 1000, with a total simulation time of $t_D = 10$. The observation point is at ($x_D = 0.5, z_D = 0.1$) for unsaturated zone (u_D) and ($x_D = 0.5, z_D = -0.1$) for saturated zone (h_D). The results are shown in Figure 3.4, from which we can see that the semi-analytical solution fits very well with the numerical simulation. We will then compare the present solution with the base case of Liang et al. (2017), which excluded the streambed effect. For convenience, the solution of Liang et al. (2017) will be noted as "Liang solution" hereinafter.

3.5 Results

3.5.1 Effects of streambed on hydraulic head

The parameters used for simulation are the same as in Section 3.4 (see Table 3.2). The results are shown in Figure 3.5. Figure 3.5 reveals the dimensionless hydraulic head changes in both saturated and unsaturated zones after two infiltration events. The first infiltration event starts at t_D = 1 and ends at t_D = 1.5 with a constant rate of I_D=0.5. The second infiltration event starts at t_D = 4.5 and ends at t_D = 5 with a constant rate of I_D=1. The first infiltration event has a lower amplitude and represents a light precipitation event. The second infiltration event has a higher amplitude and represents a heavy precipitation event. The choice of these two events

provides us the ability to study the responses in the unsaturated and saturated zones under different precipitation situations. We use two step functions to describe these two infiltration events.

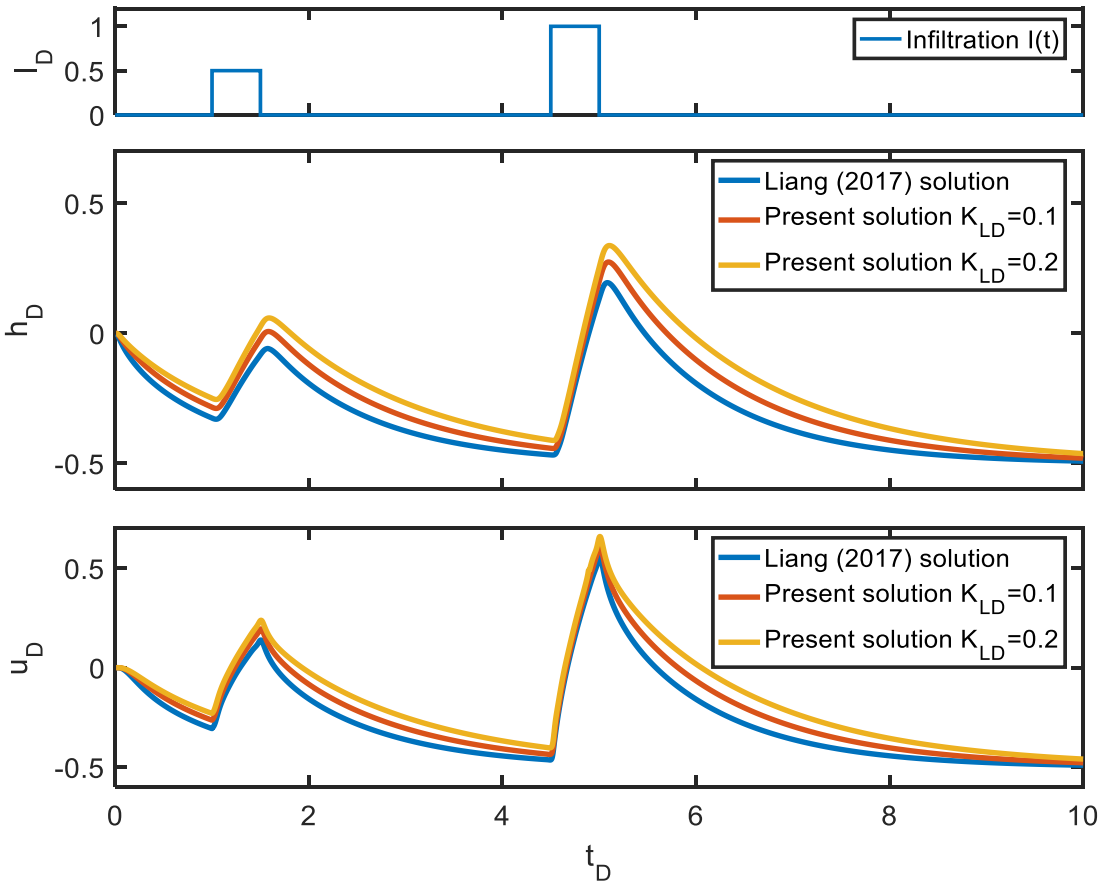

Figure 3. 5 Hydraulic head response in the saturated and unsaturated zones after two infiltration events. The first infiltration event starts at t_D = 1 and ends at t_D = 1.5 with a constant rate of I_D=0.5. The second infiltration event starts at t_D = 4.5 and ends at t_D = 5 with a constant rate of I_D=1.

In the Liang solution, the stream does not have a streambed, or the streambed thickness is zero. So the special case of the present solution with a streambed index $K_{LD} = 0$ is identical to

the Liang solution. First, let us look at the saturated zone hydraulic head responses in Figure 3. If comparing different K_{LD} values in Figure 3.5, we can see that a higher K_{LD} value will lead to a higher hydraulic head response. This means that if the streambed has a lower hydraulic conductance, the hydraulic head response due to an infiltration event is greater. Thus, the hydraulic head solution using the new model of this study is greater than that using the Liang solution. This result agrees with the general understanding that the streambed inhibits the interaction between groundwater and surface water. Hypothetically, if one has an extremely small streambed hydraulic conductance, the interaction between groundwater and surface water could be eliminated completely. So the hydraulic head increase after the infiltration event would be higher.

The K_{LD} value not only affects the peak value, but also affects the decay rate of hydraulic head. The hydraulic head decay curve is much sharper in the unsaturated zone than that in the saturated zone. Figure 3.5 also shows that a higher K_{LD} value results in a slower decay trend of hydraulic head.

3.5.2 Effects of streambed with different unsaturated zone thickness and κ_D value

To study the streambed effect with different unsaturated zone thickness, we fix all parameters except for K_{LD}, H_{uD}, and κ_D. The results of hydraulic head response in the saturated zone are shown in Figures 3.6 and 3.7 when these three parameters vary. From Figures 3.6 and 3.7 we can see that the hydraulic head in the saturated zone responds to streambed and unsaturated zone thickness differently. If we compare the dash plot (higher K_{LD} values) with the solid line plot (lower K_{LD} values) in both figures, we will find that a higher K_{LD} value leads to a higher hydraulic head response in the saturated zone. If we compare the blue color plot (greater H_{uD} values) with the red color plot (lower H_{uD} values) in both figures, we can see that a higher

unsaturated zone H_{uD} value will result in a lower hydraulic head response in the saturated zone during the infiltration event. This is because total infiltration amount is fixed and a thicker unsaturated zone implies that more water will be held by the unsaturated zone, thus less water will move down to recharge the saturated zone. Another interesting point is that when we compare plots with different κ_D values, we can see that the hydraulic head in Figure 3.6 changes more rapidly than that in Figure 3.7. This is because for a larger κ_D value, the saturated zone receives more water from the overlying unsaturated zone, resulting in a higher hydraulic head and a slower decaying rate of hydraulic head in the saturated zone.

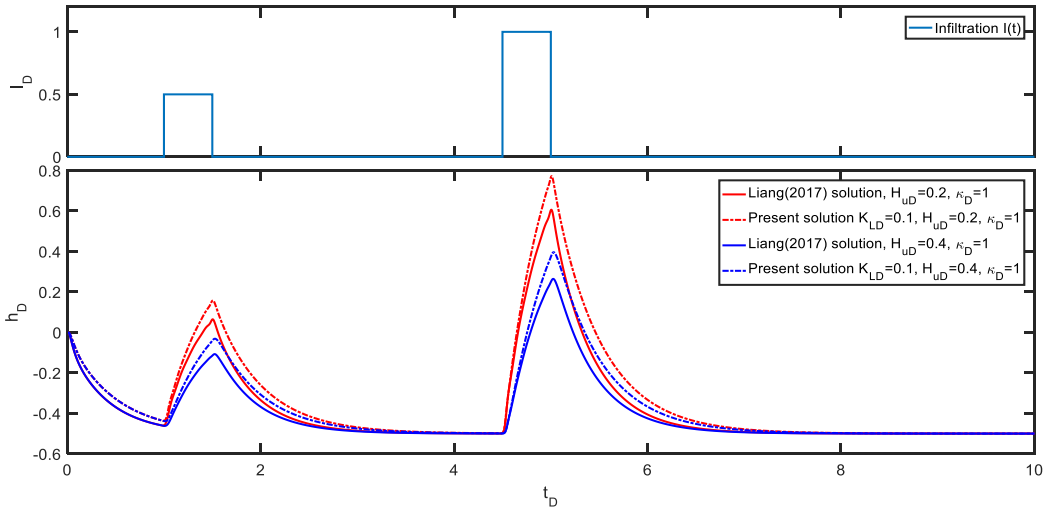

Figure 3. 6 Hydraulic head response in the saturated zone with $\kappa_D = 1$.

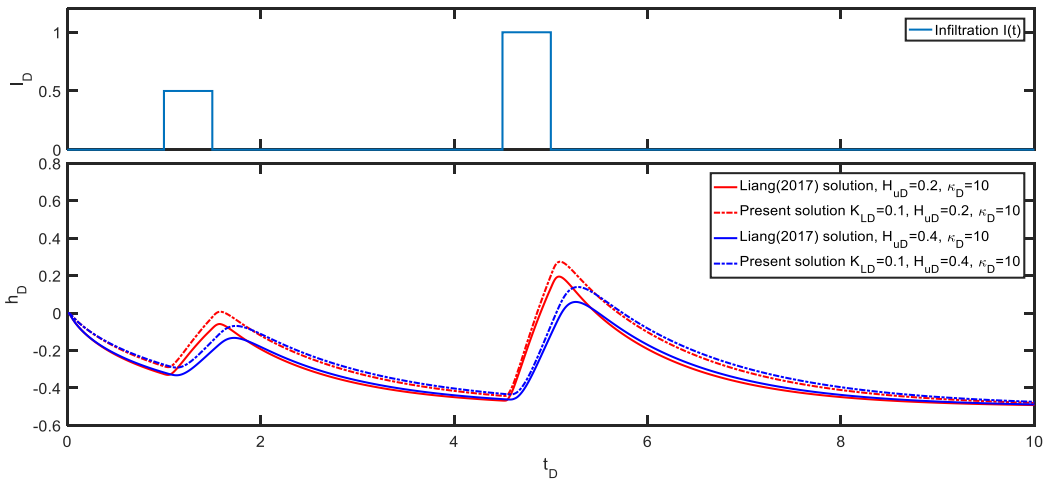

Figure 3. 7 Hydraulic head response in the saturated zone with $\kappa_D = 10$.

3.5.3 Effects of streambed on saturated zone discharge and unsaturated zone discharge

In this portion, the parameters for studying discharge to the stream are the same as in Section 5.1. Figure 3.8 shows the dimensionless discharges from both the saturated and unsaturated zones to the stream. The Liang solution is the blue line while other curves referring to different K_{LD} values equaling to 0.1 and 0.2. The middle diagram in Figure 3.8 shows the saturated zone discharge to the stream, and we observe that the Liang solution (K_{LD}=0) is the curve with the steepest increase response and the fastest decay rate. A higher K_{LD} value leads to a lower peak value of the flux rate and a slower decaying rate. There is a "cross-over" point where the higher K_{LD} value curve intercepts with the lower K_{LD} value curve. This is because the K_{LD} value can only change the groundwater discharge rate to the stream, but not the discharge volume, which is obtained by integrating the discharge rate over time. That is to say, this "cross-over" point works like a balance point between early and late time discharge volumes. The

bottom diagram in Figure 3.8 shows that the unsaturated zone discharge to the stream declines rapidly right after the infiltration event.

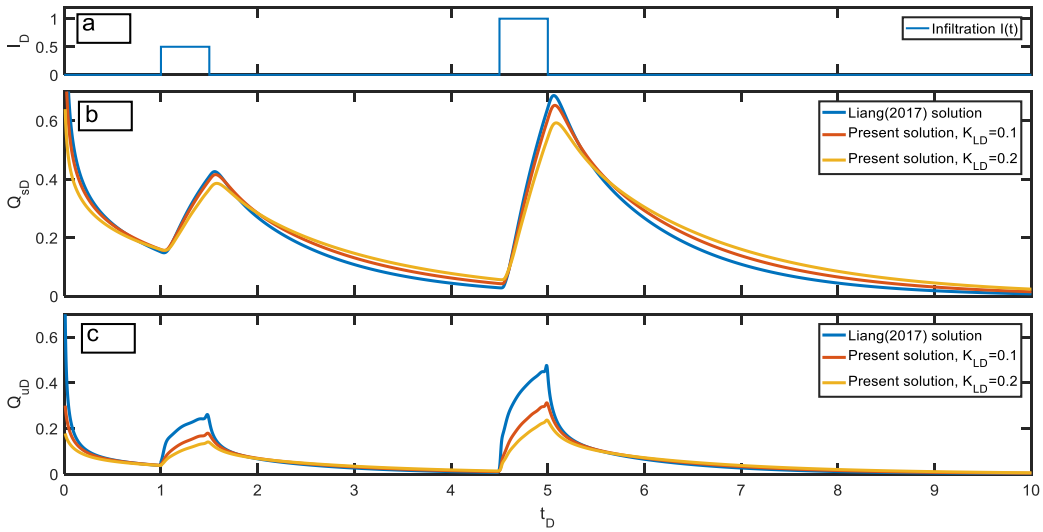

Figure 3. 8 Dimensionless discharge from the saturated zone and unsaturated zone to the stream. a) Infiltration events. b) Dimensionless discharge rate to the stream in the saturated zone. c) Dimensionless discharge rate to the stream in the unsaturated zone.

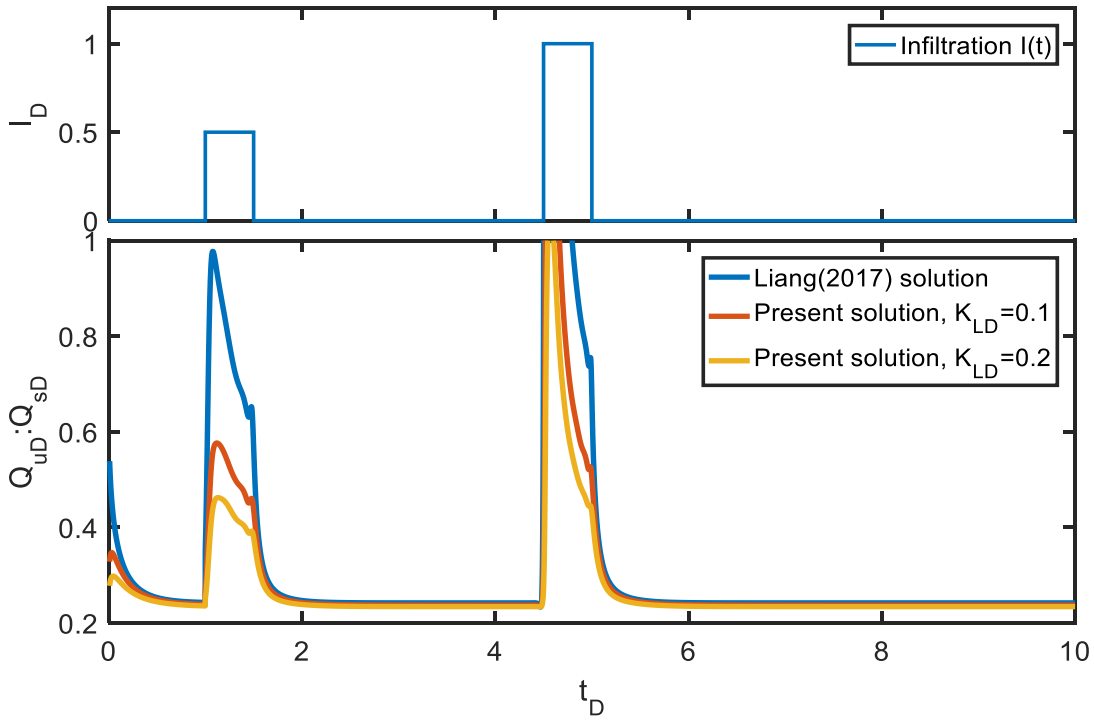

Figure 3. 9 The ratio of unsaturated zone dimensionless discharge to saturated zone dimensionless discharge. The Liang (2017) solution stands for no streambed case. Present solution K_{LD}=0.1 and K_{LD}=0.2 stand for different streambed index cases.

Figure 3.9 shows the ratio of unsaturated zone and saturated zone discharge to the stream. During the infiltration event, the ratio is relatively high. This means that the horizontal flow in the unsaturated zone is significantly large compared to the saturated zone during the infiltration event. After the infiltration event, the ratio drops to a constant ratio about 0.24 in spite of different K_{LD} values. This suggests that the K_{LD} value has much less impact on the ratio of unsaturated zone discharge and the saturated zone discharge after the infiltration event.

Since we want to see the impact of streambed on discharge redistribution, we use the present solution $K_{LD} = 0.1$ to compare with the Liang solution to quantify the difference

between those two solutions at a given time t_D. Figure 3.10 (a) shows the infiltration event, Figure 3.10 (b) shows the difference between $Q_{sD}(K_{LD} = 0.1)$ and $Q_{sD}(K_{LD} = 0)$. Figure 3.10 (c) shows the ratio between $Q_{sD}(K_{LD} = 0.1)$ and $Q_{sD}(K_{LD} = 0)$.

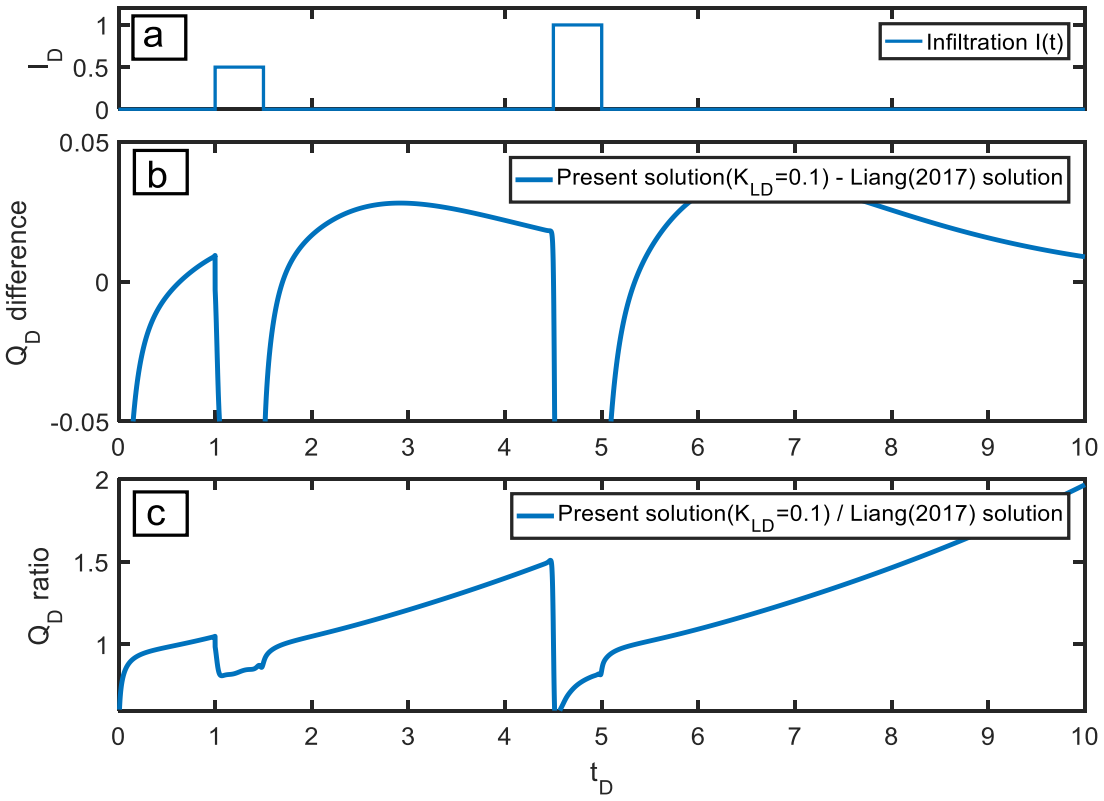

Figure 3. 10 The saturated zone dimensionless discharge difference between no streambed and with streambed. a) Infiltration events. b) Dimensionless discharge difference between K_{LD}=0.1 case and no streambed case. c) Dimensionless discharge ratio between K_{LD}= 0.1 case (present solution) and no streambed case (Liang solution).

Since the two infiltration events are from t_D=1 to t_D=1.5 and t_D=4.5 to t_D=5, we can see that the difference between these two solutions is negative at the initial state of the decaying process from Figure 3.10. Then the difference becomes positive and then declines until the next

infiltration event. However, if we look at the relative discharge ratio curve, we find that the ratio increases monotonically with time between the two infiltration events. The highest ratio will be 2 near $t_D = 10$. This means that the baseflow flux with the presence of a streambed (whose parameters are given in Table 3.2) is nearly twice (200%) of the baseflow flux without a streambed at $t_D = 10$. This finding suggests that streambed can exert significant impact on the late time baseflow.

3.5.4 Effects of streambed on the ratio of horizontal flow and vertical flow

When dealing with flow in an unconfined aquifer, flow in the unsaturated zone above the water table is usually assumed to be primarily vertical, driven by gravitational potential (Freeze and Cherry, 1979; Domenico and Schwartz, 1998; Fetter, 2001). This is found to be not true for the setting of Liang et al. (2017) and this study in which horizontal flow in the unsaturated zone can be as important as the vertical flow. However, up to present, there is no study that precisely quantify the relative importance of horizontal versus vertical flow components in the unsaturated zone and to figure out how is such a ratio varies with space and time. Similarly, conventional theory of flow in the saturated zone mostly concerns the horizontal flow, and treat vertical flow there as a secondary effect. However, such a conventional thinking also appears to be not true for a setting that mimics a watershed aquifer.

To precisely understand the relative importance of horizontal versus vertical flows in a coupled unsaturated and saturated system, we define the ratio between horizontal flow flux and vertical flow flux at a specific location as $\gamma(x_D, z_D, t_D) = \frac{q_x}{q_z} = (K_x \frac{\partial h}{\partial x}) / (K_z \frac{\partial h}{\partial z})$. We have calculated the ratio γ at three different depths: z_D= 0.1 (in the unsaturated zone), z_D= 0 (at free water table surface) and z_D= -0.1 (in the saturated zone). The parameters involved in the calculation are the same as in Section 5.1 (see Table 3.2). Since the ratio γ is a function of x_D, t_D

at a designated depth, we decide to choose three locations to show the changing of γ versus t_D. The three locations are x_D=0.1, 0.5 and 0.9. The reason of choosing these three locations is that they respectively represent far (x_D=0.1), intermediate (x_D=0.5), and close (x_D=0.9) regions from the stream. The results of γ for those three locations in the unsaturated zone (z_D= 0.1), free water table surface (z_D= 0) and saturated zone (z_D= -0.1) are shown in Figure 3. (11-13), respectively.

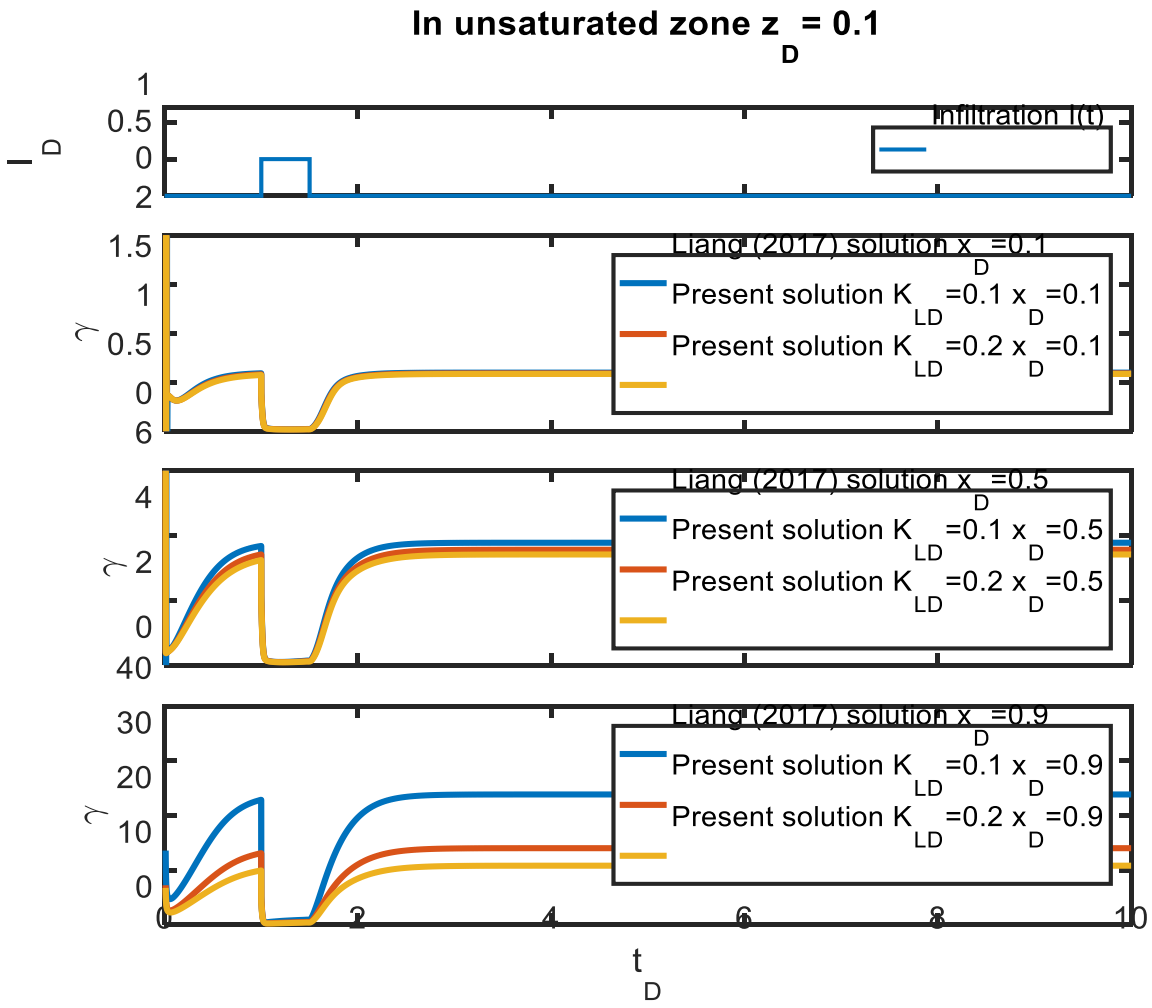

Figure 3. 11 The ratio of horizontal flow versus vertical flow (γ) as a function of time at different locations when z_D= 0.1 (in the unsaturated zone).

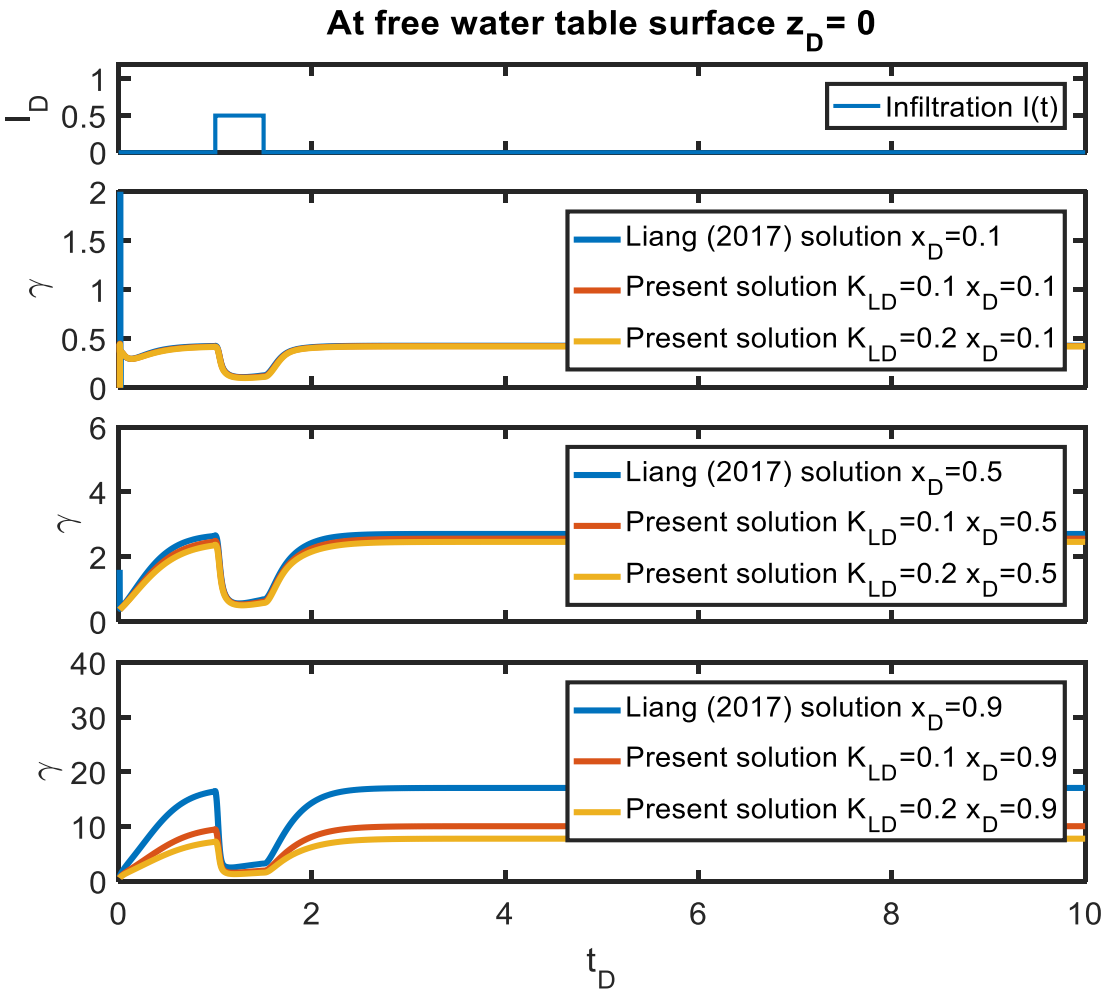

Figure 3. 12 The ratio of horizontal flow versus vertical flow (γ) as a function of time at different locations when z_D= 0 (at free water table surface).

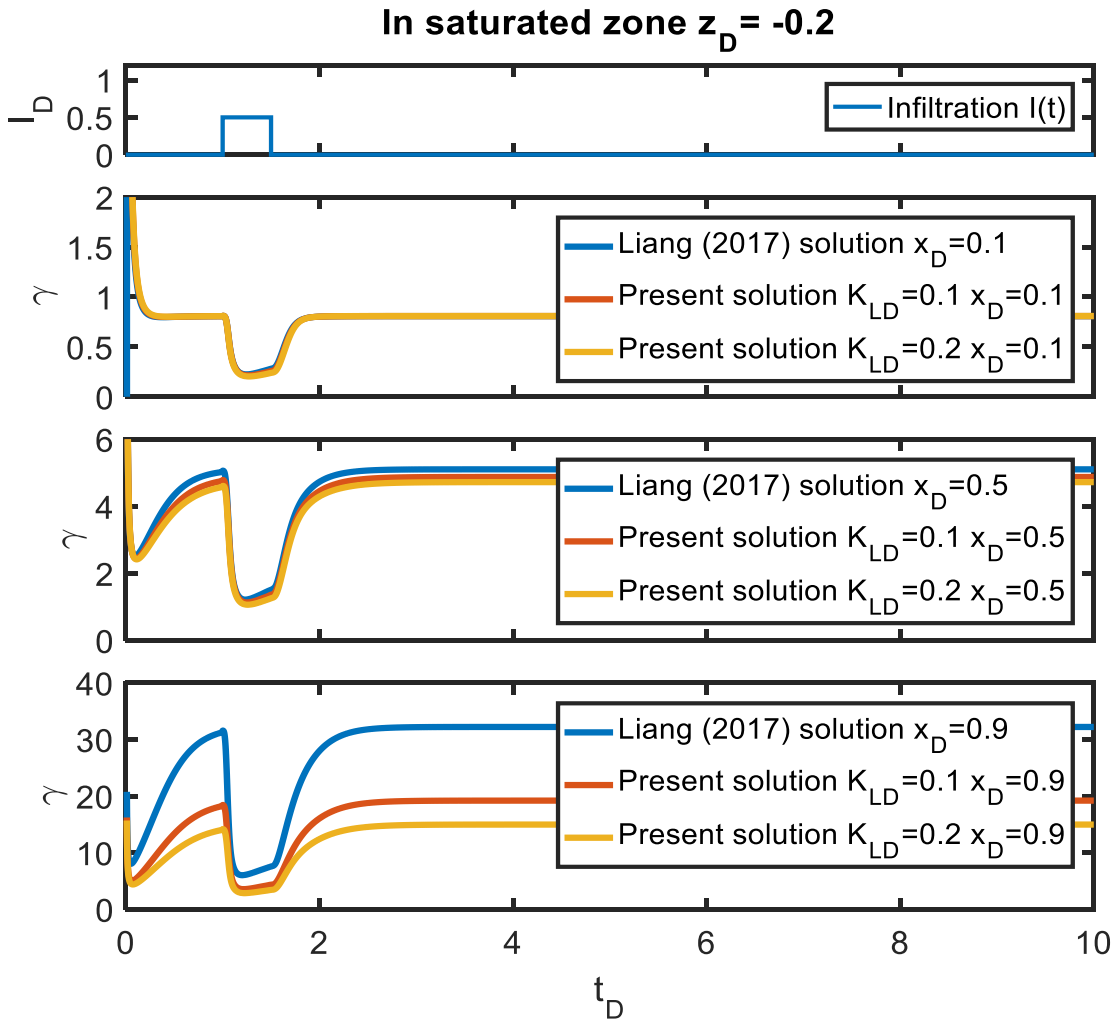

Figure 3. 13 The ratio of horizontal flow versus vertical flow (γ) as a function of time at different locations when z_D= -0.2 (in the saturated zone).

In Figure 3.11, at the location of x_D=0.1, the ratio of horizontal flow flux to vertical flow flux ranges from 0.02 to 0.5. If we compare the γ value for x_D=0.1, x_D=0.5 and x_D=0.9 cases, we can see that the x_D=0.9 case is the greatest and x_D=0.1 is the least at a given time. This means that horizontal flow becomes more significant with proximity to the stream. The streambed can

slightly lower the γ value when the location is intermediate or far from the stream, while it can lower the γ value considerably when the location is close to the stream. Since the γ value is lower in a case with a streambed than the case without a streambed, we can conclude that streambed generally suppresses the horizontal flow rather than the vertical flow. Also, the streambed only has noticeable suppressive effect on horizontal flow in regions near the stream. When we compare Figure 3. (11-13) for x_D=0.1 during the infiltration event, the γ value is the lowest (0.02) in the unsaturated zone (Figure 3.11) and the highest (0.2) in the saturated zone (Figure 3.13). This indicates that during the infiltration event, vertical flow in the unsaturated zone is more dominant than that in the saturated zone. One can see that right after the infiltration event starts, the γ value rapidly drops to a minimum and recovers slowly during the infiltration event. When the infiltration event is over, the γ value recovers to an equilibrium value quickly. Figure 3.14 shows a three-dimensional view of γ value as a function of x_D and t_D when z_D=0 (at the water table) and K_{LD}=0.1. With the help of Figure 3.14, we can have a better visualization of how the γ value changes with t_D and x_D.

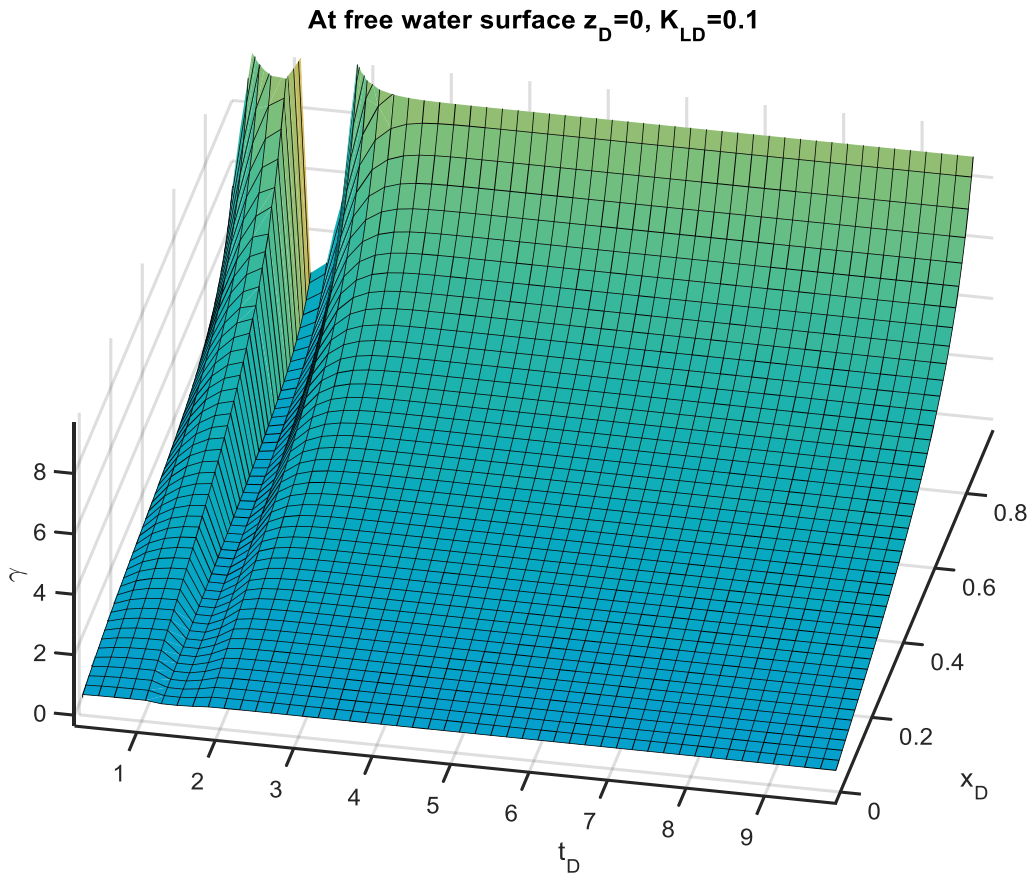

Figure 3. 14 The 3D view of the γ value varies over x_D and t_D when z_D= 0 and K_{LD}= 0.1.

3.5.5 Effects of streambed on slope recession hydrographs

Since the focus of this section is on the slope recession hydrograph, we can set the infiltration here as 0. And the rest of the parameter values are the same as in Section 3.5.1 (see Table 3.3). Following the same lines of Liang et al. (2017), we introduce the linearized Boussinesq solution (LB solution) and the linearized Laplace equation (LL solution) derived by van de Giesen et al. (2005). The LB solution uses Dupuit assumption and only considers the horizontal flow in the saturated zone, while the LL solution uses the Laplace equation and

considers both the vertical flow and the horizontal flow in the saturated zone. A notable point is that unsaturated flow discharge is not a concern in both the LL and LB solutions.

The LB solution is:

$$Q_s(t) = \sum_{n=1,3,5}^{\infty}\left(\frac{4K_x(-H)(H_s+H)}{L} exp\left(-\frac{K_x(H_s+H)(n\pi)^2}{S_y L^2}t\right)\right), \quad (3.7)$$

and the LL solution is:

$$Q_s(t) = \sum_{n=1,3,5}^{\infty}\left(\frac{4K_x(-H)}{n\pi} tanh\left(\frac{n\pi(H_s+H)}{L}\right) exp\left(-\frac{K_x}{S_y} tanh\left(\frac{n\pi(H_s+H)}{L}\right)\frac{n\pi}{L}t\right)\right). \quad (3.8)$$

From Equation (3.7)-(3.8) we can see that the LB solution can be achieved from LL solution by linearizing $tanh(x) = x + O(x^3)$ for $x \ll 1$. When $\frac{n\pi(H_s+H)}{L} \ll 1$, the LL solution becomes the LB solution. More details about the LB and LL solutions can be found in van de Giesen et al. (2005). We decide to compare the present solution with the LL solution, the LB solution and the Liang solution to see the unsaturated-saturated coupling process, vertical water flow effect and streambed effect.

Table 3. 3 Simulation parameters for studying slope recession hydrographs

$L = 100\ m$	$K_x = 1\ m/d$
$K_z = 1\ m/d$	$H_s = 11\ m$
$K_{LD} = \frac{K_x B''}{K'' L} = 0, 0.1$	$\kappa_D = 0.01, 1, 100$
$S_y = 0.1$	$S_s = 1 * 10^{-6}\ m$
$H = -1\ m$	$I_D = 0$

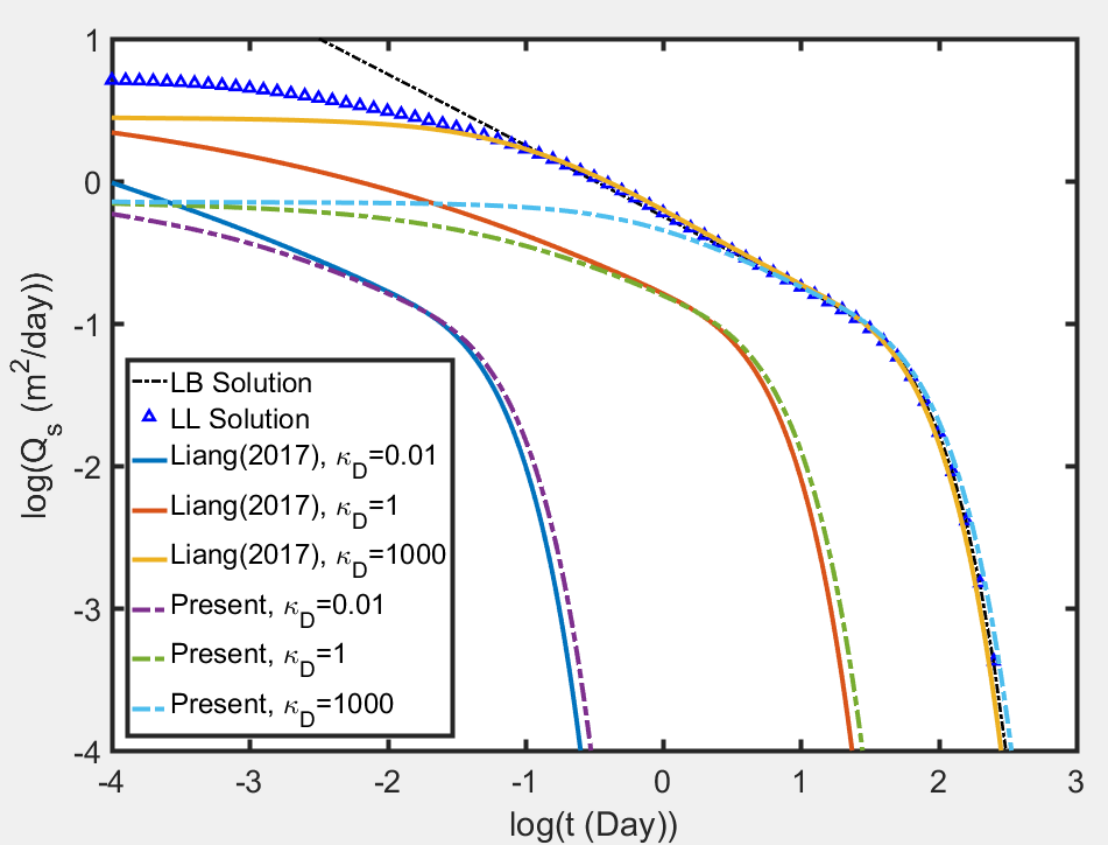

Figure 3. 15 The log-log plot of Q_s $(m^2 day^{-1})$ versus time (day). Q_s is the saturated discharge rate to the stream. The solid lines stand for the case without a streambed, which is the Liang solution. The dash lines stand for present solution considering streambed effect.

The log-log plot of the total discharge rate to the stream along with the LL solution, the LB solution and the Liang solution are shown in Figure 3.15. A higher κ_D value implies a smaller retention capacity of the unsaturated zone, and closer to the LL solution. It is obvious to see that the horizontal discharge rate during the early time will be affected greatly by the K_{LD} value. For the Liang solution ($K_{LD} = 0$), the horizontal discharge rate intends to be higher; while for a streambed case when $K_{LD} = 0.1$, the horizontal discharge rate is much lower. This is consistent with the effect of streambed that it slows down the initial baseflow flux.

Recession hydrographs are often used for determining the aquifer parameters using the two line method proposed by Brutsaert and Nieber (1977). The steps to apply this method is as following. First, plotting $-\frac{dQ}{dt}$ and Q in log-log scales and finding the lower envelope of the data, which refers to data that have the smallest $|\frac{dQ}{dt}|$ at a given *Q*. Then, fitting the lower envelope of the early time data with a slope=3 line and fitting the lower envelope of the late time data with a slope=1 line. Second, from those two lines, we can get the value of $a_1 = \frac{\pi^2 K H_S L_r^2}{S_y A^2}$ for slope=1 line and $a_2 = \frac{1.133}{K S_y H_s^3 L_r^2}$ for slope=3 line, where K is aquifer hydraulic conductivity, S_y is specific yield, H_s is the saturated aquifer thickness, L_r is the total length of upstream channels, and *A* is the area of the watershed. So as long as one of the three parameters (K, S_y, H_s) is given, the other two can be calculated. Detailed computational steps can be found in many previous studies and will not repeat here (Brutsaert and Nieber, 1977; Troch et al., 1993; van de Giesen et al., 2005).

However, we want to point out that there are different opinions towards how to get $\frac{dQ}{dt}$. Brutsaert and Nieber (1977) first introduced the constant time step (CTS) method for calculation and this method has been widely used ever since (Troch et al., 1993; Brutsaert and Lopez, 1998; Ghosh et al., 2016; Jepsen et al., 2016; Liang et al., 2017; Liang et al., 2018). While some researchers observed that the CTS method might have potential bias and uncertainty for the interpretation, an exponential time step method is proposed (Rupp and Selker, 2006b; Rupp and Selker, 2006a; Roques et al., 2018). In this study, we have adopted the most widely accepted CTS method for calculating $\frac{dQ}{dt}$. Further elaboration on the use of this method can be seen from Liang et al. (2018).

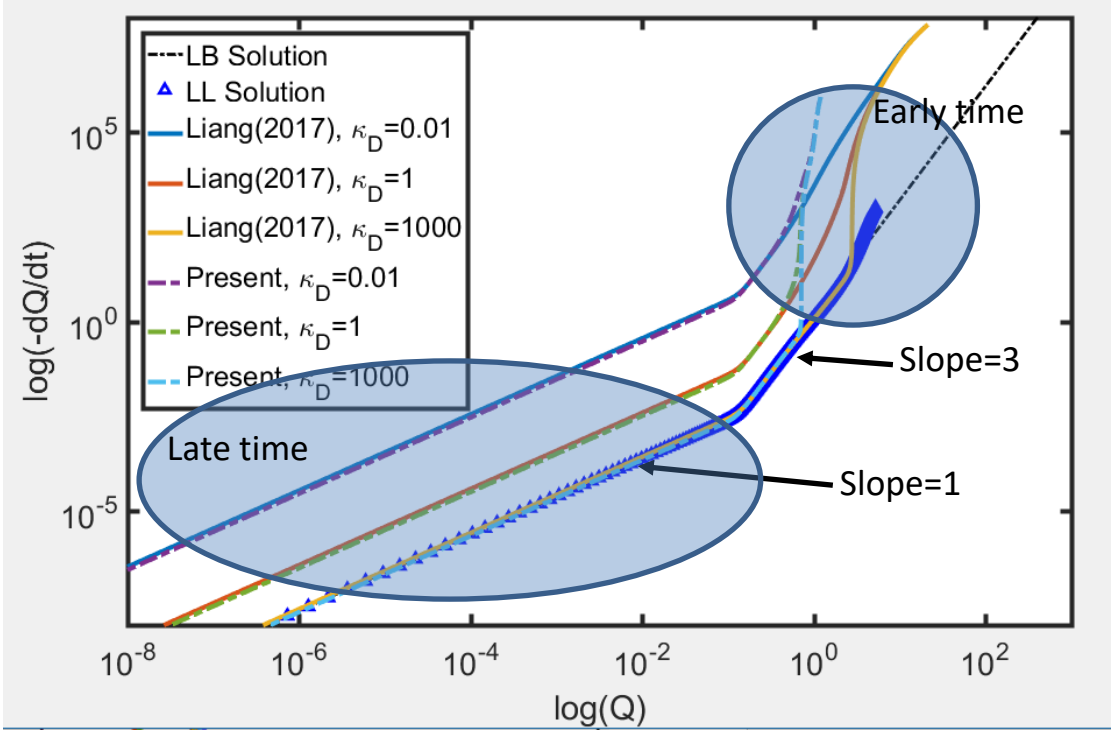

Figure 3. 16 The effect of streambed on slope recession hydrographs. The solid lines stand for no streambed case (Liang solution) and dash lines stand for present solution with a streambed index of $K_{LD} = 0.1$.

If we plot $-\frac{dQ}{dt}$ and Q in log-log scales, we can get the slope recession hydrographs as below. In Figure 3.16, the right side of the figure relates to high baseflow flux values so it stands for early time. The left side of the figure relates to low baseflow flux values so it stands for late time. For the LL and LB solutions, the slope for early time is 3 and for late time is 1. For present solution with streambed effect, the slope quickly drops from infinity to 3 at early time, and for late time the slope of present solution is also 1. This tells us that streambed does not have a great influence on late time slope recession hydrograph. But it does have influence on early time with an elevated slope. Figure 3.16 also compares the influence of streambed under different κ_D

values. It shows that the difference between present solution and the Liang solution mainly happens at early time for all κ_D values.

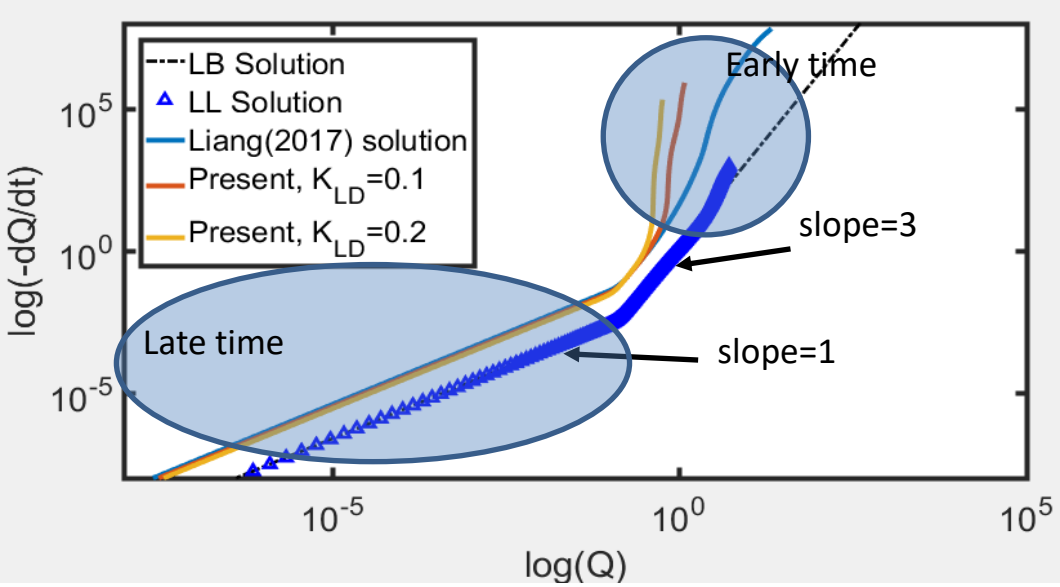

Figure 3. 17 The effect of K_{LD} value on recession slope curves.

To study streambed effect further, we plot $log\left(-\frac{dQ}{dt}\right)$ verus log (Q) using different K_{LD} values $(0, 0.1, 0.2)$. The results are shown in Figure 3.17 which tells us how different streambed K_{LD} values affect the early time slope. From Figure 3.17 we can see that both the LB and LL solutions match very well with each and the slope for early time is 3 and late time is 1. And present solutions for $K_{LD} = 0.1$ and $K_{LD} = 0.2$ have much steeper curves during the early time. But for the late time, the present solution slope fits with that of the Liang solution. It illustrates that streambed will have great effect on the early time and not much effect on late time. For the early time data, if real world data contains the information from streambed and is still fitted by

straight line slope equals 3, the fitting line will have to move up. This will generate a larger intercept of the line and give a smaller value in K, S_y, H_s.

3.5.6 Sensitivity analysis

As an example to test the influence of different parameters on the total discharge, the following technique of sensitivity analysis is employed (Kabala, 2001).

$$SC_{i,j} = I_j \frac{O_i(I_j+\Delta I_j)-O_i(I_j)}{\Delta I_j}, \tag{3.9}$$

where $SC_{i,j}$ is the sensitivity coefficient; O_i is the output function of the model. ΔI_j is a small increment; i is the i^{th} time for O_i; j is the j^{th} parameter of the model. In this session, the output function is the dimensionless total discharge. For streambed index $K_{LD} = 0$ case and $K_{LD} = 0.1$ case, sensitivity coefficients are calculated and showed in Figure 3.18 and Figure 3.19. The base value for parameters are $L = 100\ m$, $K_x = 1\ m/d$, $K_z = 1\ m/d$, $H_s = 11\ m$, $\kappa_D = 1$, $S_y = 0.1$, $S_s = 1 * 10^{-6}\ m$, $H = -1\ m$, $I_D = 0$. The analyzed parameters are $K_{LD}, H_{sD}, H_{uD}, H_D, \kappa_D, S_y, S_s, K_D$. We choose $\frac{I_j}{\Delta I_j} = 1000$ and plot the $SC_{i,j}$ results in Figure 3.18-3.19. From Figure 3.18 sensitivity analysis results, we find that the present model is most sensitive to H_D, moderately sensitive to K_{LD}, H_{sD}, and least sensitive to $H_{uD}, \kappa_D, S_y, S_s, K_D$. The influence from H_{sD}, H_D are positive and the influence from K_{LD} is negative. Compare Figure 3.18 with Figure 3.19, the sensitivity of H_D, K_D decreases when the streambed index K_{LD} increases from 0 to 0.1, while other parameter sensitivities do not change much. Similar conclusions can be drawn from sensitivity analysis conducted on any other terms such as the hydraulic heads in the saturated and unsaturated zones.

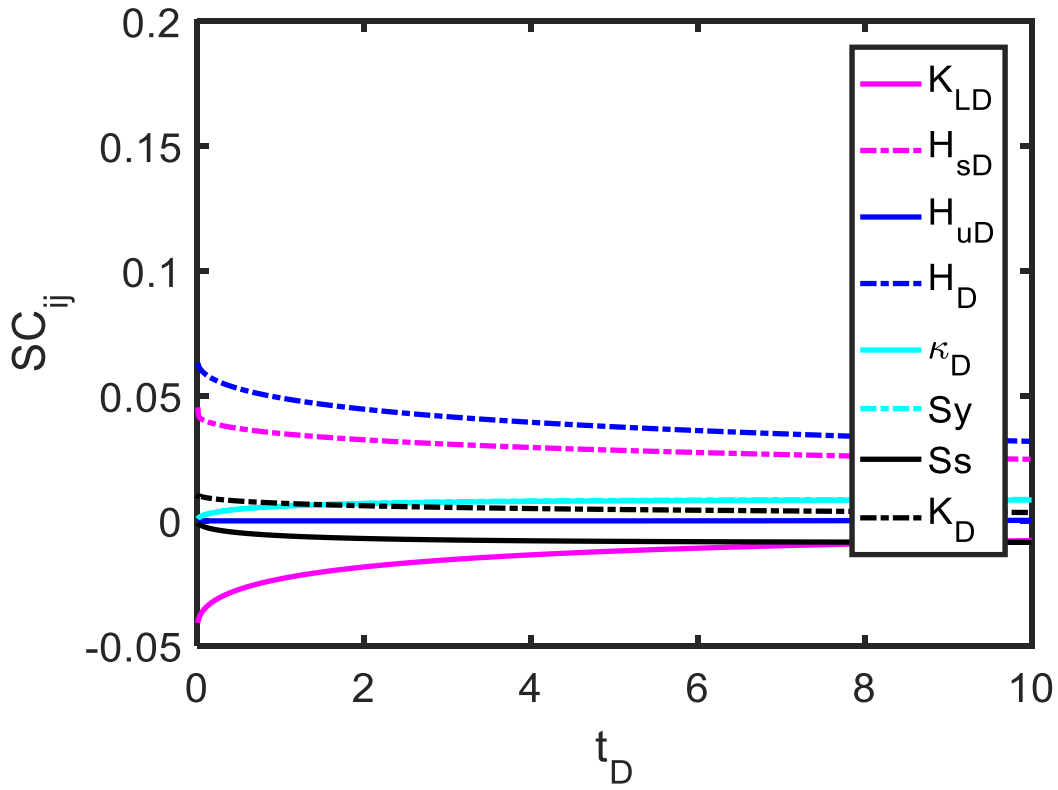

Figure 3. 18 Sensitivity analysis for different model parameters.$K_{LD} = 0.1$ is the streambed index. H_{sD} is the dimensionless saturated zone thickness. H_{uD} is the dimensionless unsaturated zone thickness. H_D is the dimensionless stream water level. κ_D is the dimensionless parameter relates to unsaturated zone effect. S_y is the specific yield. S_s is the specific storativity. K_D is the ratio of vertical hydraulic conductivity to horizontal hydraulic conductivity.

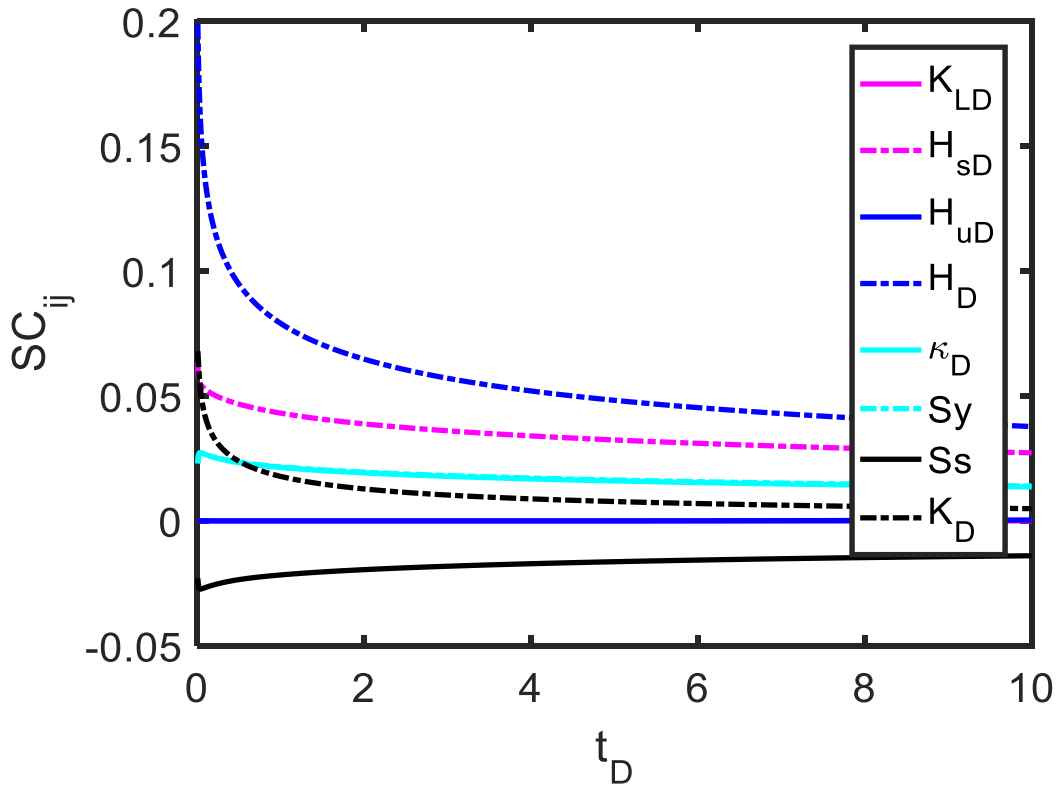

Figure 3. 19 Sensitivity analysis for no streambed model for comparison.$K_{LD} = 0$ is the no streambed case. H_{sD} is the dimensionless saturated zone thickness. H_{uD} is the dimensionless unsaturated zone thickness. H_D is the dimensionless stream water level. κ_D is the dimensionless parameter relates to unsaturated zone effect. S_y is the specific yield. S_s is the specific storativity. K_D is the ratio of vertical hydraulic conductivity to horizontal hydraulic conductivity.

3.6 Discussion

The present solution in this article takes consideration of coupled saturated-unsaturated flow process in the presence of a thin low-permeability streambed and provides a semi-analytical solution for hydraulic head distribution in both saturated zone and unsaturated zone. It also reveals the streambed effect on baseflow recession hydrograph. However, this study also has a few notable limitations.

First, the nonlinear Richard's equation governing the unsaturated flow is linearized using the approach adopted by (Kroszynski and Dagan, 1975). Therefore, all the constrains associated with such a linearization must not be overlooked, and those constrains have been documented in detail in previous studies (Kroszynski and Dagan, 1975) so will not be repeated here. One of constraint states that flow departs only slightly from the hydrostatical equilibrium.

Second, the unsaturated-saturated interface is assumed to be a fixed horizontal plane, rather than a spatiotemporally variable moving boundary, thus, the application of model requires that the hydraulic head change in the saturated zone should be relatively small as compared to the saturated zone thickness. For a dramatically variable water table, the proposed semi-analytical solution may fail and a complete numerical simulation should be applied.

Third, the streambed effect may also be studied for different seasons to evaluate the impacts of variation of streambed hydraulic conductivity with time. Furthermore, this study is a strict 2D cross-sectional investigation which does not honor the spatial variations of streambed elevation and river stage along the river channel, which is more likely to occur in real applications. Addressing this would require a three-dimensional (3D) approach to deal with.

Fourth, media heterogeneity has not been considered at the present study and may profoundly affect the hydraulic heads and discharges distribution associated with the baseflow process in a watershed.

Fifth, significant surface topography will occur near streams in many actual watersheds, so the combined effects of surface topography, heterogeneity, coupled unsaturated-saturated flow, and streambed on baseflow will be of interest to pursue in the future.

3.7 Conclusions

Trying to understand the impact of streambed hydraulic properties on baseflow in a watershed scale, considering the coupled unsaturated and saturated flow processes, we first build a 2D conceptual model of baseflow from an unsaturated-saturated zone to a stream with a thin low-permeability streambed. Then we establish a mathematical model for the coupled unsaturated and saturated flow processes, and obtain the semi-analytical solutions of spatiotemporal distributions of hydraulic heads and discharges in both the saturated and unsaturated zones. We introduced a streambed index, denoted as K_{LD}, which is a dimensionless number defined as the ratio of hydraulic conductance of the saturated zone to that of the streambed for horizontal flow, where the hydraulic conductance is defined as the ratio of hydraulic conductivity over distance of flow. Such a streambed index is a key parameter reflecting the impact of streambed. In addition, this study provides a comprehensive analysis of the relative importance of horizontal versus vertical flow in the unsaturated and saturated zones as a function of space and time. Here are some main findings:

1. When the streambed has a lower hydraulic conductance, the hydraulic head response due to an infiltration event is greater. The present solution is greater than the Liang solution due to the streambed impact.
2. A higher streambed index K_{LD} value will lead to a lower peak value of the total discharge rate to the stream. The K_{LD} value will not change the total discharge volume.
3. The relative ratio of the discharge rate to a stream with a streambed and without a streambed is a monotonically increasing function of time. The streambed will increase the late time baseflow flux.

4. The ratio of horizontal flow velocity to vertical flow velocity at water table is low when the observation location is far away from the stream and is high when the observation location is close to the stream. Streambed has an effect on such a ratio, particularly for regions close to the stream. During the infiltration event, such a ratio is much lower in the unsaturated zone than that in the saturated zone.
5. The peak value of the total discharge rate at the early time is lowered and the baseflow decaying process is prolonged when there is a streambed than the case without a streambed. The relative ratio between the late time discharge rates with and without a streambed can be as high as 200%.
6. In slope recession hydrograph analysis, the streambed affects early time slope and has little impact on late time slope. This results in an underestimation of hydraulic conductivity K, specific yield S_y and saturated aquifer thickness H_s if the streambed effect is not considered in the analysis.

4. BANK STORAGE IN UNSATURATED AND SATURATED ZONE WITH A STREAMBED

4.1 Introduction

Bank storage is defined as water infiltrating into the aquifer during high stream levels and flowing back to the stream during low stream levels (Singh, 1968). It plays a significant role in hydrological processes, such as reducing and delaying the flood hydrograph peak at downstream sites (Doble et al., 2012). Guo (1997) studied transient groundwater flow between an unconfined aquifer and a reservoir (or stream) without a low-permeability streambed while not considering the unsaturated zone water flow. Zlotnik and Huang (1999) proposed an analytical model to assess the impact of shallow stream penetration and low-permeability streambed sediments on head responses. Shallow stream means the streambed penetrating depth is much less than the aquifer thickness. They ignored the effect of the unsaturated flow process, as commonly done by other similar studies (Huang et al., 2010; Huang et al., 2012), apparently for the sake of simplifying the problem. Hilberts et al. (2005) considered the interaction of the unsaturated and saturated zones and proposed an analytical expression for specific yield that is dependent on the water table and the retention capacity of the unsaturated zone using the van Genuchten (1980) model. However, Hilberts et al. (2005) ignore the horizontal flux in the unsaturated zone. Doble et al. (2012) studied the bank storage process with different bank slopes and included unsaturated flow effects. Kong et al. (2016) showed that it was necessary to consider the unsaturated flow process to improve the accuracy of predicting groundwater flux rates at watershed outlets. Liang et al. (2017) constructed the latest model solving the coupled unsaturated-saturated zone problem which accounts for the unsaturated lateral and vertical flows. But Liang et al. (2017) did not

consider the low-permeability streambed that may affect the stream-aquifer interaction profoundly. Chen and Chen (2003) studied the stream water infiltration and bank storage caused by stream level fluctuations. Their simulation used different stream level fluctuations, aquifer properties, and considered the hydraulic conductivity of streambed sediments, recharge and evaporation processes.

In this study, we analyze the bank storage effect considering the low-permeability streambed effect during and after a flood event. We have two specific objectives. The first is to quantify the unsaturated zone bank storage effect. The second is the streambed effect on the overall bank storage processes. To serve this purpose, we developed a two-dimensional (2D) model that accounts for both unsaturated-saturated flow processes and a streambed structure. To achieve the objectives, it is crucial to have a geologically based streambed conceptual model, a nontrivial task in many occasions, as the stream geomorphology is dynamic (Hatch et al., 2010). Kalbus et al. (2009) stated that the variation of groundwater discharge to a stream was closely related to the heterogeneous properties of aquifer and streambed permeability. Sebok et al. (2015) showed the complexity of streambed structure which may have multiple layers with different grain sizes of sand, gravel, and organic layers that hinder groundwater discharge. The effect of heterogeneous hydraulic conductivities of streambeds have been investigated by Irvine et al. (2012); Schilling et al. (2017), and others. Such complexities regarding streambed geomorphology will not be taken into consideration in this study because of a few considerations. First, this study is a first attempt to include the bank storage process in a saturated-unsaturated coupled model along with a streambed analytically. Therefore, we like to start with a simple model and to use the established new model and associated solutions as references for further studies. Second, up to the present, there is still not a commonly accepted

concept model to describe the spatiotemporally variable, heterogeneous streambed. Therefore, in the present study, the streambed is represented by a thin lower-permeability layer with a uniform thickness.

The structure of this paper includes three parts. First, we will build a 2D mathematical model and derive the hydraulic head responses in both unsaturated and saturated zones during the flood event. We will further test the new solution against a finite element numerical simulation using COMSOL Multiphysics. Second, we will compare the new solution against a previous model of Liang et al. (2017) which excluded the streambed effect. Third, we will analyze the effect of the low-permeability streambed on bank storage process within a coupled saturated-unsaturated flow system.

4.2 Mathematical model

A 2D cross-sectional model of coupled saturated and unsaturated flow to a stream in a watershed is schematically shown in Figure 1(a). A low-permeability streambed with a uniform thickness and a constant hydraulic conductivity is presented. The hydraulic conductivity of the streambed is much less (at least two orders of magnitude smaller) than the hydraulic conductivity of the aquifer. The aquifer is homogeneous and anisotropic in both saturated and unsaturated zones. The streambed thickness is small when compared to the aquifer length and is assumed to

be homogeneous and isotropic. The aquifer is fully penetrated by a stream.

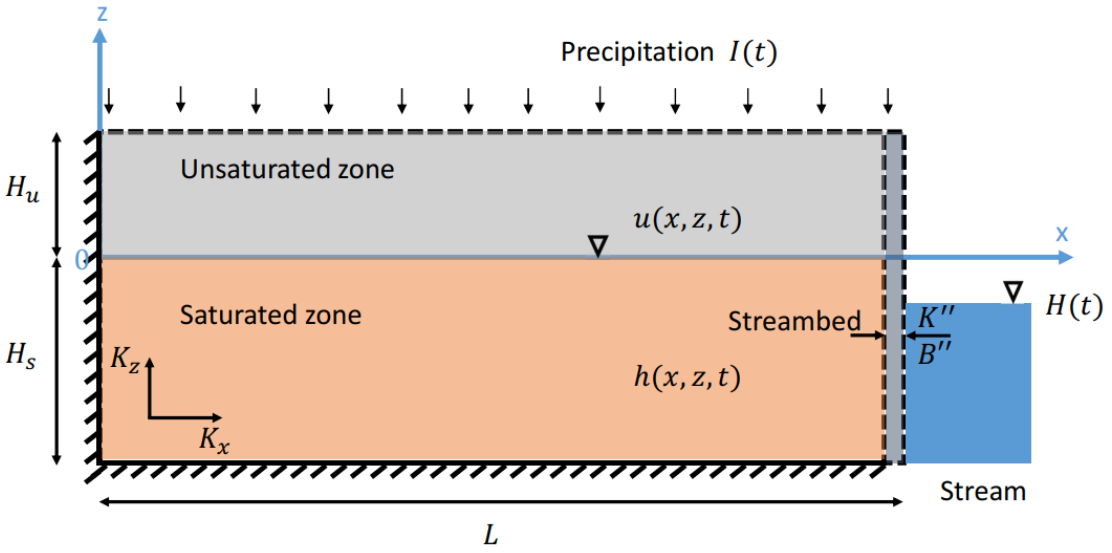

Figure 4. 1 Schematic model of unsaturated-saturated zone with a low permeability streambed.

The x-axis is horizontal and z-axis is vertically upward. The left side boundary ($x = 0$) represents the water divide (no flow boundary). The right side boundary ($x = L$) represents the streambed. The streambed hydraulic conductivity is K'' and streambed thickness is B''. The initial water table is at $z = 0$. The stream stage is dependent on time but independent of space and is described as a function of $H(t)$. The origin is set at the intercept of the initial water table with the left water divide. The unsaturated zone extends from $z = 0$ to $z = H_u$, and the saturated zone extends from $z = -H_s$ to $z = 0$. The saturated horizontal and vertical hydraulic conductivities are K_x and K_z, respectively. The base of the aquifer is impermeable. The top of the aquifer is the flat ground surface which has a second-type flow boundary condition with a prescribed, spatially uniform but temporally variable downward flux $I(t)$. One may regard $I(t)$ as the net downward infiltration rate right below the ground surface. Topographic variation of the

ground surface is likely to exist in the real world setting but is not considered here for the sake of simplicity. The topographic effect should be considered in a future study on the basis of this investigation.

After building up the conceptual model for a 2D cross-sectional flow, here comes the governing equation for the saturated zone $-H_s \le z \le 0$:

$$K_x \frac{\partial^2 h}{\partial x^2} + K_z \frac{\partial^2 h}{\partial z^2} = S_s \frac{\partial h}{\partial t}, \quad (1a)$$

$$h(x, z, 0) = 0, \quad (1b)$$

$$\frac{\partial h}{\partial x}(x, z, t)|_{x=0} = 0, \quad (1c)$$

$$\frac{K''(h(L,z,t)-H(t))}{B''} = -K_x \frac{\partial h}{\partial x}(x, z, t)|_{x=L}, \quad (1d)$$

$$\frac{\partial h}{\partial z}(x, z, t)|_{z=-H_s} = 0, \quad (1e)$$

where h is the hydraulic head in the saturated zone [L]; S_s is the specific storage [L^{-1}]; t is time [T]; H_s is the initial thickness of the saturated zone [L]; L is the distance from the water divide to the stream [L]; $H(t)$ is the time-dependent stream water level [L]. Other symbols have been explained above.

Equation (1a) is the general governing equation of flow in an unconfined aquifer. Equation (1b) is the initial condition of hydraulic head in the saturated zone. Equation (1c) is the left boundary condition representing the water divide. Equation (1d) is the right boundary condition describing the aquifer-streambed-stream system. We choose the third type boundary condition described by Equation (1d) based on a few considerations. First, the streambed is so thin with a negligible storage effect. Second, flow in the streambed is horizontal, i.e., it is perpendicular with the aquifer-streambed interface (vertical). This is because the contrast of hydraulic conductivities of the streambed and the aquifer is significant (more than two orders of

magnitude), thus flow in the low-permeability streambed is nearly perpendicular with the vertical aquifer-streambed interface, a principle sometimes called the law of refraction of flow in many hydrogeology textbooks (Freeze and Cherry, 1979; Domenico and Schwartz, 1998; Fetter, 2001). Equation (1e) is the no-flow lower boundary condition, which stands for the impermeable aquifer bottom.

In the unsaturated zone $0 \leq z \leq H_u$, flow induced by infiltrations is governed by Richards' equation. However, it is difficult to directly solve Richards' equation without any approximation. Here, we propose to use the linearized method developed by Kroszynski and Dagan (1975). The linearized 2D unsaturated flow equation can be written as follows,

$$k_0(z)K_x\frac{\partial^2 u}{\partial x^2} + K_z\frac{\partial}{\partial z}\left(k_0(z)\frac{\partial u}{\partial z}\right) = C_0(z)\frac{\partial u}{\partial t}, \quad (2a)$$

$$u(x,z,0) = 0, \quad (2b)$$

$$\frac{\partial u}{\partial x}(x,z,t)|_{x=0} = 0, \quad (2c)$$

$$\frac{K''(u(L,z,t)-H(t))}{B''} = -K_x\frac{\partial u}{\partial x}(x,z,t)|_{x=L}, \quad (2d)$$

$$K_z k_0(z)\frac{\partial u}{\partial z}(x,z,t)|_{z=H_u} = I(t), \quad (2e)$$

where u is the hydraulic head in the unsaturated zone [L], $k_0(z)$ is the zero-order approximation of the relative hydraulic conductivity [-], $C_0(z)$ is the zero-order approximation of the soil moisture capacity [L^{-1}] at the initial water content of θ_0. $k_0(z) = k(\theta_0)$ and $C_0(z) = C(\theta_0)$; k ($0 \leq k \leq 1$) and $C(\geq 0)$ are the relative hydraulic conductivity [-] and specific moisture capacity [L^{-1}], respectively, at an arbitrary water content of θ; H_u is the initial thickness of the unsaturated zone [L]. One notable point is that the saturated hydraulic conductivity of the unsaturated zone is the same as its counterpart of the saturated zone.

Equation (2b) is the initial condition of hydraulic head in the unsaturated zone. Equation (2c) is the left boundary condition represents the water divide. Equation (2d) is the right boundary condition. Equation (2e) is the upper boundary at the flat ground surface. There are several reasons about why we chose equation (2d) as the right boundary condition. We assume the water movement is horizontal in the low-permeability layer. The right side of low-permeability layer is considered as equipotential surface and without hydraulic head loss along the right side boundary. Figure 4.2 shows the conceptual assumption near the low-permeability layer. Because the low-permeability layer is thin, the water flow inside the low-permeability layer is horizontal. As soon as water moves out to the right side boundary, water will go to the stream without head loss (frictionless flow). In this way, the right side boundary can be an equipotential surface.

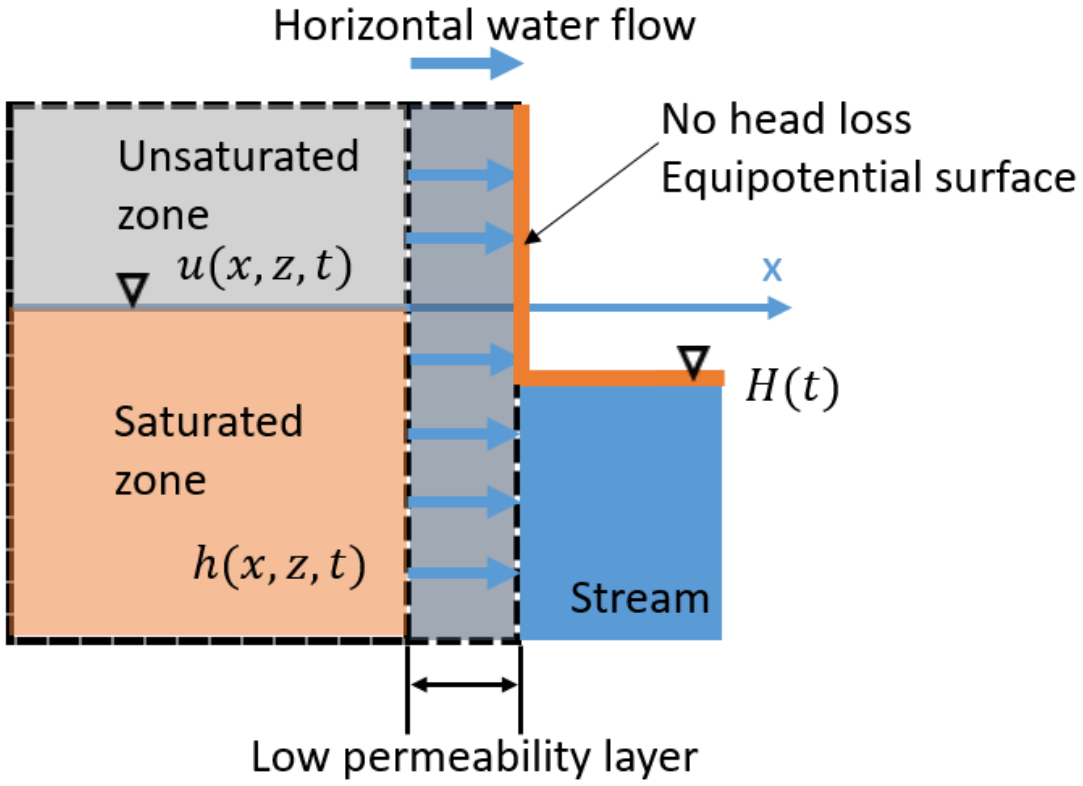

Figure 4. 2 Zoom in near the low permeability streambed. The hydraulic head on the right side of low permeability layer is the same value as $H(t)$.

To deal with $k_0(z)$ and $C_0(z)$ in Equation (2a), many previous researchers have used the Gardner (1958) exponential constitutive model for the unsaturated zone (Gardner, 1958; Kroszynski and Dagan, 1975; Tartakovsky and Neuman, 2007; Liang et al., 2017). The model is shown as follows:

$$k_0(z) = e^{-\kappa z}, \qquad (2f)$$

$$C_0(z) = S_y \kappa e^{-\kappa z}, \qquad (2g)$$

where $\kappa > 0$ is a constitutive exponent that describes the unsaturated zone medium properties [L^{-1}], S_y is the specific yield or drainable porosity [-]. We have to point out that the choice of the

Gardner (1958) exponential model is simply for the purpose of facilitating analytical treatment of the problem. If solving the problem numerically, then one is free to choose any other types of constitutive models, such as the Brooks and Corey (1966) model or the van Genuchten (1980) model. Nevertheless, the use of the Gardner (1958) exponential model here is to demonstrate the methodology in an analytical framework. In the future, it will be useful to check if the methodology and conclusions of this study still hold or not if a different constitutive model is used.

The continuous boundary condition at the saturated-unsaturated interface is as follows:

$$h(x,0,t) - u(x,0,t) = 0, \quad (3a)$$

$$\frac{\partial h}{\partial z}(x,0,t) - \frac{\partial u}{\partial z}(x,0,t) = 0 \quad (3b)$$

Base on the equation groups of (1a)-(3b), we can get the semi-analytic solution for the hydraulic head distribution in both unsaturated and saturated zones, provided that the change of hydraulic head in the saturated zone is relatively small as compared to the initial saturated thickness. After that, one can calculate the baseflow fluxes per unit width along the river in the saturated zone Q_s and unsaturated zone Q_u as:

$$Q_s(t) = \int_{-H_s}^{0} (-K_x \frac{\partial h}{\partial x}(x,z,t)|_{x=L}) dz, \quad (4a)$$

$$Q_u(t) = \int_{0}^{H_u} \left(-K_x k_0(z) \frac{\partial u}{\partial x}(x,z,t)|_{x=L}\right) dz\,. \quad (4b)$$

Total discharge rate per unit width along the river $Q(t)$ is the sum of discharge rates in the unsaturated and saturated zones.

$$Q(t) = Q_s(t) + Q_u(t). \quad (4c)$$

4.3 Semi-analytical solution

We prefer to solve the mathematical model in a dimensionless format because it can reduce the number of parameters involved in the mathematical model and recover some characteristic properties that are key controls of the dynamic system. We have obtained a new semi-analytical solution in dimensionless form and the dimensionless variables are defined in Table 4.1. $h_D, u_D, x_D, z_D, t_D, H_{sD}, H_D, H_{uD}, I_D, Q_{sD}, Q_{uD}$ are the dimensionless forms of $h, u, x, z, t, H_s, H, H_u, I, Q_s, Q_u$, respectively. $K_D, \kappa_D, \beta, \alpha, K_{LD}$ are dimensionless parameters describing the aquifer. Specifically, K_D is an anisotropy ratio defined as the ratio of vertical saturated hydraulic conductivity to horizontal saturated hydraulic conductivity. κ_D and β are two dimensionless constitutive exponents. K_{LD} is a parameter regarded as the ratio of hydraulic conductance of aquifer over that of streambed for horizontal flow, where the hydraulic conductance is defined as the ratio of hydraulic conductivity over distance of flow. K_{LD} is a key dimensionless parameter reflecting the streambed effect, and is called the "streambed index" hereinafter.

In Laplace domain, we have the semi-analytical solution as:

$$\bar{h}_D(x_D, z_D, p) = \bar{H}_D(p) + \sum_{n=0}^{\infty}\left[C_1\, exp(-\Omega_n z_D) + C_2\, exp(\Omega_n z_D) - \frac{A_n p\, sin(\omega_n)\bar{H}_D}{(\omega_n^2+p)\omega_n}\right] A_n\, cos(\omega_n x_D), \quad (5a)$$

$$\bar{u}_D(x_D, z_D, p) = \bar{H}_D(p) + \sum_{n=0}^{\infty}\left[C_3\, exp(M z_D) + C_4\, exp(N z_D) - \frac{p\beta \bar{H}_D(p) A_n sin\omega_n}{(\omega_n^2+p\beta)\omega_n}\right] A_n\, cos(\omega_n x_D), \quad (5b)$$

$$\bar{Q}_{sD}(p) = \sum_{n=0}^{\infty}\left[C_2 - C_1 + C_1\, exp(\Omega_n H_{sD}) - C_2\, exp(-\Omega_n H_{sD}) - \frac{A_n p\, sin(\omega_n)\bar{H}_D H_{sD}}{K_D \Omega_n \omega_n}\right] \frac{\omega_n sin(\omega_n)}{\Omega_n} A_n \ , \quad (6a)$$

$$\bar{Q}_{uD}(p) = \sum_{n=0}^{\infty}\left[-\frac{C_3}{M-\kappa_D} - \frac{C_4}{N-\kappa_D} + \frac{C_3\, exp\left((M-\kappa_D)H_{uD}\right)}{M-\kappa_D} + \frac{C_4\, exp\left((N-\kappa_D)H_{uD}\right)}{N-\kappa_D} + (exp(-\kappa_D H_{uD}) - 1)\frac{A_n p\beta\, sin(\omega_n)\bar{H}_D}{K_D\Psi_n^2\kappa_D\omega_n}\right]\omega_n sin(\omega_n)\, A_n \quad , \qquad (6b)$$

where the overhead bar stands for Laplace domain and the subscript "*D*" refers to the dimensionless variable, *p* is the Laplace transform parameter in respect to the dimensionless time defined in Table 4.1. The detailed derivation of the solution is presented in Supporting Information S1. Since the closed-form analytical inverse Laplace transform is difficult to execute, we will need a numerical inverse Laplace transform method to obtain the real time solution. The numerical inverse Laplace transform technique chosen here is the de Hoog et al. (1982) algorithm, which has accelerated convergence for calculation. A MATLAB script file to facilitate numerical inverse Laplace transform is modified from Hollenbeck (1998) and has a better overall accuracy than other numerical inverse Laplace transform methods (Liang et al., 2017).

Table 4. 1 The dimensionless variables.

$h_D = \frac{h}{H_s}$	$t_D = \frac{K_x}{S_s L^2} t$
$x_D = \frac{x}{L}$	$z_D = \frac{z}{L}$
$K_D = \frac{K_z}{K_x}$	$H_{sD} = \frac{H_s}{L}$
$H_{uD} = \frac{H_u}{L}$	$H_D = \frac{H}{H_s}$
$u_D = \frac{u}{H_s}$	$\kappa_D = \kappa L$
$\beta = \frac{\kappa s_y}{S_s}$	$\alpha = H_{sD} \exp(-\kappa_D H_{uD})$
$I_D = \frac{I}{K_z}$	$K_{LD} = \frac{K_x B''}{K'' L}$
$Q_{sD} = \frac{Q_s}{K_x H_s}$	$Q_{uD} = \frac{Q_u}{K_x H_s}$

4.4 Validation through COMSOL Multiphysics numerical simulation

To check the solution robustness, we use COMSOL Multiphysics (COMSOL Inc., Burlington, MA, USA) to solve Equations (1)-(3). Then compare the new semi-analytical solution with the numerical solution under a streambed index $K_{LD} = 0.1$. The parameters used for simulation are given in Table 4.2. Those parameters are from the previous study by Liang et al. (2017).

Table 4. 2 Simulation parameters for part 4.5.1

$K_D = 1.0$	$H_{sD} = 0.4$
$S_y = 0.1$	$T_{fD} = \frac{K_x T_f}{S_s L^2}$
$H_{uD} = 0.2$	$H_D = -\frac{1}{8}(1 - \cos(\frac{2\pi}{T_{fD}} * t_D))$
$K_{LD} = \frac{K_x B''}{K'' L} = 0, 0.1, 0.2$	$\kappa_D = 10$
$S_s = 1 * 10^{-3}$	$I_D = 0$

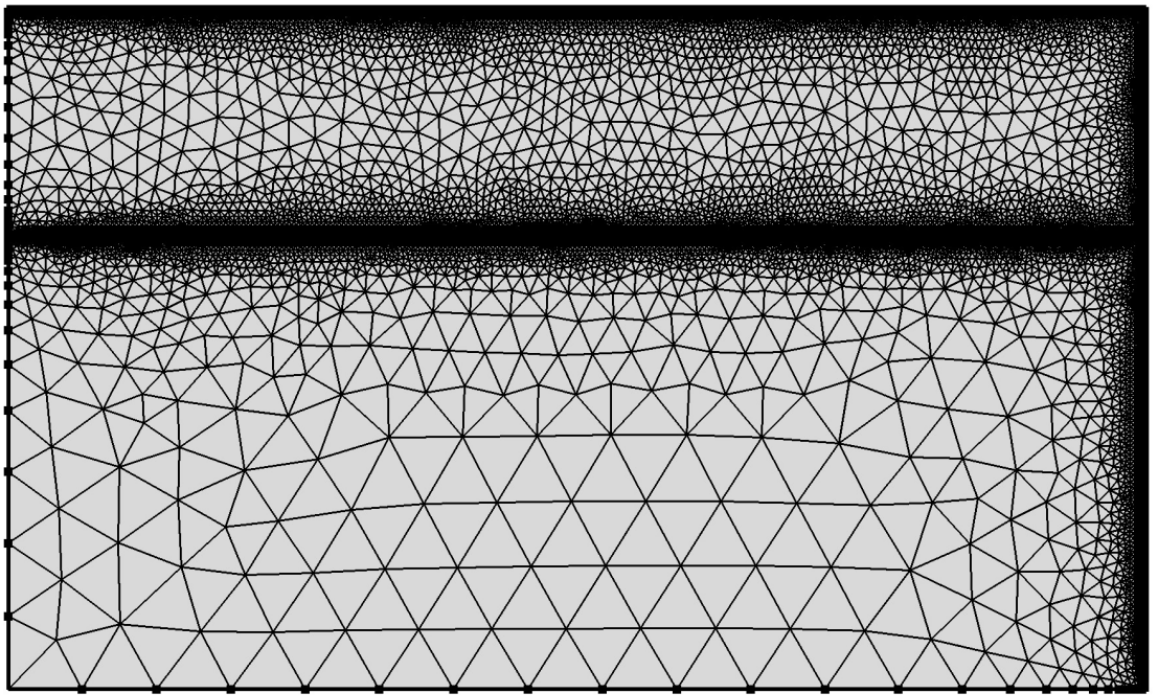

Figure 4. 3 Mesh plot for present model in the finite element simulation using COMSOL Multiphysics.

Figure 4.3 shows the mesh plot for the model. We can see that the elements near the water table and boundaries are refined to reduce the numerical errors. The number of triangular elements is 23086. The average element quality is 0.8419, which is good for simulation accuracy. In general, if the average element quality is below 0.1, it is considered as a poor mesh which then has to be redesigned to achieve an average element quality above 0.1. Numerical exercises demonstrate that the mesh used here is sufficiently fine so that the result is free from the number of elements used in the simulation.

The time step for simulation $\Delta t_D = 0.01$, and the total number of time step is 1000, with a total simulation time of $t_D = 10$. The observation point is at ($x_D = 0.9, z_D = 0.1$) for unsaturated zone (u_D) and ($x_D = 0.9, z_D = -0.1$) for saturated zone (h_D). The results are shown in Figure 4.4, from which we can see that the semi-analytical solution fits very well with the numerical simulation. We will then compare the present solution with the base case of Liang et al. (2017), which excluded the streambed effect. For convenience, the solution of Liang et al. (2017) will be noted as "Liang solution" hereinafter.

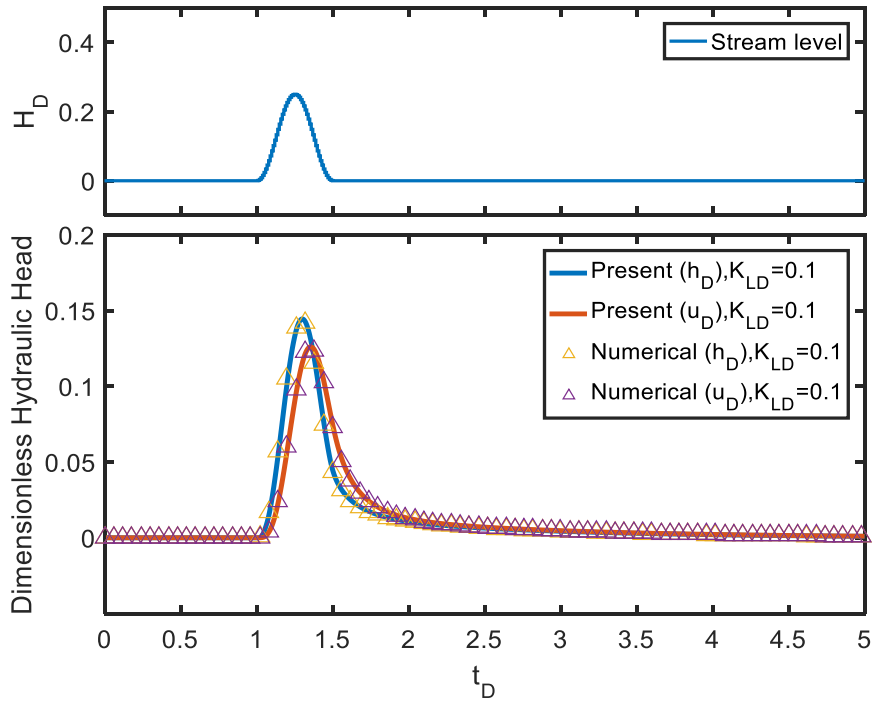

Figure 4. 4 Comparison between numerical solution and semi-analytical solution. The observation point is at ($x_D = 0.9, z_D = 0.1$) for unsaturated zone (u_D) and ($x_D = 0.9, z_D = -0.1$) for saturated zone (h_D).

4.5 Results

4.5.1 Effects of streambed on hydraulic head

The simulation parameter for this part is shown in Table 4.2. We have chosen three different locations for the observation points. The three different locations refer to near the stream ($x_D = 0.9$), half way to the stream ($x_D = 0.5$), and far away from the stream ($x_D = 0.1$). At each location, we will look at simulated observation points within unsaturated zone ($z_D = 0.1$) and saturated zone ($z_D = -0.1$). The dimensionless hydraulic head response caused by the

fluctuation of stream level results at those three locations ($z_D = 0.9, 0.5, 0.1$) are shown in Figure 4.5- 4.7, respectively. The fluctuation of stream level is defined using an equation:

$$H_D = \begin{cases} \frac{A}{2}\left(1 - \cos\frac{2\pi}{\tau}t_d\right), & when\ 0 \le t_d \le \tau \\ 0, & when\ t_d > \tau \end{cases}, \qquad (1)$$

where A describes the maximum dimensionless rise in stream water level. τ is the dimensionless period of the wave. The time period for the rise and fall of stream water level is 5 days and $\tau = 0.5$. In the Liang solution, the stream does not have a streambed (the streambed thickness is zero). So the case of $K_{LD} = 0$ reflects the Liang solution.

Firstly, let us focus on the saturated zone hydraulic head responses in Figure 4.5. If comparing different K_{LD} values in Figure 4.5, we can see that the case $K_{LD} = 0$ has the highest response and the case $K_{LD} = 0.2$ has the lowest response. This means that if the streambed has a lower hydraulic conductance (defined as the ratio of conductivity over thickness), the hydraulic head response due to stream water level rise is lower. Thus, the hydraulic head solution using the new model of this study is lower than that using the Liang solution. The results agree with general understanding of streambed that slows the interaction between the stream and aquifer, thus the influence of the stream water level rise is reduced by the streambed. If the streambed has an extremely small hydraulic conductance, the interaction between the aquifer and the stream would be lessened even more. And the hydraulic head increase from the stream water level rise would be smaller.

The K_{LD} value not only influences the hydraulic head response peak value, but also affects the rate of increase in hydraulic head during the rising phase of stream water level and the decay rate of hydraulic head during the stream flow recession. The higher K_{LD} value will result

in a slower rising rate and decaying rate of hydraulic head in the saturated zone. The K_{LD} value has similar effect in unsaturated zone just like that in saturated zone.

Secondly, if we compare the hydraulic head response in saturated zone with that in the unsaturated zone in Figure 4.5, we will find that the response in the unsaturated zone is slightly less than that in the saturated zone. This will further result in vertical water movement from the unsaturated to the saturated zone.

Thirdly, if we compare the K_{LD} value effect in saturated zone across Figure 4.5-4.7, we can see that the effect is most visible at the location of $x_D = 0.9$, which is close to the stream. For the location of $x_D = 0.1$, which is far away from the stream, the difference in hydraulic head response generated from different K_{LD} values is relatively small. This tells us that the streambed has a greater effect in near-stream region and less effect in far away from the stream region.

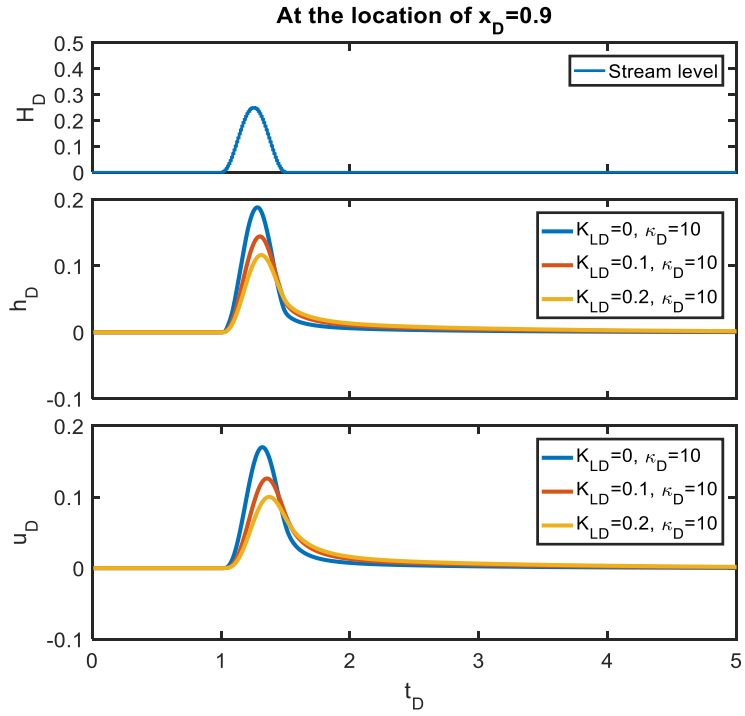

Figure 4. 5 Hydraulic response at the location of $x_D = 0.9$.

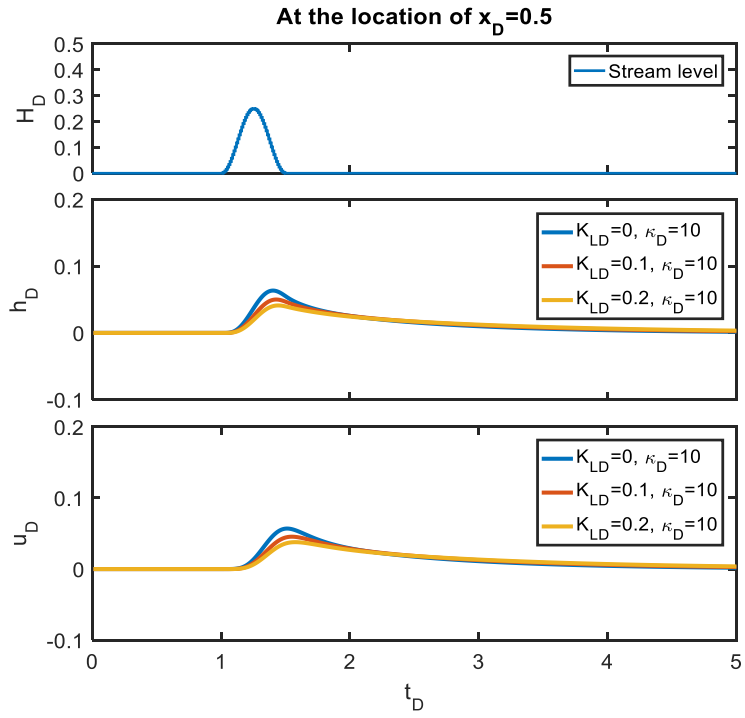

Figure 4. 6 Hydraulic response at the location of $x_D = 0.5$.

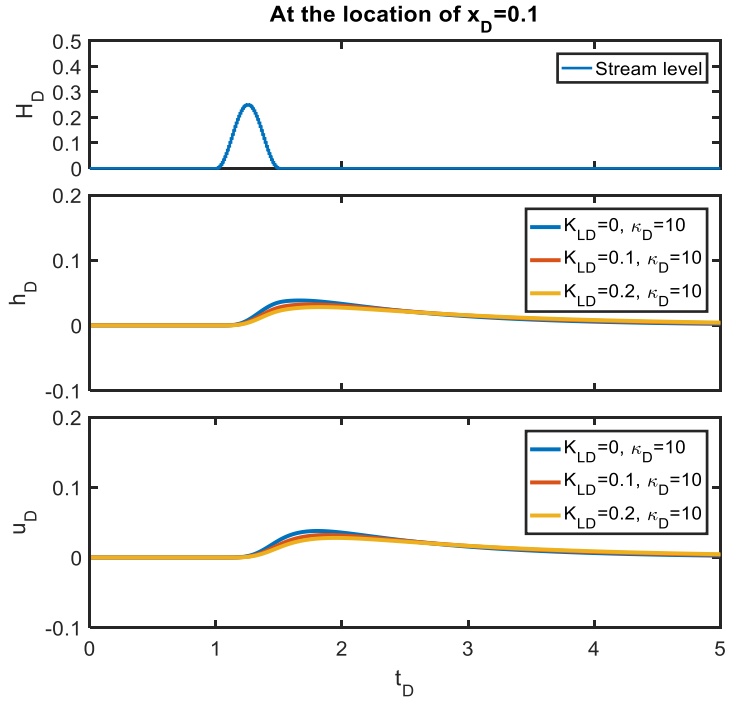

Figure 4. 7 Hydraulic response at the location of $x_D = 0.1$.

4.5.2 Effects of streambed on saturated zone and unsaturated zone flux exchange rate

The simulation parameters for this session are same as Session 4.5.1. Figure 4.8 shows the dimensionless flux exchange rate between the aquifer and the stream. The upper diagram in Figure 4.8 shows the stream water level fluctuation. The middle diagram in Figure 4.8 shows the saturated zone exchange with the stream and the lower diagram in Figure 4.8 shows the unsaturated zone exchange with the stream. Negative value of exchange rate means the water flow into the aquifer and positive value of exchange rate means the water flow into the stream. If we compare different K_{LD} value cases in the saturated zone, we can see that the higher K_{LD} value, the lower peak value of exchange rate. During the stream water level rise and fall period, the exchange rate of saturated zone value will start from zero and reach a negative peak value and then come back to a positive peak value and gradually decay to zero afterwards. The lower K_{LD} value is, the faster the whole process is. The $K_{LD} = 0$ case is the case that its exchange rate value changes from 0 to the negative peak value the fastest. For unsaturated zone, the K_{LD} value has similar effect. The higher K_{LD} value will result in a lower exchange rate. We have to point it out that in unsaturated zone, the difference between the peak value of the $K_{LD} = 0.1$ case and the $K_{LD} = 0$ case is larger than that between the peak value of the $K_{LD} = 0.1$ case and the $K_{LD} = 0.2$ case. This means the streambed effect is greater in unsaturated zone than that in saturated zone.

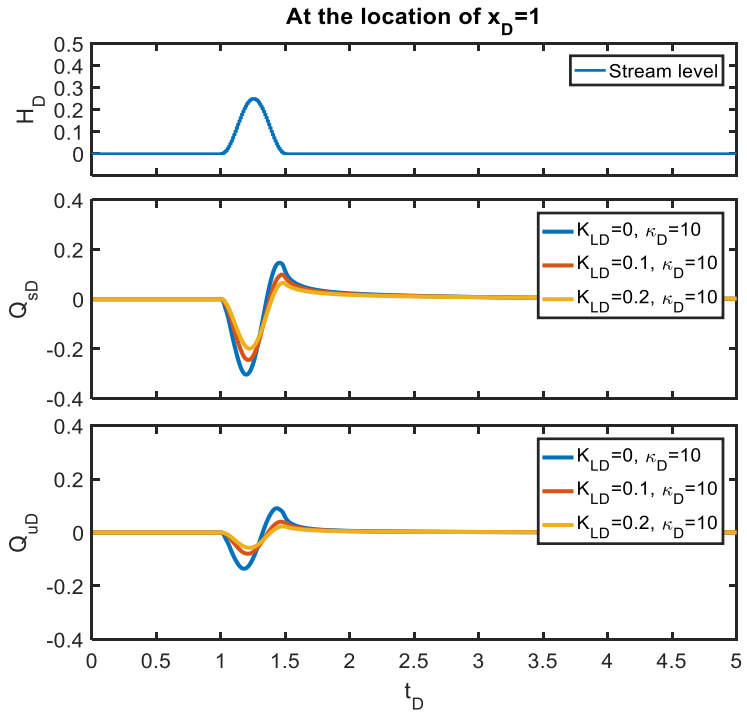

Figure 4. 8 Saturated zone and unsaturated zone flux exchange rate across the streambed. (at the location of $x_D = 1$)

4.5.3 Effects of streambed on bank storage and releasing time

The simulation parameters in this session is the same as Session 4.5.1. The bank storage per unit length of stream at time t is defined as:

$$V = -\int_0^t Q(t)dt.$$

In dimensionless form, the bank storage per unit length of stream in unsaturated zone and saturated zone can be expressed as:

$$V_{uD} = -\int_0^{t_D} Q_{uD}(t_D)dt_D.$$

$$V_{sD} = -\int_0^{t_D} Q_{sD}(t_D)dt_D.$$

So the total bank storage is the sum of unsaturated zone and saturated zone bank storage. In dimensionless form this is written as:

$V_{total} = V_{uD} + V_{sD}$.

Figure 4.9 shows the bank storage for saturated zone (V_{sD}) and unsaturated zone (V_{uD}). The diagram in the middle of Figure 4.9 is the bank storage for saturated zone. In saturated zone, the higher K_{LD} value, the lower bank storage V_{sD} peak value. This means the stream bed will lower the bank storage of the saturated aquifer. This is also true for the unsaturated zone. We also observed that the total volume of water that infiltrated into aquifer is taking more time to flow out of the aquifer for higher K_{LD} value. This means that the harder it is for water to flow from the stream into the aquifer, the less water is released from the aquifer back to the stream. If we compare the unsaturated zone bank storage with saturated zone bank storage, we find that the bank storage in the unsaturated zone is much lower than that in the saturated zone. We also have to point out that for the same K_{LD} value, unsaturated zone bank storage will be much less than that in saturated zone. This means K_{LD} value has a greater effect in unsaturated zone than that in saturated zone.

Another interesting question is that how long it will take for those water that infiltrates the bank to flow back to the stream. To answer this question, we plot V_{sD} and V_{uD} on a semi-log scale in Figure 4.10. We can see that the decaying process for the process after the flood event is nearly a straight line but not exactly. This means the decaying process is very close to exponential decay and we can denote a characteristic releasing time T_r and this T_r will be the time it takes for bank storage water to decay to $\frac{1}{e}$. And the slope of the straight line can be written as: $slope = \frac{1}{T_r}$.

Figure 4.11 shows the characteristic bank storage release time T_r value from the saturated and unsaturated zones following a flood event (after $t_D = 1.5$). We can see that the higher K_{LD} value, the longer release time T_r value for both saturated zone and unsaturated zone. If we compare the difference between the saturated and unsaturated zones, we can see that from $t_D = 1.5$ to $t_D = 2.0$, the release time T_r value for unsaturated zone is lower than that in saturated zone. This tells us that the bank storage releases faster in unsaturated zone.

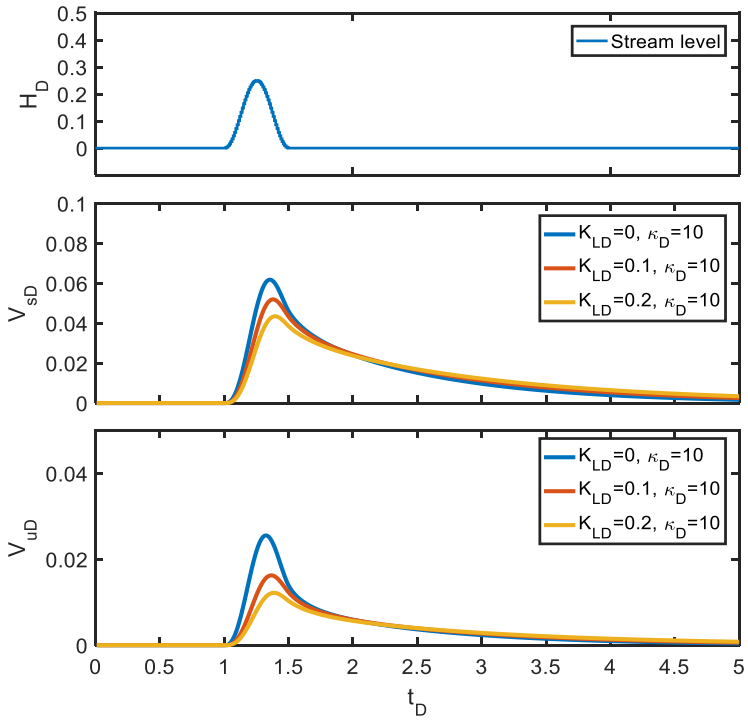

Figure 4. 9 Bank storage in unsaturated zone and saturated zone.

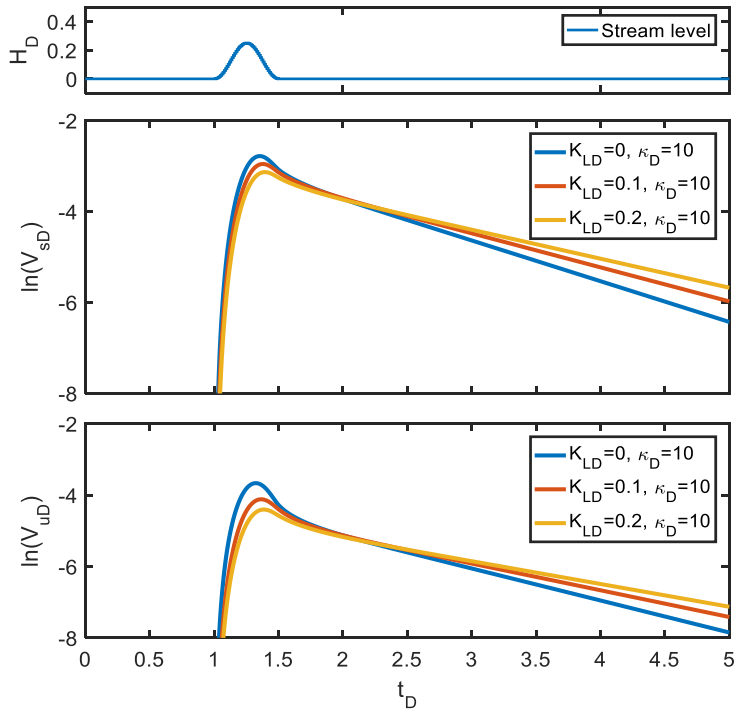

Figure 4. 10 Semi-log plot of bank storage v.s. t_D

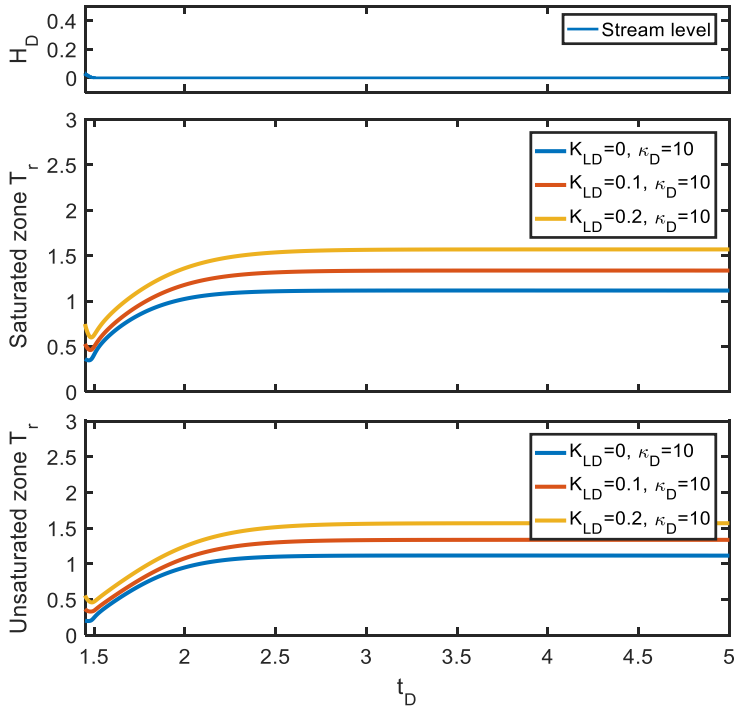

Figure 4. 11 Characteristic releasing time T_r value for unsaturated zone and saturated zone.

4.5.4 Bank storage distribution between saturated zone and unsaturated zone.

The distribution of bank storage in unsaturated zone and saturated zone is shown in Figure 4.12-4.14 with different κ_D value. From Figure 4.12 we can see the higher K_{LD} value will result in higher portion bank storage distribution in saturated zone than the unsaturated zone. It is also obvious that the $K_{LD} = 0.1$ case and $K_{LD} = 0.2$ case curve is relatively close to each other while $K_{LD} = 0$ case curve deviates away from them. This tells us that the initial K_{LD}=0.1 case presents the most effect on the distribution of bank storage between saturated zone and unsaturated zone. Further increase in K_{LD} value does not affect much on the distribution. Besides, if the κ_D value becomes larger, the portion of bank storage distribution in the saturated zone becomes higher too. This is consistent with the κ_D definition, which describes the unsaturated zone effect. The higher the κ_D value, the less the unsaturated zone effect and the saturated zone bank storage portion will become higher. For Figure 4.14, the κ_D value is extremely large, which means the unsaturated zone can be neglected. In this case, no matter what the K_{LD} value is, the portion of bank storage will all be saturated zone. That is why all three different K_{LD} value cases become one single plot.

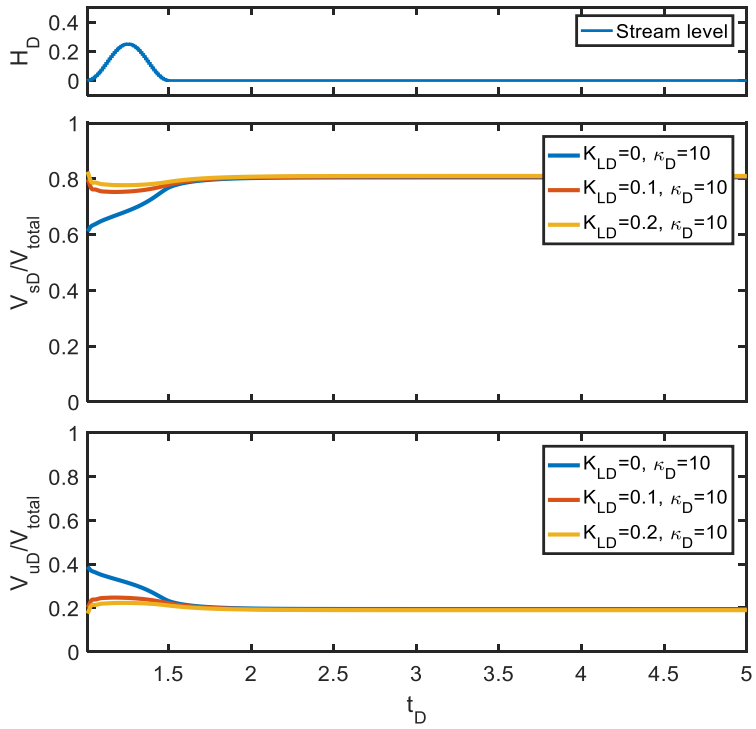

Figure 4. 12 The distribution of storage between unsaturated zone and saturated zone when $\kappa_D = 10$.

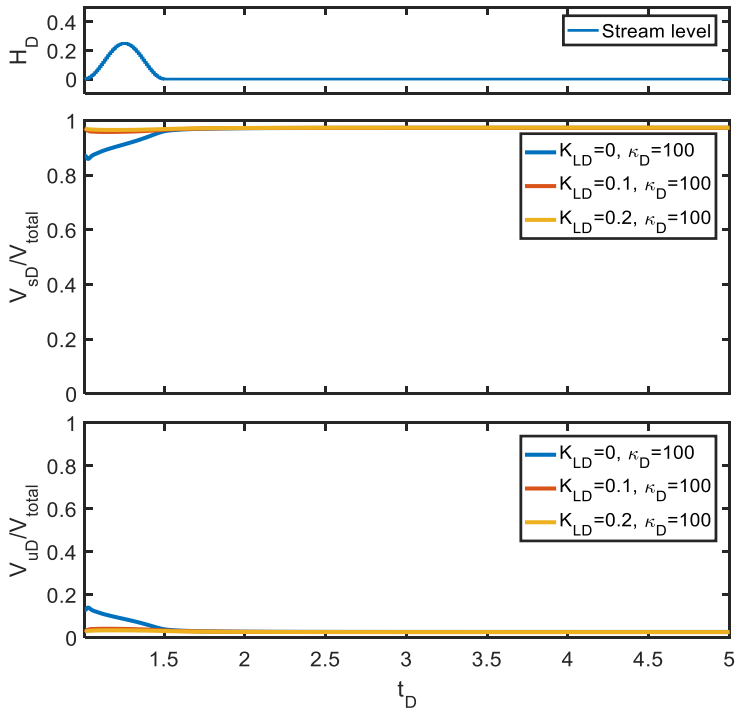

Figure 4. 13 The distribution of storage between unsaturated zone and saturated zone when $\kappa_D = 100$.

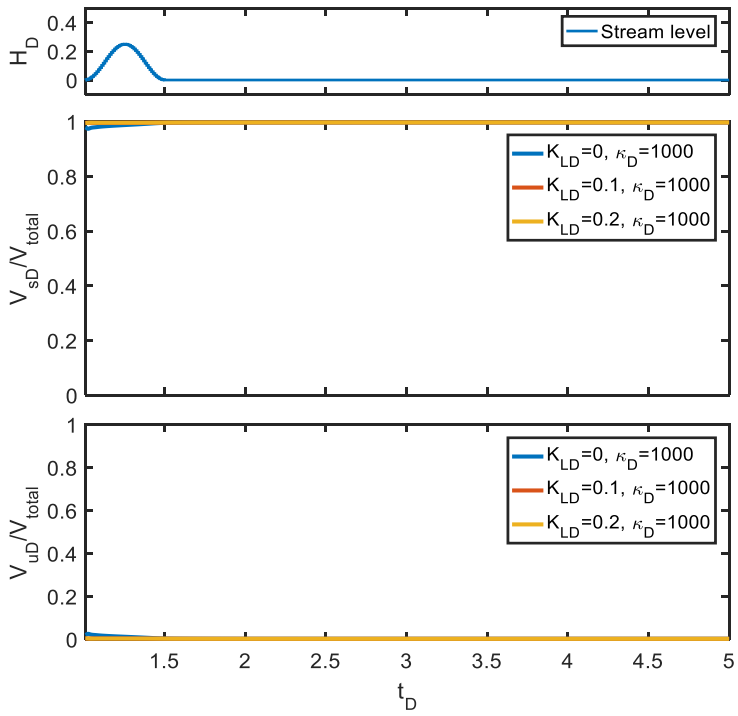

Figure 4. 14 The distribution of storage between unsaturated zone and saturated zone when $\kappa_D = 1000$.

4.5.5 Sensitivity analysis

As an example to test the influence of different parameters on the total discharge, the following technique of sensitivity analysis is employed (Kabala, 2001).

$$SC_{i,j} = I_j \frac{O_i(I_j+\Delta I_j)-O_i(I_j)}{\Delta I_j}, \qquad (9)$$

where $SC_{i,j}$ is the sensitivity coefficient; O_i is the output function of the model. ΔI_j is a small increment; i is the i^{th} time for O_i; j is the j^{th} parameter of the model. In this session, the output function is the dimensionless total discharge. The base value for this session is $L = 100\ m$, $K_x = 1\ m/d$, $K_z = 1\ m/d$, $H_s = 40\ m$, $H_u = 20\ m$, $K_{LD} = 0.1$, $\kappa_D = 10$, $S_y = 0.1$, $S_s = 1 * 10^{-3}\ m$, $I_D = 0$. The analyzed parameters are $K_{LD}, H_{sD}, H_{uD}, \kappa_D, S_y, S_s, K_D$. We choose $\frac{I_j}{\Delta I_j} =$

1000 and plot the $SC_{i,j}$ results in Figure 4.15. From the sensitivity analysis results, we find that the present model is most sensitive to S_s, H_{uD}, moderately sensitive to K_{LD}, κ_D, S_y, K_D , and least sensitive to H_{sD}. The influence from H_{sD}, H_D are positive and the influence from K_{LD} is negative. Similar conclusions can be drawn from sensitivity analysis conducted on any other terms such as the hydraulic heads in the saturated and unsaturated zones.

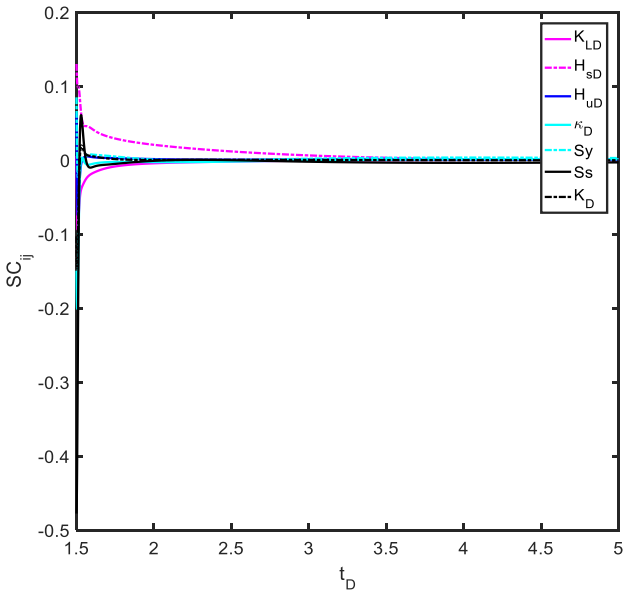

Figure 4. 15 Sensitivity analysis for different model parameters.

4.6 Discussion

The solution derived to describe bank storage in the present study takes into account coupled saturated-unsaturated flow process with the presence of a thin low-permeability streambed. It provides a semi-analytical solution for hydraulic head distribution in both saturated zone and unsaturated zone. It also reveals the streambed effect on bank storage. However, this study has a few notable limitations. For example, the nonlinear Richard's equation governing the

unsaturated flow is linearized using the approach adopted by (Kroszynski and Dagan, 1975). Therefore, all constraints that result from such a linearization must not be forgotten. Those constraints have been documented in previous studies (Kroszynski and Dagan, 1975) very specifically and will not be repeated here. Besides, the unsaturated-saturated interface is assumed to be a fixed horizontal plane. But in reality, it is a spatiotemporally variable moving boundary between unsaturated zone and saturated zone. Thus the hydraulic head change in the saturated zone should be relatively small compared to the saturated zone thickness to get accurate results. For a dramatically varying water table, the proposed semi-analytical solution may have limited capability to provide accurate results. This study is a strict 2D cross-sectional investigation which does not honor the spatial variations of streambed and river stage along the river channel, which is more likely to occur in real applications that require a three-dimensional (3D) approach to deal with. One more thing to point out is that media heterogeneity has not been considered at the present study and may profoundly affect the hydraulic heads and discharges distribution associated with the bank storage in a watershed.

4.7 Conclusion

To study the bank storage effect considering the coupled unsaturated and saturated zone, we first built a 2D conceptual model of flux exchange between an unsaturated-saturated zone and a stream with a thin low-permeability streambed. Then we introduced a mathematical model for the coupled unsaturated and saturated flow processes, and obtained the semi-analytical solutions of spatiotemporal distributions of hydraulic heads in both the saturated and unsaturated zones. We introduce a streambed index, denoted as K_{LD}, to reflect the impact of streambed. It is a dimensionless number defined as the ratio of hydraulic conductance of the saturated zone in

horizontal flow direction to the conductance of streambed, where the hydraulic conductance is defined as the ratio of hydraulic conductivity over the distance of flow. In addition, this study analyzes the timing of bank storage release under different streambed index cases. Here are some principal findings:

1. When the streambed has a lower hydraulic conductance, the hydraulic head response due to a flood event is smaller. The hydraulic head response in present solution is smaller than the Liang solution due to the streambed impact. For hydraulic head responses in aquifer, the K_{LD} value has a greater impact in the region near the stream.
2. A higher streambed index K_{LD} value will lead to a lower peak value of flux exchange rate between the aquifer and the stream. The total bank storage volume will also be smaller.
3. The bank storage release time is slightly shorter from the unsaturated zone than that from the saturated zone, which means water releases faster in unsaturated zone than that in saturated zone.
4. The distribution of bank storage between saturated zone and unsaturated zone can be influenced by a thin layer of stream (small K_{LD} value) or κ_D value, which is a description of unsaturated zone effect.

5. SUMMARY

5.1 Summary and conclusions

In this dissertation, we investigated the air compressibility on the Bouwer and Rice seepage meter, the process of baseflow to a stream with a low hydraulic conductivity thin layer streambed, and the bank storage effect in unsaturated and saturated zone with a streambed.

In the air compressibility on the Bouwer and Rice seepage meter study, a correction for calculating the seepage flux rate is provided, which considers the air compressibility inside the manometer of a B&R seepage meter. Previous works of Bouwer and Rice (1963) and Wang et al. (2014) excluded the effect of air compressibility. It will generate errors if the air compressibility is not taken into consideration under some cases. We calculated the error for ignoring the air compressibility in experiments of Wang et al. (2014) for the suction mode, and extended the calculation for two more cases for the no-suction mode.

For investigating the process of baseflow release to a stream with a low hydraulic conductivity thin layer streambed, a 2D conceptual model of baseflow from an unsaturated-saturated zone to a stream with a thin low-permeability streambed was developed. With the help of this conceptual model, we can try to understand the influence of a streambed on baseflow in a watershed scale. After having the conceptual model, a mathematical model for the coupled unsaturated and saturated flow processes is established. Then we obtained the semi-analytical solutions of spatiotemporal distributions of hydraulic heads and discharges in both the saturated and unsaturated zones. We introduced a streambed index, which defined as the ratio of hydraulic conductance of the saturated zone to that of the streambed for horizontal flow. This streambed index will be the key parameter to reflect the impact of a streambed.

For Bank storage effect study to consider the coupled unsaturated and saturated zone, a 2D conceptual model of flux exchange between an unsaturated-saturated zone and a stream with a thin low-permeability streambed is established. Mathematical model for the coupled unsaturated and saturated flow processes is also introduced and the semi-analytical solutions of spatiotemporal distributions of hydraulic heads in both the saturated and unsaturated zones are obtained. Streambed index, which reflects the impact of streambed, is studied for bank storage effect. The releasing time of bank storage under different streambed index cases are investigated within the scope of research.

The following conclusions can be drawn:

1. The effect of air compressibility in the manometer increases with the volume of air in the manometer. Applying suction to the manometer reduces the air compressibility effect and is preferred. The correction of this study will work as a quantitative tool to determine if air compressibility can be neglected or not for a B&R seepage meter test with and without suction applied.
2. When the streambed has a lower hydraulic conductance, the hydraulic head response due to an infiltration event is greater. The present solution is greater than the Liang solution due to the streambed impact. A higher streambed index K_{LD} value will lead to a lower peak value of the total discharge rate to the stream. The K_{LD} value will not change the total discharge volume. The relative ratio of the discharge rate in a stream with a streambed and one without a streambed monotonically increases as a function of time. The presence of a low-K streambed will increase the late time baseflow flux. The ratio of horizontal flow velocity to vertical flow velocity is high when observation point is close to the stream. Streambed has an effect on such a ratio,

particularly for locations close to the stream. During the infiltration event, such a ratio is much lower in the unsaturated zone than that in the saturated zone. The peak value of the total discharge rate at the early time is lowered and the baseflow decaying process is prolonged when there is a streambed than the case without a streambed. In slope recession hydrograph analysis, the streambed affects early time slope and has little impact on late time slope. This results in an underestimation of hydraulic conductivity K, specific yield S_y and saturated aquifer thickness H_s if the streambed effect is not considered in the analysis.

3. When the streambed has a lower hydraulic conductance, the hydraulic head response due to a flood event is smaller. The hydraulic head response of the present solution is smaller than that of the Liang solution due to the streambed impact. The K_{LD} value has a greater impact in regions closer to the stream. A higher streambed index K_{LD} value will lead to a lower peak value of flux exchange rate between the aquifer and the stream. The total bank storage volume will also be smaller. The bank storage releasing time is slightly shorter in the unsaturated zone than that in the saturated zone. The distribution of bank storage between the saturated and unsaturated zones can be influenced by the stream index and the unsaturated flow process (reflected in the κ_D value).

5.2 Contribution

The contribution of this study can be summarized as follows:

1. This dissertation for the first time bring in a quantitative tool to determine if air compressibility can be neglected or not for a B&R seepage meter test with and without suction applied.
2. This study provides rigorous semi-analytical solutions for a 2D conceptual model of flux exchange between an unsaturated-saturated zone and a stream with a thin low-permeability streambed. It helps to understand the impact of streambed on baseflow in a watershed scale. It first introduced a streambed index, which is a key parameter for studying the impact of streambed. In addition, this study provides a comprehensive analysis of the relative importance of horizontal versus vertical flow in the unsaturated and saturated zones as a function of space and time.
3. This study is the first attempt ever to include the interaction of streambed with saturated-unsaturated flow processes analytically in bank storage studies. This study also applies the streambed index concept to bank storage.

5.3 Future scope

Up to now, most of the Bouwer and Rice seepage meter studies have not considered the temperature effect. If temperature is found to change considerably during the experiment, its effect on air compressibility may have to be taken into account. In the future work, further investigation of temperature on B&R seepage meter could be studied. For baseflow recession studies, media heterogeneity has not been considered at the present study and may profoundly affect the hydraulic heads and discharges distribution associated with the baseflow process in a watershed. Additionally, surface topography is also likely to be an influence factor in an actual

watershed, so the combined effects of surface topography, heterogeneity, coupled unsaturated-saturated flow, and streambed on baseflow could be a direction to investigate. In the future, it will be useful to check if the methodology and conclusions of this study still hold if a different constitutive model is used.

REFERENCES

Belanger, T.V., Montgomery, M.T., 1992. Seepage Meter Errors. Limnology and Oceanography, 37(8): 1787-1795.

Boulton, A.J., Findlay, S., Marmonier, P., Stanley, E.H., Valett, H.M., 1998. The functional significance of the hyporheic zone in streams and rivers. Annu Rev Ecol Syst, 29: 59-81. DOI:DOI 10.1146/annurev.ecolsys.29.1.59

Boussinesq, J., 1877. Essai sur la théorie des eaux courantes. Imprimerie nationale.

Boussinesq, J., 1903a. Sur le débit, en temps de sécheresse, d'une source alimentée par une nappe d'eaux d'infiltration. CR Hebd. Seanc. Acad. Sci. Paris, 136: 1511-1517.

Boussinesq, J., 1903b. Théorie analytique de la chaleur: mise en harmonie avec la thermodynamique et avec la théorie mécanique de la lumière, 2. Gauthier-Villars.

Boussinesq, J., 1904. Recherches théoriques sur l'écoulement des nappes d'eau infiltrées dans le sol et sur le débit des sources. Journal de mathématiques pures et appliquées, 10: 5-78.

Bouwer, H., Rice, R.C., 1963. Seepage meters in seepage and recharge studies. Journal of the Irrigation and Drainage Division, 89(1): 17-42.

Brooks, R.H., Corey, A.T., 1966. Properties of porous media affecting fluid flow. Journal of the Irrigation and Drainage Division, 92(2): 61-90.

Brunner, P., Cook, P.G., Simmons, C.T., 2009a. Hydrogeologic controls on disconnection between surface water and groundwater. Water Resources Research, 45(1): n/a-n/a. DOI:10.1029/2008wr006953

Brunner, P., Cook, P.G., Simmons, C.T., 2011. Disconnected surface water and groundwater: from theory to practice. Ground Water, 49(4): 460-467. DOI:10.1111/j.1745-6584.2010.00752.x

Brunner, P., Simmons, C.T., Cook, P.G., 2009b. Spatial and temporal aspects of the transition from connection to disconnection between rivers, lakes and groundwater. Journal of Hydrology, 376(1-2): 159-169. DOI:10.1016/j.jhydrol.2009.07.023

Brutsaert, W., Lopez, J.P., 1998. Basin-scale geohydrologic drought flow features of riparian aquifers in the southern Great Plains. Water Resources Research, 34(2): 233-240. DOI:10.1029/97wr03068

Brutsaert, W., Nieber, J.L., 1977. Regionalized Drought Flow Hydrographs from a Mature Glaciated Plateau. Water Resources Research, 13(3): 637-644. DOI:10.1029/WR013i003p00637

Burden, R.L., Faires, J.D., 2010. Numerical Analysis, , 9th ed. New York: Brooks/Cole.

Carr, M.R., Winter, T.C., 1980. An annotated bibliography of devices developed for direct measurement of seepage. 2331-1258, US Dept. of the Interior, Geological Survey.

Chen, X., Chen, X.H., 2003. Stream water infiltration, bank storage, and storage zone changes due to stream-stage fluctuations. Journal of Hydrology, 280(1-4): 246-264. DOI:10.1016/S0022-1694(03)00232-4

Cherkauer, D.A., McBride, J.M., 1988. A Remotely Operated Seepage Meter for Use in Large Lakes and Rivers. Ground Water, 26(2): 165-171. DOI:10.1111/j.1745-6584.1988.tb00379.x

de Hoog, F.R., Knight, J.H., Stokes, A.N., 1982. An Improved Method for Numerical Inversion of Laplace Transforms. Siam J Sci Stat Comp, 3(3): 357-366. DOI:Doi 10.1137/0903022

Doble, R., Brunner, P., McCallum, J., Cook, P.G., 2012. An Analysis of River Bank Slope and Unsaturated Flow Effects on Bank Storage. Ground Water, 50(1): 77-86. DOI:10.1111/j.1745-6584.2011.00821.x

Domenico, P.A., Schwartz, F.W., 1998. Physical and chemical hydrogeology, 506. Wiley New York.

Fetter, C., 2001. Applied Hydrogeology (4 th). Supplemental website http://www. appliedhydrogeology. info. Upper Saddle River, NJ: Prentice Hall: 598.

Freeze, R.A., Cherry, J.A., 1979. Groundwater, Prentice Hall Inc., Upper Saddle River.

Gardner, W.R., 1958. Some Steady-State Solutions of the Unsaturated Moisture Flow Equation with Application to Evaporation from a Water Table. Soil Science, 85(4): 228-232. DOI:10.1097/00010694-195804000-00006

Ghosh, D.K., Wang, D., Zhu, T., 2016. On the transition of base flow recession from early stage to late stage. Advances in Water Resources, 88: 8-13. DOI:10.1016/j.advwatres.2015.11.015

Guo, W.X., 1997. Transient groundwater flow between reservoirs and water-table aquifers. Journal of Hydrology, 195(1-4): 370-384. DOI:Doi 10.1016/S0022-1694(96)03200-3

Hall, F.R., 1968. Base-Flow Recessions-A Review. Water Resources Research, 4(5): 973-983. DOI:10.1029/WR004i005p00973

Hatch, C.E., Fisher, A.T., Ruehl, C.R., Stemler, G., 2010. Spatial and temporal variations in streambed hydraulic conductivity quantified with time-series thermal methods. Journal of Hydrology, 389(3-4): 276-288. DOI:10.1016/j.jhydrol.2010.05.046

Hendricks, D., Warnick, C., 1961. A study of the control of canal seepage. Engineering Experiment Station, University of Idaho.

Hilberts, A.G.J., Troch, P.A., Paniconi, C., 2005. Storage-dependent drainable porosity for complex hillslopes. Water Resources Research, 41(6). DOI:10.1029/2004wr003725

Hollenbeck, K., 1998. A matlab function for numerical inversion of Laplace transforms by the de Hoog algorithm.

Huang, C.-S., Tsou, P.-R., Yeh, H.-D., 2012. An analytical solution for a radial collector well near a stream with a low-permeability streambed. Journal of Hydrology, 446-447: 48-58. DOI:10.1016/j.jhydrol.2012.04.028

Huang, Y., Zhou, Z.-f., Yu, Z.-b., 2010. Analytical solution based on stream-aquifer interactions in partially penetrating streams. Water Science and Engineering, 3(3): 292-303. DOI:https://doi.org/10.3882/j.issn.1674-2370.2010.03.005

Irvine, D.J., Brunner, P., Franssen, H.-J.H., Simmons, C.T., 2012. Heterogeneous or homogeneous? Implications of simplifying heterogeneous streambeds in models of losing streams. Journal of Hydrology, 424-425: 16-23. DOI:10.1016/j.jhydrol.2011.11.051

Israelsen, O.W., Reeve, R.C., 1944. Canal lining experiments in the delta area, Utah.

Jepsen, S.M., Harmon, T.C., Shi, Y., 2016. Watershed model calibration to the base flow recession curve with and without evapotranspiration effects. Water Resources Research, 52(4): 2919-2933. DOI:10.1002/2015wr017827

Kabala, Z.J., 2001. Sensitivity analysis of a pumping test on a well with wellbore storage and skin. Advances in Water Resources, 24(5): 483-504. DOI:10.1016/s0309-1708(00)00051-8

Kalbus, E., Schmidt, C., Molson, J.W., Reinstorf, F., Schirmer, M., 2009. Influence of aquifer and streambed heterogeneity on the distribution of groundwater discharge. Hydrol Earth Syst Sc, 13(1): 69-77. DOI:10.5194/hess-13-69-2009

Kong, J., Shen, C.J., Luo, Z.Y., Hua, G.F., Zhao, H.J., 2016. Improvement of the hillslope-storage Boussinesq model by considering lateral flow in the unsaturated zone. Water Resources Research, 52(4): 2965-2984. DOI:10.1002/2015wr018054

Kroszynski, U.I., Dagan, G., 1975. Well pumping in unconfined aquifers: The influence of the unsaturated zone. Water Resources Research, 11(3): 479-490. DOI:10.1029/WR011i003p00479

Lee, D.R., 1977. A device for measuring seepage flux in lakes and estuaries1. Limnology and Oceanography, 22(1): 140-147. DOI:10.4319/lo.1977.22.1.0140

Lee, D.R., Cherry, J.A., 1979. A field exercise on groundwater flow using seepage meters and mini-piezometers. Journal of Geological Education, 27(1): 6-10.

Liang, X., Zhan, H., Zhang, Y.-K., Schilling, K., 2017. Base flow recession from unsaturated-saturated porous media considering lateral unsaturated discharge and aquifer compressibility. Water Resources Research, 53(9): 7832-7852. DOI:10.1002/2017wr020938

Liang, X., Zhan, H., Zhang, Y.-K., Schilling, K., 2018. Reply to Comment by Roques et al. on "Base Flow Recession from Unsaturated-Saturated Porous Media considering Lateral Unsaturated Discharge and Aquifer Compressibility". Water Resources Research. DOI:10.1002/2017wr022378

Murdoch, L.C., Kelly, S.E., 2003. Factors affecting the performance of conventional seepage meters. Water Resources Research, 39(6). DOI:10.1029/2002wr001347

Pauwels, V.R.N., Troch, P.A., 2010. Estimation of aquifer lower layer hydraulic conductivity values through base flow hydrograph rising limb analysis. Water Resources Research, 46(3). DOI:10.1029/2009wr008255

Peng, X., Zhan, H., 2017. Air Compressibility Effect on Bouwer and Rice Seepage Meter. Ground Water, 55(6): 899-905. DOI:10.1111/gwat.12550

Robinson, A., Rohwer, C., 1952. Study of seepage losses from irrigation channels. US Department of Agriculture, Soil Conservation Service Progress Report, 42.

Roques, C., Rupp, D.E., Jachens, E., Selker, J.S., 2018. Comment on "Base Flow Recession from Unsaturated-Saturated Porous Media considering Lateral Unsaturated Discharge and Aquifer Compressibility" by Liang, X., H. Zhan, Y.-K. Zhang, and K. Schilling (2017). Water Resources Research. DOI:10.1002/2017wr022085

Rosenberry, D.O., 2008. A seepage meter designed for use in flowing water. Journal of Hydrology, 359(1-2): 118-130. DOI:10.1016/j.jhydrol.2008.06.029

Rosenberry, D.O., Pitlick, J., 2009. Local-scale variability of seepage and hydraulic conductivity in a shallow gravel-bed river. Hydrological Processes, 23(23): 3306-3318. DOI:10.1002/hyp.7433

Rupp, D.E., Selker, J.S., 2005. Drainage of a horizontal Boussinesq aquifer with a power law hydraulic conductivity profile. Water Resources Research, 41(11). DOI:10.1029/2005wr004241

Rupp, D.E., Selker, J.S., 2006a. Information, artifacts, and noise in dQ/dt-Q recession analysis. Advances in Water Resources, 29(2): 154-160. DOI:10.1016/j.advwatres.2005.03.019

Rupp, D.E., Selker, J.S., 2006b. On the use of the Boussinesq equation for interpreting recession hydrographs from sloping aquifers. Water Resources Research, 42(12). DOI:10.1029/2006wr005080

Schilling, O.S., Irvine, D.J., Hendricks Franssen, H.-J., Brunner, P., 2017. Estimating the Spatial Extent of Unsaturated Zones in Heterogeneous River-Aquifer Systems. Water Resources Research, 53(12): 10583-10602. DOI:10.1002/2017wr020409

Sebok, E., Duque, C., Engesgaard, P., Boegh, E., 2015. Spatial variability in streambed hydraulic conductivity of contrasting stream morphologies: channel bend and straight channel. Hydrological Processes, 29(3): 458-472. DOI:10.1002/hyp.10170

Singh, K.P., 1968. Some Factors Affecting Baseflow. Water Resources Research, 4(5): 985-999. DOI:10.1029/WR004i005p00985

Solder, J.E., Gilmore, T.E., Genereux, D.P., Solomon, D.K., 2016. A Tube Seepage Meter for In Situ Measurement of Seepage Rate and Groundwater Sampling. Ground Water, 54(4): 588-95. DOI:10.1111/gwat.12388

Sophocleous, M., 2002. Interactions between groundwater and surface water: the state of the science. Hydrogeology Journal, 10(1): 52-67. DOI:10.1007/s10040-001-0170-8

Szilagyi, J., Parlange, M.B., 1998. Baseflow separation based on analytical solutions of the Boussinesq equation. Journal of Hydrology, 204(1-4): 251-260. DOI:10.1016/s0022-1694(97)00132-7

Szilagyi, J., Parlange, M.B., Albertson, J.D., 1998. Recession flow analysis for aquifer parameter determination. Water Resources Research, 34(7): 1851-1857. DOI:10.1029/98wr01009

Taniguchi, M. et al., 2003. Spatial and temporal distributions of submarine groundwater discharge rates obtained from various types of seepage meters at a site in the Northeastern Gulf of Mexico. Biogeochemistry, 66(1-2): 35-53. DOI:DOI 10.1023/B:BIOG.0000006090.25949.8d

Taniguchi, M., Fukuo, Y., 1993. Continuous Measurements of Ground-Water Seepage Using an Automatic Seepage Meter. Ground Water, 31(4): 675-679. DOI:10.1111/j.1745-6584.1993.tb00601.x

Tartakovsky, G.D., Neuman, S.P., 2007. Three-dimensional saturated-unsaturated flow with axial symmetry to a partially penetrating well in a compressible unconfined aquifer. Water Resources Research, 43(1). DOI:10.1029/2006WR005153

Troch, P.A., Detroch, F.P., Brutsaert, W., 1993. Effective water-table depth to describe initial conditions prior to storm rainfall in humid regions. Water Resources Research, 29(2): 427-434. DOI:10.1029/92wr02087

Troch, P.A., Paniconi, C., van Loon, E.E., 2003. Hillslope-storage Boussinesq model for subsurface flow and variable source areas along complex hillslopes: 1. Formulation and characteristic response. Water Resources Research, 39(11): 1316, doi:10.1029/2002WR001728. DOI:10.1029/2002wr001728

van de Giesen, N., Steenhuis, T.S., Parlange, J.Y., 2005. Short- and long-time behavior of aquifer drainage after slow and sudden recharge according to the linearized Laplace equation. Advances in Water Resources, 28(10): 1122-1132. DOI:10.1016/j.advwatres.2004.12.002

van Genuchten, M.T., 1980. A closed-form equation for predicting the hydraulic conductivity of unsaturated soils. Soil science society of America journal, 44(5): 892-898.

Wang, W.K. et al., 2014. Estimating streambed parameters for a disconnected river. Hydrological Processes, 28(10): 3627-3641. DOI:10.1002/hyp.9904

Warnick, C., 1951. Methods of measuring seepage loss in irrigation canals. Engineering Experiment Station, University of Idaho.

Yamada, H., Nakamura, F., Watanabe, Y., Murakami, M., Nogami, T., 2005. Measuring hydraulic permeability in a streambed using the packer test. Hydrological Processes, 19(13): 2507-2524. DOI:10.1002/hyp.5688

Zhu, T., Fu, D., Jenkinson, B., Jafvert, C.T., 2015. Calibration and application of an automated seepage meter for monitoring water flow across the sediment-water interface. Environ Monit Assess, 187(4): 171. DOI:10.1007/s10661-015-4388-7

Zlotnik, V.A., Huang, H., 1999. Effect of shallow penetration and streambed sediments on aquifer response to stream stage fluctuations (analytical model). Ground Water, 37(4): 599-605. DOI:DOI 10.1111/j.1745-6584.1999.tb01147.x

APPENDIX A

DERIVATION OF SEEPAGE RATE USING EQUATION 2. (2) CONSIDERING AIR COMPRESSIBILITY:

We use Boyle's ideal gas law to address air compressibility:

$$P_a V_a = C, \tag{A1}$$

where Pa and Va are respectively the air pressure and air volume at a given constant temperature inside the manometer, and C denotes a constant. If the manometer's cross-section area is σ, water levels in tube A and tube B are denoted as hA and hB, respectively, the height of the manometer is H and the bottom of the manometer is set at the stream water surface, then the volume of air in the manometer is as follow:

$$V_a = \sigma(2H - h_A - h_B). \tag{A2}$$

Taking the derivative of equation (A1), one has:

$$\frac{dP_a}{P_a} = -\frac{dV_a}{V_a}, \tag{A3}$$

here dPa and dVa are respectively the air pressure and volume changes during a short period of time. Note that dPa is negative because the air pressure in the manometer is decreasing while air volume is increased.

Differentiation of equation (A2) leads to:

$$\frac{dV_a}{V_a} = \frac{-dh_A - dh_B}{2H - h_A - h_B}, \tag{A4}$$

here dhA and dhB are respectively the changes of water levels in tube A and tube B, and dhA is negative while dhB is positive.

Air pressure in the manometer can be written as:

$$P_a = P_0 - \rho g h_B, \tag{A5}$$

where the constant air pressure above stream water surface is noted as P0 (101.3 kPa), ρ is water density (998.2 kg/m3 at 20 °C), and g is acceleration constant (9.81 m/s2).

Taking the derivative of equation (A5) leads to:

$$dP_a = -\rho g dh_B. \tag{A6}$$

From equations (A3)-(A6), one can have:

$$\frac{dh_B}{-(P_0/\rho g)+h_B} = \frac{dh_A + dh_B}{2H - h_A - h_B}. \tag{A7}$$

Reorganizing equation (A7) leads to:

$$-\frac{dh_A}{dh_B} = \frac{2H - h_A - 2h_B + (P_0/\rho g)}{(P_0/\rho g) - h_B} = 1 + \frac{2H - h_A - h_B}{(P_0/\rho g) - h_B} = 1 + \kappa, \tag{A8}$$

where

$$\kappa = \frac{2H - h_A - h_B}{(P_0/\rho g) - h_B}. \tag{A9}$$

The numerator of the right side of equation (A9) actually stands for the total length of air inside the manometer, and it is always positive. The denominator of the right side of equation (A9) is always positive as well, because ($P_0/\rho g$) term is 10.34 m and hB is smaller than the height of the manometer H, which is much less than 10.34 m. κ can be regarded as a correction term due to the air compressibility in the manometer. If the air compressibility effect is neglected, κ=0; otherwise, κ is positive.

If we rewrite equation (A1) using equation (A2) and equation (A5), we can have:

$$(P_0 - \rho g h_B)(2H - h_A - h_B) = C/\sigma. \tag{A10}$$

The right side of equation (A10) is a constant, so the left side of equation (A10) is also a constant.

To show how the correction term κ affects the new seepage flux (V_e'), one needs to know the relationship between the new seepage flux rate (V_e') and the rate of water level change in the manometer tube A. From equation (A6), one can see that the air pressure inside the manometer is decreased by -dPa. Since the water level in the manometer tube A is decreased by -dhA, the hydraulic head in the seepage bell must have decreased by$-dP_a - \rho g dh_A$. Therefore, the pressure balance inside the seepage bell leads to:

$$-dP_a - \rho g dh_A = -\rho g dh, \tag{A11}$$

where dh is the water-level decrease in the falling-head reservoir during a short period of time. If the manometer tube diameter is small enough and it can be ignored when compared to the falling head reservoir diameter, the seepage rate V_e' should be the same as the falling head reservoir water level falling rate ($-dh/dt$):

$$V_e' = -dh/dt. \tag{A12}$$

From equations (A6) and (A11), one gets

$$dh = dh_A - dh_B. \tag{A13}$$

Combining equations (A8), (A12) and (A13), one can get

$$V_e' = \frac{2+\kappa}{1+\kappa}\left(-\frac{dh_A}{dt}\right) = \frac{2+\kappa}{1+\kappa}V_s, \tag{A14}$$

where Vs is the absolute value of slope of curve A at the intersection point 1 in Figure 2.3.

APPENDIX B

DERIVATION OF EQUATIONS (3.5a), (3.5b), (3.6a) AND (3.6b)

For saturated zone, after nondimensionalization, governing equation and the associated initial and boundary conditions can be written as:

$$\frac{\partial^2 h_D}{\partial x_D^2} + K_D \frac{\partial^2 h_D}{\partial z_D^2} = \frac{\partial h_D}{\partial t_D}, \; -H_{sD} \le z_D < 0, \tag{B.1a}$$

$$h_D(x_D, z_D, 0) = 0, \tag{B.1b}$$

$$\frac{\partial h_D}{\partial x_D}(x_D, z_D, t_D)|_{x_D=0} = 0, \tag{B.1c}$$

$$h_D(1, z_D, t_D) - H_D(t_D) = -K_{LD} \frac{\partial h_D}{\partial x_D}(1, z_D, t_D), \tag{B.1d}$$

$$\frac{\partial h_D}{\partial z_D}(x_D, z_D, t_D)|_{z_D=-H_{sD}} = 0. \tag{B.1e}$$

Conducting the Laplace transform, one has:

$$\frac{\partial^2 \bar{h}_D}{\partial x_D^2} + K_D \frac{\partial^2 \bar{h}_D}{\partial z_D^2} = p\bar{h}_D, \; -H_{sD} \le z_D \le 0, \tag{B.2a}$$

$$\frac{\partial \bar{h}_D}{\partial x_D}(x_D, z_D, p)|_{x_D=0} = 0, \tag{B.2b}$$

$$\bar{h}_D(1, z_D, p) - \bar{H}_D(p) = -K_{LD} \frac{\partial \bar{h}_D}{\partial x_D}(1, z_D, t_D), \tag{B.2c}$$

$$\frac{\partial \bar{h}_D}{\partial z_D}(x_D, z_D, p)|_{z_D=-H_{sD}} = 0, \tag{B.2d}$$

where the overhead bar represents the term in Laplace domain, *p* is the Laplace transform parameter in respect to the dimensionless time. Using the following variable substitution:

$$\bar{h}_{D2}(x_D, z_D, p) = \bar{h}_D(x_D, z_D, p) - \bar{H}_D(p), \tag{B.3}$$

Then equations (B.2a)-(B.2d) become:

$$\frac{\partial^2 \bar{h}_{D2}}{\partial x_D^2} + K_D \frac{\partial^2 \bar{h}_{D2}}{\partial z_D^2} = p\bar{h}_{D2} + p\bar{H}_D(p), \; -H_{sD} \le z_D \le 0, \tag{B.4a}$$

$$\frac{\partial \bar{h}_{D2}}{\partial x_D}(x_D, z_D, p)|_{x_D=0} = 0, \tag{B.4b}$$

$$\bar{h}_{D2}(1, z_D, p) = -K_{LD} \frac{\partial \bar{h}_{D2}}{\partial x_D}(1, z_D, t_D), \quad \text{(B.4c)}$$

$$\frac{\partial \bar{h}_{D2}}{\partial z_D}(x_D, z_D, p)|_{z_D=-H_{sD}} = 0, \quad \text{(B.4d)}$$

The Cosine transform of $\bar{h}_{D2}(x_D, z_D, p)$ can be defined as

$$\tilde{\bar{h}}_{D2}(z_D, p) = \int_0^1 \bar{h}_{D2}(x_D, z_D, p) A_n \cos(\omega_n x_D) dx_D, \quad \text{(B.5a)}$$

where A_n is a coefficient, $\omega_n$is a frequency, both to be determined based on the boundary conditions. The corresponding inversion formula is defined as

$$\bar{h}_{D2}(x_D, z_D, p) = \sum_{n=0}^{\infty} \tilde{\bar{h}}_{D2}(z_D, p) A_n \cos(\omega_n x_D), \quad \text{(B.5b)}$$

where *n* is a non-negative integer. Substituting equation (B.5b) into equation (B.4c) leads to:

$$\sum_{n=0}^{\infty} \tilde{\bar{h}}_{D2}(z_D, p) A_n cos(\omega_n x_D)|_{x_D=1} = -K_{LD} \sum_{n=0}^{\infty} \tilde{\bar{h}}_{D2}(z_D, p) A_n (-\omega_n) sin(\omega_n x_D)\,|_{x_D=1}\,, \quad \text{(B.6a)}$$

which can be rearranged into:

$$\sum_{n=0}^{\infty} \tilde{\bar{h}}_{D2}(z_D, p) A_n (cos(\omega_n) - K_{LD} \omega_n\, sin(\omega_n)) = 0. \quad \text{(B.6b)}$$

Then we will have:

$$cos(\omega_n) - K_{LD} \omega_n\, sin(\omega_n) = 0, \quad \text{(B.6c)}$$

which means:

$$\omega_n\, tan(\omega_n) = \frac{1}{K_{LD}}. \quad \text{(B.6d)}$$

Equation (B.6d) is for calculating ω_n.

Now multiplying equation (B.5b) by $A_m cos(\omega_m x_D)$ and integrating from 0 to 1 to get:

$$\tilde{\bar{h}}_{D2}(z_D, p) = \int_0^1 \sum_{n=0}^{\infty} \tilde{\bar{h}}_{D2}(z_D, p) A_n \cos(\omega_n x_D)\, A_m \cos(\omega_m x_D) dx_D\,. \quad \text{(B.7a)}$$

So only when $m = n$ the integral is non-zero and we will have:

$$A_n^2 \left(\frac{1}{2} + \frac{sin(2\omega_n)}{4\omega_n}\right) = 1. \quad \text{(B.7b)}$$

Equation (B.7b) is for calculating A_n.

Multiplying equation (B.4a) by $A_n cos(\omega_n x_D)$, and integrating from 0 to 1 to get:

$$-\omega_n^2 \bar{\tilde{h}}_{D2} + K_D \frac{d^2 \bar{\tilde{h}}_{D2}}{dz_D^2} = p\bar{\tilde{h}}_{D2} + \frac{p\bar{H}_D(p)A_n sin\omega_n}{\omega_n}, \ -H_{sD} \le z_D \le 0, \qquad \text{(B.8a)}$$

The solution for equation (B.8a) can be written as:

$$\bar{\tilde{h}}_{D2} = C_1\, exp(-\Omega_n z_D) + C_2\, exp(\Omega_n z_D) - \frac{p\bar{H}_D(p)A_n sin\omega_n}{(\omega_n^2+p)\omega_n}, \qquad \text{(B.9)}$$

where $\Omega_n = \sqrt{\frac{\omega_n^2+p}{K_D}}$, C_1 and C_2 are z-independent variables and will be evaluated later.

So the solution for equation (B.2a) can be written as:

$$\bar{h}_D(x_D, z_D, p) = \bar{H}_D(p) + \sum_{n=0}^{\infty} \Big[C_1\, exp(-\Omega_n z_D) + C_2\, exp(\Omega_n z_D) -$$

$$\frac{A_n p\, sin(\omega_n)\bar{H}_D}{(\omega_n^2+p)\omega_n} \Big] A_n\, cos(\omega_n x_D), \qquad \text{(B.10)}$$

For unsaturated zone, after nondimensionalization and using equation (2f) and equation (2g).

Equation (2a) to (2e) can be written as:

$$\frac{\partial^2 u_D}{\partial x_D^2} + K_D \frac{\partial^2 u_D}{\partial z_D^2} - K_D \kappa_D \frac{\partial u_D}{\partial z_D} = \beta \frac{\partial u_D}{\partial t_D}, \ 0 \le z_D \le H_{uD}, \qquad \text{(B.11a)}$$

$$u_D(x_D, z_D, 0) = 0, \qquad \text{(B.11b)}$$

$$\frac{\partial u_D}{\partial x_D}(x_D, z_D, t_D)|_{x_D=0} = 0, \qquad \text{(B.11c)}$$

$$u_D(1, z_D, t_D) - H_D(t_D) = -K_{LD} \frac{\partial u_D}{\partial x_D}(1, z_D, t_D), \qquad \text{(B.11d)}$$

$$\alpha \frac{\partial u_D}{\partial z_D}(x_D, z_D, t_D)|_{z_D=H_{uD}} = I_D(t_D), \qquad \text{(B.11e)}$$

After applying Laplace transform, we get:

$$\frac{\partial^2 \bar{u}_D}{\partial x_D^2} + K_D \frac{\partial^2 \bar{u}_D}{\partial z_D^2} - K_D \kappa_D \frac{\partial \bar{u}_D}{\partial z_D} = \beta p \bar{u}_D, \ 0 \le z_D \le H_{uD}, \qquad \text{(B.12a)}$$

$$\frac{\partial \bar{u}_D}{\partial x_D}(x_D, z_D, p)|_{x_D=0} = 0, \qquad \text{(B.12b)}$$

$$\bar{u}_D(1, z_D, p) - \bar{H}_D(p) = -K_{LD}\frac{\partial \bar{u}_D}{\partial x_D}(1, z_D, t_D), \quad \text{(B.12c)}$$

$$\alpha\frac{\partial \bar{u}_D}{\partial z_D}(x_D, z_D, p)|_{z=H_{uD}} = \bar{I}_D(p). \quad \text{(B.12d)}$$

Using the following variable substitution:

$$\bar{u}_{D2}(x_D, z_D, p) = \bar{u}_D(x_D, z_D, p) - \bar{H}_D(p), \quad \text{(B.13)}$$

then equations (B.12a)-(B.12d) become:

$$\frac{\partial^2 \bar{u}_{D2}}{\partial x_D^2} + K_D\frac{\partial^2 \bar{u}_{D2}}{\partial z_D^2} - K_D\kappa_D\frac{\partial \bar{u}_{D2}}{\partial z_D} = \beta p(\bar{u}_{D2} + \bar{H}_D(p)),\ 0 \le z_D \le H_{uD},$$

(B.14a)

$$\frac{\partial \bar{u}_{D2}}{\partial x_D}(x_D, z_D, p)|_{x_D=0} = 0, \quad \text{(B.14b)}$$

$$\bar{u}_{D2}(1, z_D, p) = -K_{LD}\frac{\partial \bar{u}_{D2}}{\partial x_D}(1, z_D, t_D), \quad \text{(B.14c)}$$

$$\alpha\frac{\partial \bar{u}_{D2}}{\partial z_D}(x_D, z_D, p)|_{z=H_{uD}} = \bar{I}_D(p). \quad \text{(B.14d)}$$

The Cosine transform of $\bar{u}_{D2}(x_D, z_D, p)$ can be defined as

$$\tilde{\bar{u}}_{D2}(z_D, p) = \int_0^1 \bar{u}_{D2}(x_D, z_D, p)B_n\cos(\omega_{bn}x_D)dx_D, \quad \text{(B.15a)}$$

and the corresponding inversion formula is defined as

$$\bar{u}_{D2}(x_D, z_D, p) = \sum_{n=0}^{\infty}\tilde{\bar{u}}_{D2}(z_D, p)B_n\cos(\omega_{bn}x_D), \quad \text{(B.15b)}$$

where B_n is a coefficient and ω_{bn} is a frequency, both will be determined later.

Substituting equation (B.15b) into equation (B.14c) to have:

$$\sum_{n=0}^{\infty}\tilde{\bar{u}}_{D2}(z_D, p)B_n cos(\omega_{bn}x_D) = -K_{LD}\sum_{n=0}^{\infty}\tilde{\bar{u}}_{D2}(z_D, p)B_n(-\omega_{bn})sin(\omega_{bn}x_D)|_{x_D=1},$$

(B.16a)

which can be rearranged into:

$$\sum_{n=0}^{\infty}\tilde{\bar{u}}_{D2}(z_D, p)B_n(cos(\omega_{bn}) - K_{LD}\omega_{bn}\, sin(\omega_{bn})) = 0. \quad \text{(B.16b)}$$

Then we will have:

$$cos(\omega_{bn}) - K_{LD}\omega_{bn}\, sin(\omega_{bn}) = 0, \qquad \text{(B.16c)}$$

which means:

$$\omega_{bn}\, tan(\omega_{bn}) = \frac{1}{K_{LD}}. \qquad \text{(B.16d)}$$

Equation (B.16d) is for calculating ω_{bn}. And we can see that ω_{bn} is the same as ω_n.

Then we multiply equation (B.15b) by $B_m cos(\omega_{bm} x_D)$ and integrate from 0 to 1 to get:

$$\tilde{\bar{u}}_{D2}(z_D, p) = \int_0^1 \sum_{n=0}^{\infty} \tilde{\bar{u}}_{D2}(z_D, p) B_n \cos(\omega_{bn} x_D)\, B_m \cos(\omega_{bm} x_D) dx_D\ , \qquad \text{(B.17a)}$$

So only when $m = n$ the integral is non-zero and we will have:

$$B_n^2 \left(\frac{1}{2} + \frac{sin(2\omega_{bn})}{4\omega_{bn}}\right) = 1, \qquad \text{(B.17b)}$$

Equation (B.17b) is for calculating B_n. And we can see B_n equaling to A_n .

Then, multiplying equation (B.14a) by $A_n cos(\omega_n x_D)$, and integrating from 0 to 1 to get:

$$-\omega_n^2 \tilde{\bar{u}}_{D2} + K_D \frac{d^2\tilde{\bar{u}}_{D2}}{dz_D^2} - K_D\kappa_D \frac{d\tilde{\bar{u}}_{D2}}{dz_D} = p\beta\tilde{\bar{u}}_{D2} + \frac{p\beta \bar{H}_D(p) A_n sin\omega_n}{\omega_n}\ ,\ 0 \le z_D \le H_{uD},$$

(B.18a)

$$K_D \frac{d^2\tilde{\bar{u}}_{D2}}{dz_D^2} - K_D\kappa_D \frac{d\tilde{\bar{u}}_{D2}}{dz_D} - (\omega_n^2 + p\beta)\tilde{\bar{u}}_{D2} = \frac{p\beta \bar{H}_D(p) A_n sin\omega_n}{\omega_n},\ 0 \le z_D \le H_{uD},$$

(B.18b)

The solution for equation (B.18b) can be written as:

$$\tilde{\bar{u}}_{D2} = C_3\, exp(Mz_D) + C_4\, exp(Nz_D) - \frac{p\beta \bar{H}_D(p) A_n sin\omega_n}{(\omega_n^2 + p\beta)\omega_n}\ , \qquad \text{(B.19)}$$

where $M = \frac{K_D\kappa_D + \sqrt{K_D^2\kappa_D^2 + 4K_D(\omega_n^2 + p\beta)}}{2K_D}$, and $N = \frac{K_D\kappa_D - \sqrt{K_D^2\kappa_D^2 + 4K_D(\omega_n^2 + p\beta)}}{2K_D}$, C_3 and C_4 are z-independent variables and will be evaluated along with C_1 and C_2.

Now, we can write the solution for the hydraulic head in the unsaturated zone as:

$$\bar{u}_D(x_D, z_D, p) = \bar{H}_D + \sum_{n=0}^{\infty}\left[C_3\exp(Mz_D) + C_4\exp(Nz_D) - \frac{p\beta\bar{H}_D(p)A_n sin\omega_n}{(\omega_n^2+p\beta)\omega_n}\right]A_n\cos(\omega_n x_D), \tag{B.20}$$

In order to determine C_1 , C_2 , C_3 and C_4, we need to start with continuous boundary condition at the interface *z*=0,

$$h - u = 0, \tag{B.21a}$$

$$\frac{\partial h}{\partial z} - \frac{\partial u}{\partial z} = 0, \tag{B.21b}$$

After changing equations (B.21a) and (B.21b) into dimensionless forms and applying Laplace transform, Fourier Cosine transform and using equations (B.3) and (B.13), we can get :

$$\tilde{\bar{h}}_{D2} - \tilde{\bar{u}}_{D2} = 0, \qquad z_D = 0, \tag{B.22a}$$

$$\frac{\partial\tilde{\bar{h}}_{D2}}{\partial z_D} - \frac{\partial\tilde{\bar{u}}_{D2}}{\partial z_D} = 0, \qquad z_D = 0. \tag{B.22b}$$

Multiplying equation (B.4d) by $A_n cos(\omega_n x_D)$ and integrating from 0 to 1 to get

$$\frac{\partial\tilde{\bar{h}}_{D2}}{\partial z_D}(x_D, z_D, p)|_{z_D=-H_{sD}} = 0, \tag{B.23a}$$

Multiplying equation (B.14d) by $A_n cos(\omega_n x_D)$ and integrating from 0 to 1 leads to

$$\alpha\frac{\partial\tilde{\bar{u}}_{D2}}{\partial z_D}(\omega_n, z_D, p)|_{z_D=H_{uD}} = \frac{A_n\bar{I}_D(p)sin\omega_n}{\omega_n}. \tag{B.23b}$$

Now we can use equations (B.22a), (B.22b), (B.23a), (B.23b) to determine C_1, C_2, C_3, C_4 as:

$$C_1 = \frac{\exp(-H_{uD}M)(N-M)\eta+\left[1-\exp\left(H_{uD}(N-M)\right)\right]MN\lambda}{\Omega_n[\exp(2\Omega_n H_{sD})-1]\left[\xi N-M+N(1-\xi)\exp\left(H_{uD}(N-M)\right)\right]}, \tag{B.24a}$$

$$C_2 = \frac{\exp(-H_{uD}M)(N-M)\eta+\left[1-\exp\left(H_{uD}(N-M)\right)\right]MN\lambda}{\Omega_n[1-\exp(-2\Omega_n H_{sD})]\left[\xi N-M+N(1-\xi)\exp\left(H_{uD}(N-M)\right)\right]}, \tag{B.24b}$$

$$C_3 = \frac{\exp(-H_{uD}M)(N\xi/M-1)\eta-\exp\left(H_{uD}(N-M)\right)N\lambda}{\xi N-M+N(1-\xi)\exp\left(H_{uD}(N-M)\right)}, \tag{B.24c}$$

$$C_4 = \frac{\exp(-H_{uD}M)(1-\xi)\eta+M\lambda}{\xi N-M+N(1-\xi)\exp(H_{uD}(N-M))}, \quad \text{(B.24d)}$$

where

$$\eta = \frac{A_n \sin(\omega_n)}{\omega_n \alpha} \bar{I}_D , \quad \text{(B.25a)}$$

$$\xi = \frac{M[1+\exp(-2\Omega_n H_{sD})]}{\Omega_n[1-\exp(-2\Omega_n H_{sD})]}, \quad \text{(B.25b)}$$

$$\lambda = \frac{A_n p \sin(\omega_n)\omega_n(1-\beta)}{(\omega_n^2+p\beta)(\omega_n^2+p)} \bar{H}_D. \quad \text{(B.25c)}$$

Then the baseflow flux in the saturated zone Q_s can be calculated as:

$$Q_s(t) = \int_{-H_s}^{0}(-K_x \frac{\partial h}{\partial x}(x,z,t)|_{x=L})dz, \quad \text{(B.26)}$$

After nondimensionalization and Laplace transform:

$$\bar{Q}_{sD}(p) = -\int_{-H_{sD}}^{0} \frac{\partial \overline{h_D}}{\partial x_D}(1, z_D, p)dz_D \quad \text{(B.27)}$$

Combining equations (B.10) and (B.27), we will get

$$\bar{Q}_{sD}(p) = \sum_{n=0}^{\infty}\Big[C_2 - C_1 + C_1\, exp(\Omega_n H_{sD}) - C_2\, exp(-\Omega_n H_{sD}) - \frac{A_n p\, sin(\omega_n)\bar{H}_D H_{sD}}{K_D \Omega_n \omega_n}\Big]\frac{\omega_n sin(\omega_n)}{\Omega_n} A_n \quad \text{(B.28)}$$

The discharge in the unsaturated zone can be similarly computed:

$$\bar{Q}_{uD}(p) = \sum_{n=0}^{\infty}\Big[-\frac{C_3}{M-\kappa_D} - \frac{C_4}{N-\kappa_D} + \frac{C_3\, exp((M-\kappa_D)H_{uD})}{M-\kappa_D} + \frac{C_4\, exp((N-\kappa_D)H_{uD})}{N-\kappa_D} + (exp(-\kappa_D H_{uD}) - 1)\frac{A_n p\beta\, sin(\omega_n)\bar{H}_D}{K_D \Psi_n^2 \kappa_D \omega_n}\Big]\omega_n sin(\omega_n)\, A_n \ , \quad \text{(B.29)}$$